

Data Assimilation in the Geosciences

An overview on methods, issues and perspectives

Alberto Carrassi*, Marc Bocquet[†], Laurent Bertino* and Geir Evensen^{‡*}

Article Type: Overview

Abstract

State estimation theory in geosciences is commonly referred to as *data assimilation*. This term encompasses the entire sequence of operations that, starting from the observations of a system, and from additional statistical and/or dynamical information (such as an evolution model), provides the best possible estimate of its state. Data assimilation is common practice in numerical weather prediction but its application is becoming widespread in many other areas of climate, atmosphere, ocean and environment modeling; in all those circumstances where one intends to estimate the state of a large dynamical system based on limited information. While the complexity of data assimilation, and of the methods thereof, stands on its interdisciplinary nature across statistics, dynamical systems and numerical optimization, when applied to geosciences an additional difficulty arises by the, constantly increasing, sophistication of the environmental models. Thus, in spite of data assimilation being nowadays ubiquitous in geosciences, it has so far remained a topic mostly reserved for experts. This overview article is aimed at geoscientists with a background in mathematical and physical modelling, who have heard of the rapid development of data assimilation and its growing domains of application in environmental science, but so far have not delved into its conceptual and methodological complexities.

*Nansen Environmental and Remote Sensing Center, Bergen, Norway

[†]CEREA, joint laboratory École des Ponts ParisTech and EDF R&D, Université Paris-Est, Champs-sur-Marne, France

[‡]IRIS, Bergen, Norway

1 Introduction

The purpose of this article is to provide a comprehensive, state-of-the-art overview of the methods and challenges of the data assimilation (DA) in the geosciences. It is aimed at geoscientists who are confronted with the problem of combining data with models and need to learn DA, but who are intimidated by the vast, and technical, literature. This work may guide them through a first journey into the topic while being at the same time as complete and precise as possible.

The finest mathematical details, at the crossing between different areas such as numerical methods, algebra, statistics or dynamical systems, are key to grasp the sense of the DA problem, to reveal its interdisciplinary nature and, for many, its beauty. While keeping this in mind, we have nevertheless avoided all technicalities that were not, in our opinion, strictly necessary and have worked to make the narrative intelligible for geoscientists, or climate scientists, who do not usually possess a strong background in mathematics.

We did our best to provide the readers with an extensive bibliography, but also recognize that it is beyond the scope of this work to make it fully exhaustive. In the last decade or so, DA has attracted much attention and the topic has recently been upgraded to the rank of a discipline per-se, as testified by the appearance of books such as Van Leeuwen et al.¹, Reich and Cotter², Law et al.³ or Asch et al.⁴. These works have mainly concerned to the mathematical dimension and formulation of the DA problem and complement seminal books on DA (e.g., Daley⁵, Kalnay⁶ or Evensen⁷), that had spread the knowledge about DA and shaped it as independent discipline. The present article places itself somehow in between these two classes of textbook and aims at bridging the mathematical side of the DA methods with the practicalities and the physical intuitions and know-how that have guided its dramatic development in the climate science and geosciences in general.

The paper is structured so as to provide a first general formulation of the estimation problem, from a Bayesian perspective, in Sect. 2. Having defined the issue, and illustrated the intrinsic difficulties to adopt the Bayesian approach in the geosciences, the two most popular families of DA algorithms, both based on a Gaussian approximation, namely the Kalman filter and the variational methods, are described in Sect. 3. Section 4 is completely

devoted to the ensemble methods, from their origin, through the most relevant successful variants and up to the new frontier of hybrid ensemble-variational methods. Four selected topics, characterizing the DA problems in the geosciences, are the subjects of Sect. 5, and are exemplar of the specific type of approximations and compromises, as well as the level of innovations DA has achieved. Finally Sect. 6 presents a prospect of the nowadays challenges and current directions of research and developments, with special attention to two of them, the particle filter and coupled DA.

2 State estimation: formulation of the problem

2.1 Premises

The problem we intend to solve is the estimation of the state of a system, say the atmosphere, the ocean or any component of the Earth system or its whole, at any arbitrary past, present and future time. We possess two complementary, but both incomplete and inaccurate, sources of information: the *observations* and the *model*. Data assimilation provides the conceptual and methodological tools to tackle the problem by bringing synergy between model and observations and by exploiting their respective informational content. Given the nature of the modeling and observation infrastructure in the geosciences, DA is conveniently formalized as a discrete-model/discrete-observation estimation problem, as we will do in this overview. We remark however that, the *nudging method* (e.g., Hoke and Anthes⁸, Lakshmivarahan and Lewis⁹), one of the simplest and most straightforward approach to assimilate data in a dynamical model, is better formulated as continuous-model/continuous-data problem. Nudging will not be tackled in this overview, but it is worth mentioning that it has recently awaken new attention which has also brought to the introduction of new advanced formulations (e.g., Auroux and Blum¹⁰, Pazo et al.¹¹), and to the study of its connection with the synchronization problem¹². Interested readers can find complete treatment of the continuous-continuous and discrete-continuous cases in many textbooks on estimation theory (see, e.g., Jazwinski¹³, Bain and Crisan¹⁴). We shall formalize hereafter the two ingredients entering the estimation problem.

The dynamical model - Let us assume that a model of the physical processes of interest is given as a discrete stochastic-dynamical system in the m -dimensional Euclidean space \mathbb{R}^m ,

$$\mathbf{x}_k = \mathcal{M}_{k:k-1}(\mathbf{x}_{k-1}, \boldsymbol{\lambda}) + \boldsymbol{\eta}_k. \quad (1)$$

Here $\mathbf{x}_k \in \mathbb{R}^m$ and $\boldsymbol{\lambda} \in \mathbb{R}^p$ are the model state and parameter vectors respectively, $\mathcal{M}_{k:k-1} : \mathbb{R}^m \rightarrow \mathbb{R}^m$ is usually a nonlinear, possibly chaotic, map from time t_{k-1} to t_k , and $\boldsymbol{\eta}_k \in \mathbb{R}^m$ stands for model error, represented here as a stochastic additive term. The model parameters may include the external forcings or the boundary-condition terms. Throughout the text we will use the notation $\mathbf{x}(t_k) = \mathbf{x}_k$.

The model error term, $\boldsymbol{\eta}_k$, is intended to represent the error of a model prediction of the true unknown process at time t_k , initialized from the true state (perfect initial condition) at time t_{k-1} . It accounts for the cumulative effect, over the interval $t_k - t_{k-1}$, of errors in the parameters, $\boldsymbol{\lambda}$, errors in the numerical schemes used to integrate Eq. (1) as well as the effect of the unresolved scales. The two latter arise from the spatio-temporal discretization from physical laws (e.g., the Navier Stokes equations) expressed as partial differential equations on a continuous media, into difference equations on a discrete grid or finite spectral modes. The appropriateness of the stochastic formulation of the model error is questionable in many cases (see, e.g., Nicolis¹⁵). Nevertheless it has the advantage of fitting very well to the probabilistic Bayesian approach to the DA problem, as we will clarify later. Alternative forms of model error treatment in DA have been proposed recently, including a deterministic one (see Carrassi and Vannitsem¹⁶ and references therein), but they will not be tackled in this overview.

The dynamical model can also include an explicit dependency in time (i.e., be non-autonomous), and it will be so if the system is subject to climate change driven by a time-dependent forcing, such as radiative forcing, anthropogenic changes in greenhouse gas and aerosol concentrations. In this case the system may not possess an attractor nor an invariant measure on it, a situation that again would hamper the development of a consistent statistical framework for DA. Recent studies on the so called pullback or random attractor^{17,18} may open the path to suitable formulations of the estimation problem for non-autonomous systems.

The observation model - Noisy observations of \mathbf{x}_k are available at discrete times and

are represented as components of the observation vector $\mathbf{y}_k \in \mathbb{R}^d$. Assuming the noise is additive, they are related to the model state vector through

$$\mathbf{y}_k = \mathcal{H}_k(\mathbf{x}_k) + \boldsymbol{\epsilon}_k. \quad (2)$$

Equation (2) defines the, possibly nonlinear, observation operator, $\mathcal{H} : \mathbb{R}^m \rightarrow \mathbb{R}^d$, and it may involve spatial interpolations in finite-difference models or spectral-to-physical space transformation in spectral models. Transformations based on physical laws for indirect measurements, such as radiative fluxes used to infer temperatures, can also be represented in this way (e.g., Kalnay⁶). To simplify the notation, we have omitted the dependency of the observation vector size; so that we assumed $d_k = d$.

Similarly to model error, the observational error, $\boldsymbol{\epsilon}_k$, is also represented as a stochastic additive term, and accounts for the instrumental error of the observing devices, deficiencies in the formulation of the observation operator itself, and the *error of representation (or representativeness)*^{19,20}. The latter arises from the presence of unresolved scales and represents their effect on the scales explicitly resolved by the model. The error of representativeness is difficult to estimate, but ubiquitous in Earth science, because the description of a continuum fluid is afforded by an inevitably limited (albeit always growing) number of discrete grid points (or spectral modes); see Cohn²¹ for a discussion on this issue. Note that the additivity of noise is also a simplification since more general noisy observations $\mathbf{y}_k = \mathcal{H}_k(\mathbf{x}_k, \boldsymbol{\epsilon}_k)$ could be considered.

Confronting model with data is inherent to the scientific methods since Galileo's era. Nevertheless, the DA problem in Earth science has some characteristic criticalities that makes it unique. In geosciences we usually have $d \ll m$, i.e., the amount of available data is insufficient to fully describe the system and one cannot strongly rely on a data-driven approach: the model is paramount. It is the model that fills the spatial and temporal gaps in the observational network: it propagates information from observed-to-unobserved areas and from the observing times to any other causally related. This capability has been pivotal in DA for NWP with notable examples being the ocean areas and the Southern Hemisphere, where the lack of routine observations platforms has been compensated by the dynamical

model (see, e.g., Daley⁵, Kalnay⁶). The other peculiarity is the use of massive dataset ($d \approx \mathcal{O}(10^7)$) and huge numerical models ($m \approx \mathcal{O}(10^9)$). Thus, DA methods are designed to achieve the best possible use of a never sufficient (albeit constantly growing) amount of data, and to attain an efficient data-model fusion, in a short period of time (typically 3 – 6 hours for NWP). This poses a formidable computational challenge, and makes DA an example of current big-data problems.

2.2 Bayesian formulation of the state estimation problem

With the two complementary pieces of information in hand, model and data, we can move forward and formalize their fusion. Because of the assumed random nature of both the model and observational error, they can be described in terms of *probability density functions* (pdfs), and the Bayesian approach offers a natural framework to shape the DA problem. Our main focus here is on state estimation, i.e., the issue of estimating \mathbf{x} , based on the model and the observation. Nevertheless, in many physical applications, one is often interested in the joint estimate of the system’s state and of its parameter, $\boldsymbol{\lambda}$ (see, e.g., Evensen²² and references therein). We shall allude to parameter estimation in a number of instances, but its extensive exposition is beyond the spirit of this overview.

In the Bayesian formulation, the output of the estimation process is the *posterior distribution* $p(\mathbf{x}|\mathbf{y})$ of the unknown process \mathbf{x} conditioned on the data \mathbf{y} , which can be obtained using *Bayes’ rule*

$$p(\mathbf{x}|\mathbf{y}) = \frac{p(\mathbf{y}|\mathbf{x})p(\mathbf{x})}{p(\mathbf{y})}. \quad (3)$$

In Eq. (3), the three components of the Bayesian inference appear: $p(\mathbf{x})$ is the *prior pdf* that encodes all the knowledge about the process before assimilating the new observations, $p(\mathbf{y}|\mathbf{x})$ is the likelihood of the data conditioned on the unknown state \mathbf{x} , and $p(\mathbf{y})$ is the marginal distribution of the observation $p(\mathbf{y}) = \int d\mathbf{x} p(\mathbf{y}|\mathbf{x})p(\mathbf{x})$. The latter is usually independent of \mathbf{x} and plays the role of a normalization coefficient. The use of a prior is a distinctive feature of the Bayesian approach, and allows for the introduction of additional information about the system before data are processed. Its choice is subjective and one can in principle use any distribution that suits a study’s specific purposes, based on climatology (i.e., from

an historical knowledge about the system), on general physical principles or even on subjective expert's opinion. However, in many practical circumstances, the search for a good informative prior is not straightforward, although its choice may strongly, and sometimes negatively, affect the results. In NWP it is usually given by a short-range forecast (3 – 6 hours) initialized from the past best-possible estimate of the weather state.

Both the model and the observational error sequences, $\{\boldsymbol{\eta}_k : k = 1, \dots, K\}$ and $\{\boldsymbol{\epsilon}_k : k = 1, \dots, K\}$ are assumed to be white-in-time, mutually independent and distributed according to the pdfs $p_{\boldsymbol{\eta}}$ and $p_{\boldsymbol{\epsilon}}$, respectively. These pdfs stand as the transitional kernel for the probabilistic transition from \mathbf{x}_{k-1} to \mathbf{x}_k , and the likelihood of the observations \mathbf{y}_k conditioned on the state \mathbf{x}_k ,

$$p(\mathbf{x}_k|\mathbf{x}_{k-1}) = p_{\boldsymbol{\eta}}[\mathbf{x}_k - \mathcal{M}_{k:k-1}(\mathbf{x}_{k-1})], \quad (4)$$

$$p(\mathbf{y}_k|\mathbf{x}_k) = p_{\boldsymbol{\epsilon}}[\mathbf{y}_k - \mathcal{H}_k(\mathbf{x}_k)], \quad (5)$$

where the model dependency on the parameters, $\boldsymbol{\lambda}$, has been dropped to simplify the notation. Let us define the sequences of system states and observations within the interval $[t_0, t_K]$ as $\mathbf{x}_{K:0} = \{\mathbf{x}_K, \mathbf{x}_{K-1}, \dots, \mathbf{x}_0\}$ and $\mathbf{y}_{K:1} = \{\mathbf{y}_K, \mathbf{y}_{K-1}, \dots, \mathbf{y}_1\}$ respectively, and we have used the lower case to indicate the dummy index and the upper case to identify the time window length. Because the observational errors are assumed to be white-in-time we have

$$p(\mathbf{y}_{K:1}|\mathbf{x}_{K:0}) = \prod_{k=1}^K p(\mathbf{y}_k|\mathbf{x}_k) = \prod_{k=1}^K p_{\boldsymbol{\epsilon}}[\mathbf{y}_k - \mathcal{H}_k(\mathbf{x}_k)], \quad (6)$$

meaning that the conditional likelihood of the observations in the interval $t_K - t_0$ is the product of the individual likelihoods. We will further assume that the process is Markovian, so that the state at time t_k , once conditioned on all past states, only depends on the state at time t_{k-1}

$$p(\mathbf{x}_{K:0}) = p(\mathbf{x}_0) \prod_{k=1}^K p(\mathbf{x}_k|\mathbf{x}_{k-1}) = p(\mathbf{x}_0) \prod_{k=1}^K p_{\boldsymbol{\eta}}[\mathbf{x}_k - \mathcal{M}_{k:k-1}(\mathbf{x}_{k-1})]. \quad (7)$$

By combining Eq. (6) and (7) using Bayes' rule, Eq. (3), we get the posterior distribution

$$p(\mathbf{x}_{K:0}|\mathbf{y}_{K:1}) \propto p(\mathbf{x}_0) \prod_{k=1}^K p(\mathbf{y}_k|\mathbf{x}_k)p(\mathbf{x}_k|\mathbf{x}_{k-1}) = p(\mathbf{x}_0) \prod_{k=1}^K p_{\boldsymbol{\epsilon}}[\mathbf{y}_k - \mathcal{H}_k(\mathbf{x}_k)]p_{\boldsymbol{\eta}}[\mathbf{x}_k - \mathcal{M}_{k:k-1}(\mathbf{x}_{k-1})]. \quad (8)$$

Equation (8) is of central importance: it states that a new update can be obtained as soon as new data are at disposal; it is known as a hidden Markov model in the field of statistics.

Depending on the time period when observations are distributed and over which the state estimate is pursued, it is possible to define *three estimation problems*²³:

1. **Prediction:** estimate $p(\mathbf{x}_l|\mathbf{y}_{k:1})$ with $l > k$.
2. **Filtering:** estimate $p(\mathbf{x}_k|\mathbf{y}_{k:1})$.
3. **Smoothing:** estimate $p(\mathbf{x}_{K:0}|\mathbf{y}_{K:1})$, or marginals of this pdf, such as $p(\mathbf{x}_l|\mathbf{y}_{K:1})$, with $0 \leq l < K$.

A schematic illustration of the three problems is given in Fig. 1.

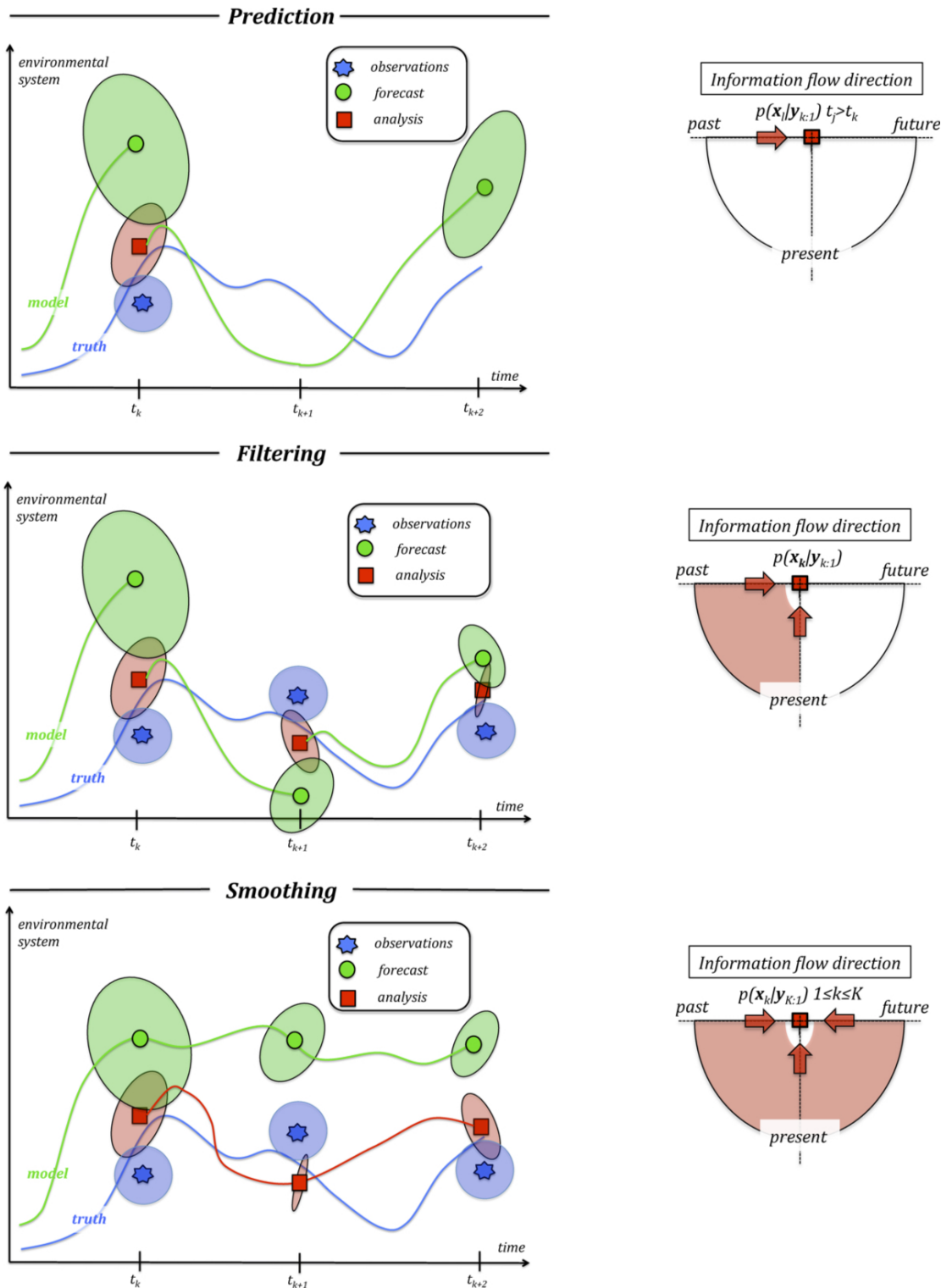


Figure 1: Illustration of the three estimation problems: *prediction* (top), *filtering* (middle) and *smoothing* (bottom). In the right column the information flow directions are displayed for the three cases, illustrating how the information is carried from the past during a prediction, from the past and present in the filter estimate, while from past, present and future in the smoother estimate. The latter can only be obtained after the data have been collected.

The *prediction problem* (Fig. 1 top panel) is formally addressed by solving the corresponding Chapman-Kolmogorov equation for the propagation of a pdf under the model dynamics

$$p(\mathbf{x}_l|\mathbf{y}_{k:1}) = \int d\mathbf{x}_k p_\eta[\mathbf{x}_l - \mathcal{M}_{l:k}(\mathbf{x}_k)]p(\mathbf{x}_k|\mathbf{y}_{k:1}), \quad (9)$$

given the conditional pdf at time t_k , $p(\mathbf{x}_k|\mathbf{y}_{k:1})$.

The *filtering problem* (Fig. 1 mid panel) is the most common one in geophysical applications, and it is characterized by sequential processing, in which measurements are utilized as they become available^{13,24}. An *analysis step*, in which the conditional pdf, $p(\mathbf{x}_k|\mathbf{y}_{k:1})$, is updated using the latest observation, \mathbf{y}_k , alternates with a forecast step in which this pdf is propagated forward until the time of a new observation. The analysis is based on the application of Bayes' Eq. (3), which becomes

$$p(\mathbf{x}_k|\mathbf{y}_{k:1}) = \frac{p_\epsilon[\mathbf{y}_k - \mathcal{H}_k(\mathbf{x}_k)]p(\mathbf{x}_k|\mathbf{y}_{k-1:1})}{\int d\mathbf{x}_k p_\epsilon[\mathbf{y}_k - \mathcal{H}_k(\mathbf{x}_k)]p(\mathbf{x}_k|\mathbf{y}_{k-1:1})}, \quad (10)$$

while in the *prediction step* one integrates the Chapman-Kolmogorov equation (9), with $l \rightarrow k$ and $k \rightarrow (k - 1)$. The process is then repeated, sequentially, with the outcome of the Chapman-Kolmogorov equation providing the prior distribution for the next analysis step.

Estimating the conditional pdf of the state at any time t_k , $0 \leq k \leq K$, based on all observations (past, present and future), is known as the *smoothing problem* (Fig. 1 bottom panel). This is relevant when one is interested in a retrospective analysis after the observations have been collected, and it is very useful in generating *reanalysis* as well as in the estimation of the parameters $\boldsymbol{\lambda}$. Reanalysis programs (see, e.g., Dee et al.²⁵) offer an homogeneous reconstructed estimate of Earth system based on observations over an extended period of time (up to a century), using a state-of-the-art model and DA procedure at the time when reanalysis is produced. Reanalysis are paramount in climate diagnosis and some NWP and climate centers worldwide issue their own reanalysis product (e.g., Dee et al.²⁵, Xie et al.²⁶).

The joint smoothing pdf is given in Eq. (8), and is based on the recursive use of the Bayes formula for the update at each t_k , and the Chapman-Kolmogorov equation for the pdf propagation from t_{k-1} to t_k . To see this, write the smoothing distribution at time t_k using the states at time t_{k+1}

$$p(\mathbf{x}_k|\mathbf{y}_{K:1}) = \int d\mathbf{x}_{k+1} p(\mathbf{x}_k|\mathbf{x}_{k+1}, \mathbf{y}_{K:1})p(\mathbf{x}_{k+1}|\mathbf{y}_{K:1}). \quad (11)$$

Furthermore, note the following

$$p(\mathbf{x}_k | \mathbf{x}_{k+1}, \mathbf{y}_{K:1}) = p(\mathbf{x}_k | \mathbf{x}_{k+1}, \mathbf{y}_{k:1}) = \frac{p(\mathbf{x}_{k+1} | \mathbf{x}_k) p(\mathbf{x}_k | \mathbf{y}_{k:1})}{p(\mathbf{x}_{k+1} | \mathbf{y}_{k:1})}, \quad (12)$$

where we used again the fact that observations $\{\mathbf{y}_{k+1}, \dots, \mathbf{y}_K\}$ are independent of \mathbf{x}_k given \mathbf{x}_{k+1} (see Sect. 2.2), and $p(\mathbf{x}_k | \mathbf{y}_{k:1})$ is the filter solution (the analysis) at time t_k . Together, Eq. (11) and (12) suggest a forward-backward recursive algorithm, in which a forward filtering is followed by a backward smoothing. Starting from $p(\mathbf{x}_0)$, the forward phase consists of a sequential filter from t_1 to t_K which allows one to estimate, and to store, the sequence of filter pdfs $p(\mathbf{x}_k | \mathbf{y}_{k:1})$. In the backward phase, from t_{K-1} to t_1 , one evaluates Eq. (12) using the previously stored filter solutions, and finally estimate the smoothing pdf recursively via Eq. (11) using the smoothing pdf, $p(\mathbf{x}_{k+1} | \mathbf{y}_{K:1})$, from the previous iteration. We will see in Sect. 3.1.2 that the above recursion possesses an analytic solution when the dynamical and observational model are linear and all error pdfs are Gaussian.

We conclude the section with some comparative considerations between the filter and smoother. The filtering solution at an arbitrary t_k ($0 \leq k \leq K$) is obtained by sequential updating until t_k and it thus accounts for all observations up to t_k . In contrast, the smoothing solution at the same time t_k , which is formally obtained by marginalizing $p(\mathbf{x}_{K:0} | \mathbf{y}_{K:1})$ over $\{\mathbf{x}_0, \mathbf{x}_1, \dots, \mathbf{x}_{k-1}, \mathbf{x}_{k+1}, \dots, \mathbf{x}_{K-1}, \mathbf{x}_K\}$, also accounts for future observations until t_K , and it is thus generally more accurate than the filtering one. At the final time t_K both solutions have incorporated the same amount of data, so that in the absence of approximations, they will coincide.

3 A route to solutions: the Gaussian approximation

With the pdfs defined in Eqs. (8–10) in hands, it still remains to be decided which is the estimator that better suits the specific problem. Two "natural" options, the *mean* of the distribution or its *mode*, characterize two distinct approaches to state estimation. Methods designed to estimate the mean are named *minimum squared error* estimators because, independent of the properties of the conditional pdf (i.e., whether or not it is symmetric and unimodal), the mean is the minimum squared error estimate¹³. The mode is the peak of the

distribution, the most probable state, and methods based on it are referred to as *maximum a posteriori* estimators. Other possible options are viable, such as the median, but they are generally more difficult to compute do not have the same wide range of applicability as the mean and the mode.

Despite its appealing and clear logic, the huge dimension of the typical models and datasets used in environmental science hampers the use of a fully Bayesian approach. The problem dimension renders it extremely difficult, or practically impossible, to define and to evolve the pdfs. To overcome this computational, albeit fundamental, issue it is usually assumed that the uncertainties of each piece of information (observations, model and prior) are Gaussian distributed. This hypothesis leads to a substantial simplification: the pdfs can now be described completely in terms of their first and second moments, the mean and covariance matrix.

The Gaussian approximation is at the core of most of the DA procedures successfully used in the geosciences, and this overview will largely discuss methods that rely upon it to different extents. This section presents two main approaches to the estimation problem on which the DA in the geosciences is rooted: the minimum variance Kalman-like and the maximum a posteriori variational methods.

3.1 The linear and Gaussian case - The Kalman filter and smoother

The dynamical and observational models, Eqs. (1) and (2), are both assumed to be linear

$$\mathbf{x}_k = \mathbf{M}_{k:k-1}\mathbf{x}_{k-1} + \boldsymbol{\eta}_k, \quad \boldsymbol{\eta}_k \sim \mathcal{N}(\mathbf{0}, \mathbf{Q}_k), \quad (13)$$

$$\mathbf{y}_k = \mathbf{H}_k\mathbf{x}_k + \boldsymbol{\epsilon}_k, \quad \boldsymbol{\epsilon}_k \sim \mathcal{N}(\mathbf{0}, \mathbf{R}_k), \quad (14)$$

with $\mathbf{M}_{k:k-1}$ and \mathbf{H}_k being matrices in $\mathbb{R}^{m \times m}$ and $\mathbb{R}^{d \times m}$, respectively. The observational and model noises are assumed to be white-in-time, unbiased, and Gaussian distributed with covariances $\mathbf{R}_k \in \mathbb{R}^{d \times d}$ and $\mathbf{Q}_k \in \mathbb{R}^{m \times m}$ respectively.

3.1.1 Kalman filter

Under the aforementioned hypotheses of all sources of errors being Gaussian and both the observational and dynamical models being linear, the Kalman filter is the exact (optimal) solution to recursively estimate the conditional mean and the associated uncertainty, the conditional covariance, of the filtering pdf $p(\mathbf{x}_k|\mathbf{y}_{k:0})$. The process is sequential, meaning that observations are assimilated as they become available, and the KF alternates a *forecast step*, when the mean and covariance of the prediction conditional pdf, $p(\mathbf{x}_k|\mathbf{y}_{k-1:0})$, are evolved, with an *analysis step* in which the mean and covariance of the filtering conditional pdf, $p(\mathbf{x}_k|\mathbf{y}_{k:0})$, are updated. By virtue of the Gaussian assumption, the mean and covariance suffice to fully describe the pdfs and the KF provides an exact set of closed equations. The KF formulae are given below without their derivation, which goes beyond the scope of this overview, but the reader can find numerous alternative ways in classical books or reviews on filtering^{13,14,21,24,27,28}.

Let us indicate the forecast/analysis mean state and covariance as $\mathbf{x}^{\text{f/a}}$ and $\mathbf{P}^{\text{f/a}}$ respectively. The KF recursive equations then read

$$\text{Forecast Step} \quad \mathbf{x}_k^{\text{f}} = \mathbf{M}_{k:k-1}\mathbf{x}_{k-1}^{\text{a}}, \quad (15)$$

$$\mathbf{P}_k^{\text{f}} = \mathbf{M}_{k:k-1}\mathbf{P}_{k-1}^{\text{a}}\mathbf{M}_{k:k-1}^{\text{T}} + \mathbf{Q}_k. \quad (16)$$

$$\text{Analysis step} \quad \mathbf{K}_k = \mathbf{P}_k^{\text{f}}\mathbf{H}_k^{\text{T}}(\mathbf{H}_k\mathbf{P}_k^{\text{f}}\mathbf{H}_k^{\text{T}} + \mathbf{R}_k)^{-1}, \quad (17)$$

$$\mathbf{x}_k^{\text{a}} = \mathbf{x}_k^{\text{f}} + \mathbf{K}_k(\mathbf{y}_k - \mathbf{H}_k\mathbf{x}_k^{\text{f}}), \quad (18)$$

$$\mathbf{P}_k^{\text{a}} = (\mathbf{I}_k - \mathbf{K}_k\mathbf{H}_k)\mathbf{P}_k^{\text{f}}. \quad (19)$$

Given the statistical, observational and dynamical parameter matrices, \mathbf{Q}_k , \mathbf{R}_k , \mathbf{H}_k and \mathbf{M}_k , for $k \geq 1$, and initial condition for the conditional mean, $\mathbf{x}_0^{\text{a}} = \mathbf{x}_0$, and conditional error covariance, $\mathbf{P}_0^{\text{a}} = \mathbf{P}_0$, Eqs. (15)–(19) estimate sequentially the state and the associated error covariance at any future time $k > 1$. The matrix $\mathbf{K}_k \in \mathbb{R}^{m \times d}$ is the Kalman gain and it contains the regression coefficients of the optimal linear combination between the prior, the forecast \mathbf{x}_k^{f} , and the observations. The resulting state estimate, the analysis \mathbf{x}_k^{a} , has minimum variance and is unbiased.

3.1.2 Kalman smoother

We discussed in Sect. 2.2 that a recursive estimate of the pdf of the system state at any arbitrary time in the observing window, conditioned on all observations in the window, i.e. the pdf $p(\mathbf{x}_k|\mathbf{y}_{K:1})$, can be obtained using a forward and backward recursions, in which a forward-in-time filter is followed by a backward-in-time smoother. Under the hypotheses of linear dynamical and observational models and Gaussian errors, this bi-directional recursion can be solved analytically and it is referred to as the *Kalman smoother*¹³. Like for the KF, we describe the KS formulae in the following, but we do not provide their derivation which can be found, for instance, in Jazwinski¹³.

Assume that a forward in time KF has been implemented using Eqs. (15–19) for $k = 1, \dots, K$, and the forecast and analysis means and covariances, $\mathbf{x}_k^{f/a}$ and $\mathbf{P}_k^{f/a}$, have been computed and stored. With the filtering solutions at disposal we can run the KS recursion backward in time, for $k = K - 1, \dots, 1$, to compute the smoothing mean and covariance, \mathbf{x}_k^{sm} and \mathbf{P}_k^{sm} , according to

$$\mathbf{S}_k = \mathbf{P}_k^a \mathbf{M}_{k+1:k}^T (\mathbf{M}_{k+1:k} \mathbf{P}_k^a \mathbf{M}_{k+1:k}^T + \mathbf{Q}_{k+1})^{-1} = \mathbf{P}_k^a \mathbf{M}_{k+1:k}^T \mathbf{P}_{k+1}^{-f}, \quad (20)$$

$$\text{KS Mean} \quad \mathbf{x}_k^{\text{sm}} = \mathbf{x}_k^a + \mathbf{S}_k (\mathbf{x}_{k+1}^{\text{sm}} - \mathbf{x}_{k+1}^f), \quad (21)$$

$$\text{KS Covariance} \quad \mathbf{P}_k^{\text{sm}} = \mathbf{P}_k^a + \mathbf{S}_k (\mathbf{P}_{k+1}^{\text{sm}} - \mathbf{P}_{k+1}^f) \mathbf{S}_k^T \quad (22)$$

with initial conditions, at time t_K , $\mathbf{x}_K^{\text{sm}} = \mathbf{x}_K^a$ and $\mathbf{P}_K^{\text{sm}} = \mathbf{P}_K^a$. As anticipated in Sect. 2.2, the KF and KS solutions at final time t_K are equivalent, but they are not so at any other time within the window. The KS formulation given above is also known as *Rauch-Tung-Striebel* smoother; more details on the smoothing techniques can be found in Cosme et al.²⁹.

3.1.3 Some properties of the Kalman filter and smoother

Although the straightforward use of the KF and KS in geosciences is obviously hampered by the computational limitations and by the inconsistency of their statistical/dynamical hypotheses (Gaussianity and linearity), yet they represent the backbone of many practical DA algorithms. The history of the use of KF-like methods in geosciences is the one of a never-ending search for suitable approximations that, even if sub-optimal, can still work

satisfactorily in a nonlinear, non-Gaussian, and high dimensional setting. We will see in the coming sections how the KF has served as a key conceptual and factual framework upon which several successful operational DA methods have been built for this scenario. This section briefly revises some of the key properties and issues of the KF and KS. Our discussion here mainly pertain to the KF, but most of the conclusions apply to the KS as well.

Time dependent prior - The KF analysis will be closer to either the observations or the prior depending on their respective accuracy, i.e., on our belief about them as estimated via the covariances \mathbf{R}_k and \mathbf{P}_k^f respectively. In the geosciences, the number of observations, albeit large, is usually insufficient to fully cover the state space ($d \ll m$) so that much of how the information is spread from observed to unobserved areas is controlled by the prior. Having an informative, accurate, and reliable prior is thus of great importance. As mentioned at the end of Sect. 2.1, the situation $d \ll m$ is endemic in NWP, and the use of a short-range numerical forecast in a cyclic DA procedure has been key to the success of DA in that context (see, e.g., Daley⁵, Kalnay⁶). The KF recursion provides a time-dependent estimate of the prior (its mean and covariance) that is highly desirable in environmental systems that are usually chaotic, so that the actual error associated with \mathbf{x}_k^f is itself strongly time-dependent. We will see in Sect. 5.1 that this property of the chaotic dynamics, while representing a challenge to the state estimation process, can also be exploited explicitly in the design of DA algorithms for this class of systems.

Filter divergence - Filter divergence is the name used to refer to the situation in which the solution of the KF deviates dramatically from the true signal that it was supposed to track³⁰. The phenomena is irreversible, in the sense that the KF is not longer able to pull back its solution close to the truth. Filter divergence is often the result of progressive and repeated under-estimation of the actual error, $\mathbf{P}_k^a < \mathbf{P}_k^{\text{truth}}$ (the matrices order relationship is that of the cone of the positive semi-definite matrices³¹). Under the action of the dynamics, Eq. (16), the analysis error covariance, \mathbf{P}_{k-1}^a , is transformed into the forecast one at the next time, \mathbf{P}_k^f . If the dynamical model is chaotic (or just unstable) then at least one of the eigenvalues of $\mathbf{M}_{k:k-1}$ is larger than one and $\mathbf{P}_k^f \geq \mathbf{P}_{k-1}^a$: the estimated error grows during the forecast phase. However, for generic stable dynamics such an error growth is not guaranteed.

At the analysis times, the term $(\mathbf{I}_k - \mathbf{K}_k \mathbf{H}_k)$ in Eq. (18) and (19) represents the forcing due to the observations, and it has a stabilizing effect since its eigenvalues are bounded to be lower or equal to one³². This implies that the estimated analysis error covariance is always smaller or equal to the forecast (prior) error covariance, $\mathbf{P}_k^a \leq \mathbf{P}_k^f$. The overall fate of the KF error covariance comes by the balances between the (possible) growth during the forecast phases and the (certain) decrease at analysis times. If the dynamics is not able to counteract the covariance decrease occurring at analysis times, the KF error covariance will progressively decrease, and once $\mathbf{H}_k \mathbf{P}_k^f \mathbf{H}_k^T \ll \mathbf{R}_k$ the filter solution may start to ignore the observations. This is not an issue in itself, as long as the actual error is also decreasing and the KF solution is properly tracking the desired signal. Nevertheless, when this is not the case, i.e., when the KF error estimates decrease but the actual error does not, the KF solution starts to deviate from the observations, eventually diverging completely from the true signal.

Several factors may be at the origin of filter divergence, notably in the misspecification in the DA setup, such as a too strong influence from the measurements (from wrongly specified error statistics, neglected measurement error covariances, etc.), or wrongly specified or neglected model errors (using a model representation that poorly represents reality without accounting for this misrepresentation). Filter divergence also occurs in ensemble-based DA (see Sect. 4) and we will see in Sect. 4.4 which countermeasures have been placed in order to deal with this issue in real applications.

A diagnostic tool - A remarkable property of the KF, originating from the linear and Gaussian assumption, is that the error covariances, \mathbf{P}_k^f and \mathbf{P}_k^a do not depend on the observation values: they are thus unconditional covariance. This is a direct consequence of the first and second moments of the system's state pdf being independent from each other (and uncoupled with higher order moments); a behavior that does no longer hold in a nonlinear and non-Gaussian scenario. Another peculiar feature, which serves as a measure of the filter deviations from optimality, is that the innovation vector sequence, $\mathbf{v}_k = \mathbf{y}_k - \mathbf{H}_k \mathbf{x}_k^f$, is Gaussian and white-in-time¹³: one can thus keep monitoring the innovations to asses the KF optimality and, possibly, to implement corrections⁵.

Bias and covariance estimation - The optimality of the KF relies upon the veracity of its assumptions: the linearity of the model and observational operator, and the Gaussianity of

the true error pdfs. Any mismatch between the real conditions on which the KF operates and its working hypotheses will negate its optimality. Nevertheless, even when the hypotheses are correct, the KF will still depend on the correct specification of its statistical inputs: the model and observational error covariances. The initial conditions, \mathbf{x}_0^a and \mathbf{P}_0^a , are also input but their impact on the filter performance is discussed separately in the following paragraph.

Recall from Eqs. (13)–(14) that, $\boldsymbol{\eta}_k \sim \mathcal{N}(\mathbf{0}, \mathbf{Q}_k)$ and $\boldsymbol{\epsilon}_k \sim \mathcal{N}(\mathbf{0}, \mathbf{R}_k)$. If either the actual model or observational errors are biased (or both), the KF analysis will be biased too, unless those biases are removed from the forecast before the analysis update, Eqs. (18)–(19). These biases can be estimated recursively in time, along with the system’s state, using an approach known as *state augmentation* in which the state is formally augmented with the bias term (e.g., Dee³³). The state augmentation strategy is also the classical choice to deal with the simultaneous model state and parameter estimation¹³.

Likewise, discrepancies can also be present between the actual model and observation error covariances and those stipulated in the filter setup. In contrast to the bias though, the covariances cannot be corrected using the state augmentation approach, and an additional procedure is required. A possibility is again on the use of the innovations: when all error covariances entering the KF are correct, the innovations are distributed according to²¹ $\mathbf{v}_k \sim \mathcal{N}(\mathbf{0}, \boldsymbol{\Sigma}_k)$, with $\boldsymbol{\Sigma}_k = \mathbf{H}_k(\mathbf{M}_{k:k-1}\mathbf{P}_{k-1}^a\mathbf{M}_{k:k-1}^T + \mathbf{Q}_k)\mathbf{H}_k^T + \mathbf{R}_k$. It is then possible, in principle, to estimate the "best" \mathbf{Q}_k and/or \mathbf{R}_k as those maximizing the conditional probability, $p(\mathbf{v}_k|\mathbf{Q}_k, \mathbf{R}_k)$, where the innovation is treated as a random variable³⁴. Given the large dimension of \mathbf{Q}_k and \mathbf{R}_k , such a maximum likelihood approach can only be feasible if \mathbf{Q}_k and \mathbf{R}_k are parametrized based on a very small number of parameters.

In any case, suitable parametrizations of the covariance matrices are necessary, particularly for model error, given the huge size of the geophysical models and the wide range of possible error sources. The former problem implies the need to estimate large matrices based on a limited number of available observations. The second is related to the multiple sources of model error, such as incorrect parametrization, numerical discretization, and the lack of description of some relevant scale of motion, which makes difficult to set a unified parametrization. Recent works have proposed efficient combinations of Bayesian estimation procedures with Monte Carlo approximation to estimate both the observational and model

error covariances^{35–39}.

The computation of the Kalman gain, Eq. (17), requires the inversion of the matrix $(\mathbf{H}_k \mathbf{P}_k^f \mathbf{H}_k^T + \mathbf{R}_k)^{-1} \in \mathbb{R}^{d \times d}$. To make it computationally tractable, \mathbf{R}_k is often assumed to be diagonal (so full rank), i.e., observations are assumed to be spatially uncorrelated. The estimation of \mathbf{R}_k is reduced to the task of specifying only its diagonal. It can also affect negatively the filter’s performance when observations are indeed spatially correlated and it is typically so for remotely sensed data. The impact of neglecting observational error correlations, as well as approaches to include them efficiently in the DA setup, have been studied in several works (see, e.g., Stewart et al.⁴⁰, Miyoshi et al.⁴¹).

Dependency on the initial condition - The criticality of the choice of the initial error covariance, \mathbf{P}_0 , is related to the filter’s stability, intended as the convergence of its solutions to an asymptotic sequence, independently of the initial conditions⁴². Optimality of the filter does not guarantee stability but, for a stochastically-driven dynamical system as in Eq. (13), it also requires the filter to be (uniformly) *observable* and *controllable* (see, e.g., Jazwinski¹³, Kalman⁴³, Cohn and Dee⁴⁴). Roughly, observability is the condition that, given sufficiently many observations, the initial state of the system can be reconstructed by using a finite number of observations. Similarly, controllability can be described as the ability to move the system from any initial state to a desired one over a finite time interval, and is related to the properties of the system noise, \mathbf{Q}_k . The KF stability and convergence for purely deterministic systems (i.e., like in Eq. (13) but with $\mathbf{Q}_k = \mathbf{0}$), under the sole condition of uniform observability has been recently proved by Ni and Zhang⁴⁵ and further characterized in terms of the stability properties of the dynamics by Gurumoorthy et al.⁴⁶. The generalization to the case of degenerate (rank deficient) initial condition error covariance is given in Bocquet et al.³¹, thus corroborating reduced-rank formulations of the KF based on the system’s unstable modes⁴⁷.

3.2 Variational approach

Variational methods are designed to estimate the model trajectory that ”best fits” all the observations within a prescribed observing window $[t_0, t_K]$. Given that the model trajectory is globally adjusted to fit all observations simultaneously, the state estimate at each t_k in the

window is influenced by all observations, before, at, and after t_k . The problem is formalized as the one of minimizing an appropriate scalar *cost function* that quantifies the model-to-data misfit, with the constraint given by the model equations. Assuming to have data at each time t_k in the window (this assumption can easily be relaxed without any major changes in the exposition that follows), the variational problem reads

$$\mathbf{x}_{K:0}^a \triangleq \operatorname{argmin}(\mathcal{J}(\mathbf{x}_{K:0})) \quad \text{subject to} \quad \mathbf{x}_k = \mathcal{M}_{k:k-1}(\mathbf{x}_{k-1}) + \boldsymbol{\eta}_k \quad k = 1, \dots, K. \quad (23)$$

The cost function, $\mathcal{J}(\mathbf{x}_{K:0})$, is a function of the entire model trajectory within the window ($\mathcal{J}(\mathbf{x}_{K:0})$ is in fact a *functional*), and the variational analysis solution, the trajectory $\mathbf{x}_{K:0}^a$, provides the closest possible fit to the data, while being simultaneously consistent with the model dynamics over the entire window. Note that, in formulating the variational problem, Eq. (23), we did not require the model being linear and we have not yet made any hypothesis on the statistical nature of the errors. The most common forms of the variational problem in the geosciences are discussed and derived in Sect. 3.2.2. For example, when both model and observational noise are white in time, unbiased, and Gaussian distributed with covariances \mathbf{Q}_k and \mathbf{R}_k respectively, the cost function reads

$$\mathcal{J}(\mathbf{x}_{K:0}) = \frac{1}{2} \sum_{k=0}^K \|\mathbf{y}_k - \mathcal{H}_k(\mathbf{x}_k)\|_{\mathbf{R}_k}^2 + \frac{1}{2} \sum_{k=1}^K \|\mathbf{x}_k - \mathcal{M}_{k:k-1}(\mathbf{x}_{k-1})\|_{\mathbf{Q}_k}^2 + \frac{1}{2} \|\mathbf{x}_0 - \mathbf{x}^b\|_{\mathbf{B}}^2, \quad (24)$$

where the notation, $\|\mathbf{x}\|_{\mathbf{A}}^2 = \mathbf{x}^T \mathbf{A} \mathbf{x}$, is used to indicate the weighted Euclidean norm. In Eq. (24) we furthermore assumed to have a prior, commonly referred to as *background* in variational methods literature, for the state at the beginning of the window, under the form of a Gaussian pdf with mean, $\mathbf{x}^b \in \mathbb{R}^m$, and covariance, $\mathbf{B} \in \mathbb{R}^{m \times m}$, respectively. We will recall and derive Eq. (24) in Sect. 3.2.2.

The calculus of variations can be used to find the extremum of $\mathcal{J}(\mathbf{x}_{K:0})$ and leads to the corresponding Euler-Lagrange equations (see, e.g., Le Dimet and Talagrand⁴⁸, Bennett⁴⁹). These arise by searching for the solution of a constrained minimization problem in which the requirement that the solution has to follow the dynamics is satisfied by appending the model equations so that

$$\mathcal{L}(\mathbf{x}_{K:0}, \boldsymbol{\Gamma}) = \mathcal{J}(\mathbf{x}_{K:0}) + \sum_{k=1}^K \boldsymbol{\Gamma}_k^T (\mathbf{x}_k - \mathcal{M}_{k:k-1}(\mathbf{x}_{k-1}) - \boldsymbol{\eta}_k), \quad (25)$$

and $\mathbf{\Gamma}_k^T \in \mathbb{R}^m$ is the Lagrangian multiplier vector at time t_k . Although rigorous and formally appealing, solving the Euler-Lagrange equations for problems with the size and complexity of typical geophysical systems is practically impossible, unless drastic approximations are introduced. When the dynamics are linear and the amount of observations is not very large, the Euler-Lagrange equations can be solved with the *method of representers* which has been very successful in the early days of DA for the ocean⁴⁹, and later extended to nonlinear dynamics by Uboldi and Kamachi⁵⁰. A nice property of the representer method is that it reduces the dimension of the problem to the number of measurements (compared to the whole model state at all times or the model state dimension)⁴⁹.

Nevertheless, the representers method is far from being applicable for realistic high-dimensional problems such as NWP. An attractive alternative is represented by the *descent methods*, which make use of the gradient vector of the cost function in an iterative minimization procedure⁵¹. This latter approach, in its many variants, is adopted in most of the operational NWP centers that employ variational assimilation⁵². At the cost function minimum, its gradient must vanish and its Hessian matrix be positive definite:

$$\nabla_{\mathbf{x}_{K:0}} \mathcal{J}(\mathbf{x}_{K:0}) = \mathbf{0}, \quad \nabla_{\mathbf{x}_{K:0}}^2 \mathcal{J}(\mathbf{x}_{K:0}) > 0, \quad (26)$$

where $\mathbf{0} \in \mathbb{R}^{m \times K}$ is a matrix with all entries equal to zero, and the second inequality stands for the positive definiteness of the Hessian matrix. The *control variable* with respect to which the minimization is performed is the entire model trajectory over the observing window. The variational problem defined by Eq. (23) is usually referred to as *weak-constraint* given that the model dynamics is affected by errors and it thus constitutes a weak constraint during the minimization⁵³.

An important particular case is given by the *strong-constraint* variational assimilation in which the model is assumed to be perfect^{48,54} (i.e., $\boldsymbol{\eta}_k = 0$). In this case, the dynamical model is (assumed) purely deterministic and its solutions are uniquely determined by specifying the initial conditions. This transforms the problem from a constraint into an unconstrained one and the cost function into a function of the initial condition alone, $\mathcal{J}(\mathbf{x}_{K:0}) \Rightarrow \mathcal{J}(\mathbf{x}_0)$; its gradient with respect to the state at t_0 reads

$$\nabla_{\mathbf{x}_0} \mathcal{J}(\mathbf{x}_{K:0}) = \sum_{k=1}^K \mathbf{M}_{k:0}^T \nabla_{\mathbf{x}_k} \mathcal{J}(\mathbf{x}_k) + \nabla_{\mathbf{x}_0} \mathcal{J}(\mathbf{x}_0). \quad (27)$$

where we have used the fact that $\mathbf{x}_k = \mathcal{M}_{k:0}(\mathbf{x}_0)$, and applied the chain rule for differentiating compositions of functions. The matrix $\mathbf{M}_{k:0}^T$ is the *adjoint operator*, the adjoint of the tangent linear model, and implies a backward integration from t_k to t_0 . The gradient, Eq. (27), can be obtained through a set of operations involving both forward nonlinear and backward adjoint integration. The drastic reduction of the control variable’s number, from the entire trajectory $\mathbf{x}_{K:0}$ for the weak-constraint, into the initial state alone, \mathbf{x}_0 , for the strong-constraint case, together with the use of the adjoint methods⁵⁵, has made possible the successful use and diffusion of strong-constraint variational methods, or some suitable approximation of them, in atmospheric and oceanic DA (see, e.g., Kalnay⁶, Talagrand⁵⁶).

3.2.1 Minimization process

With the gradient in hand, the minimization is iteratively solved searching for the state vector, \mathbf{x}_0^i , at the i -th iteration that satisfies $\mathcal{J}(\mathbf{x}_0^i) < \mathcal{J}(\mathbf{x}_0^{i-1})$, and the process is repeated until a prespecified convergence criteria (a threshold on the amplitude of the cost function) is verified. These procedures are referred to as *descent methods* because the searching direction, \mathbf{v}^i , is chosen to have an angle greater than 90 degrees with respect to the gradient. Moreover, the various minimization algorithms differ on how \mathbf{v}^i and the step size along it are chosen. The most common and straightforward descent methods are the *steepest* and the *Newton* method.

In the former, \mathbf{v}^i is taken as opposite to the gradient. This strategy works very well when the cost function is uniformly strictly convex (i.e., it has a global quadratic dependence on the control variable), in which case the gradient at any arbitrary point always heads to the absolute (and unique) minimum of the cost function, and the rate of convergence is linear. The computational cost of each iteration is relatively low, but the linear convergence can be so slow that the difference, $\mathbf{x}_0^i - \mathbf{x}_0^{i-1}$, becomes smaller than computer precision. Even more critical is though the assumption of a globally convex cost function, a condition seldom encountered in the geosciences applications^{57,58}.

To cope with this, Newton’s method assumes that the cost function can be locally approximated by a quadratic expansion around the state point, \mathbf{x}^i , $\mathcal{J}(\mathbf{x}) \approx \mathcal{J}^{\text{Newt}}(\mathbf{x}) = \mathcal{J}(\mathbf{x}^i) + \nabla_{\mathbf{x}}\mathcal{J}(\mathbf{x}^i)(\mathbf{x} - \mathbf{x}^i) + \frac{1}{2}(\mathbf{x} - \mathbf{x}^i)^T \nabla_{\mathbf{x}}^2 \mathcal{J}(\mathbf{x}^i)(\mathbf{x} - \mathbf{x}^i)$. The state at i -th iteration is found by setting

the gradient of this approximation to zero, which gives $\mathbf{v}^i = -\nabla_{\mathbf{x}}^{-2} \mathcal{J}^{Newt}(\mathbf{x}^i) \nabla_{\mathbf{x}} \mathcal{J}^{Newt}(\mathbf{x}^i)$; the search direction is equal to the opposite of the Hessian matrix of the cost function multiplied by its gradient. At the minimum the Hessian of the cost function is positive definite so that the search direction verifies the condition of being oriented with an angle greater than 90 degrees from the gradient. In practice, and in contrast to steepest descent, the Newton method uses also the local information about the curvature of the cost-function in order to better point toward its minimum. Although the convergence of the Newton’s method is quite rapid, its operational use in geophysical DA is rendered difficult by the need to invert the Hessian matrix, which is usually huge size and ill conditioned.

Minimization algorithms used operationally are a trade-off between efficiency and computational limitation and have features that mimic those of the two main algorithms just described. A throughout description of the state-of-art minimization methods goes beyond the scope of this article but interested readers can find more details in, e.g., Asch et al.⁴, Fisher and Andersson⁵².

3.2.2 Statistical interpretation and 4DVar

So far we have intentionally avoided to give the cost function any specific form, while all we assumed was that it offers an appropriate quantification of the model-to-data misfit. It is however obvious that the form of the cost function reflects the way how we intend to weight up the data and the model relative to each other. Again, the statistical approach offers a natural framework to accomplish this task. A natural choice would be to set the cost function proportional to the conditional posterior, $p(\mathbf{x}_{K:0} | \mathbf{y}_{K:0})$, for which a functional suitable form, possibly smooth and derivable, must be given.

A tremendous simplification is obtained by employing the hypothesis of Gaussian errors. Recall the Gaussian assumptions done in formulating the KF and KS in Sect. 3.1, and to define the cost function Eq. (24). By applying the Bayes’s theorem, Eq. (3), the conditional

posterior is the product of three Gaussian pdfs and is itself Gaussian

$$\ln p(\mathbf{x}_{K:0}|\mathbf{y}_{K:0}) \propto - \left[\frac{1}{2} \sum_{k=0}^K \|\mathbf{y}_k - \mathcal{H}_k(\mathbf{x}_k)\|_{\mathbf{R}_k^{-1}}^2 + \frac{1}{2} \sum_{k=1}^K \|\mathbf{x}_k - \mathcal{M}_{k:k-1}(\mathbf{x}_{k-1})\|_{\mathbf{Q}_k^{-1}}^2 + \frac{1}{2} \|\mathbf{x}_0 - \mathbf{x}^b\|_{\mathbf{B}^{-1}}^2 \right], \quad (28)$$

$$\triangleq -\mathcal{J}^{\text{w4DVar}}(\mathbf{x}_{K:0}) \quad (29)$$

which provides the cost function already given in Eq. (24). Maximizing $\ln p(\mathbf{x}_{K:0}|\mathbf{y}_{K:0})$, i.e., finding the most likely trajectory, the analysis $\mathbf{x}_{K:0}^a$, is equivalent to minimizing the term between the squared brackets. Equation (29) defines the cost function of the *weak-constraint 4DVar*, w4DVar^{59–62}. The minimization can be carried out iteratively using the gradient of the cost function as mentioned in Sect. 3.2.1. The control variable for the minimization is the entire trajectory, $\mathbf{x}_{K:0}$, and the estimate at each time t_k is influenced by all observations in the window, up to and after t_k . The gradient (not shown; see Trémolet⁶¹, Carrassi and Vannitsem⁶³) with respect to \mathbf{x}_k includes a term proportional to the innovation, $\mathbf{y}_k - \mathcal{H}_k(\mathbf{x}_k)$, because data are assumed to be available at each time step. In the general case, when the model time discretization is finer than the observational temporal density, the corresponding innovation term disappears. The model error being white-in-time implies a significant simplification: the cost function requires the model error covariances only (and not the correlation), and the model error cost function term (the second one in the rhs of Eq. (28)) reduces to a single summation over the time steps weighted by the inverse of the model error covariances⁶¹. Even in this white-in-time case, the huge size of the control variable, $\approx \mathcal{O}(m \times K)$, along with the difficulty to reliably estimate the model error covariances, \mathbf{Q}_k (cf. Sect. 3.1.3), have made necessary the developments of specific solutions to make w4DVar feasible in the geosciences (see, e.g., Vidard et al.⁶⁰, Trémolet⁶², Griffith and Nichols⁶⁴). Consequently, its use in operational settings has been much limited until very recently^{65–67}. The w4DVar in the presence of a time correlated model error is described in Carrassi and Vannitsem⁶³, while the w4DVar in the context of hybrid ensemble-variational methods (cf. Sect. 4.5) has been recently studied by Amezcua et al.⁶⁸.

In the widely used *strong-constraint 4DVar*, s4DVar, it is assumed that the model is

perfect, which reduces the cost function to

$$\mathcal{J}^{\text{s4DVar}}(\mathbf{x}_0) \triangleq \frac{1}{2} \sum_{k=0}^K \|\mathbf{y}_k - \mathcal{H}_k \circ \mathcal{M}_{k:0}(\mathbf{x}_0)\|_{\mathbf{R}_k^{-1}}^2 + \frac{1}{2} \|\mathbf{x}_0 - \mathbf{x}^b\|_{\mathbf{B}^{-1}}^2, \quad (30)$$

with the \circ symbol representing the composition of operators and the control variable is now "only" the system's state at the beginning of the window, \mathbf{x}_0 . The gradient can be obtained by applying Eq. (27) and reads

$$\nabla_{\mathbf{x}_0} \mathcal{J}^{\text{s4DVar}}(\mathbf{x}_0) = - \sum_{k=0}^K \mathbf{M}_{k:0}^T \mathbf{H}_k^T \mathbf{R}^{-1} [\mathbf{y}_k - \mathcal{H}_k \circ \mathcal{M}_{k:0}(\mathbf{x}_0)] - \mathbf{B}^{-1}(\mathbf{x}_0 - \mathbf{x}^b), \quad (31)$$

which makes apparent the effects of the adjoint operator, $\mathbf{M}_{k:0}^T$, to project backward the influence of the observation at any t_k . The final analysis is obtained using an iterative process starting by providing a first guess, $\mathbf{x}_0^{i=0}$, and evaluating $\mathcal{J}^{\text{s4DVar}}(\mathbf{x}_0^i)$ and the gradient at each iteration. As explained in Sect. 3.2.1, the process is then repeated until the convergence criteria are met. From the final minimum state at \mathbf{x}_0^a the analyzed trajectory over the entire window, $\mathbf{x}_{K:0}^a$, is obtained by integrating the deterministic model from t_0 to t_K . This trajectory represents the most likely model solution fitting the observations within the window and given the prescribed initial condition and data uncertainty.

A schematic illustration of the different problems tackled by the w4DVar, s4DVar and 3DVar (Sect. 3.3.2) is given in Fig. 2.

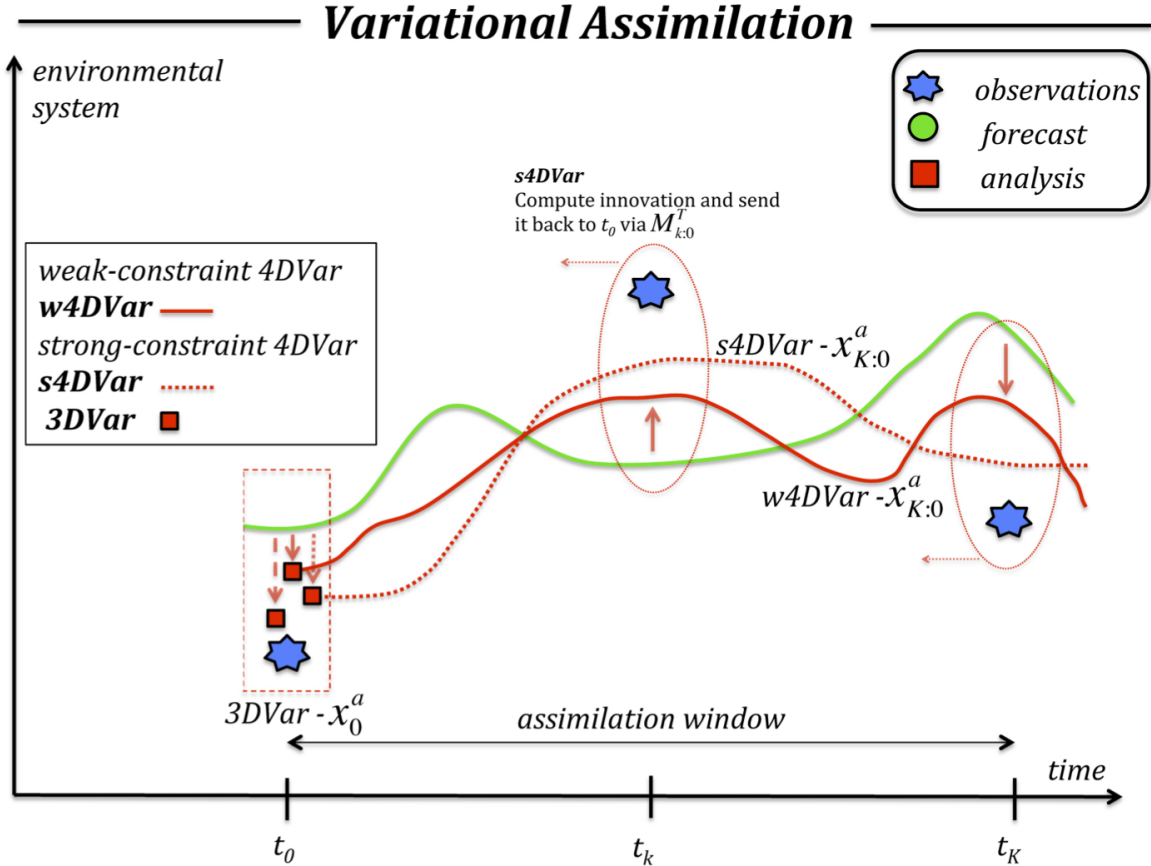


Figure 2: Illustration of the three variational problems: weak-constraint 4DVar (w4DVar; red continuous line), strong-constraint 4DVar (s4DVar; red dotted line) and 3DVar (squared mark at t_0). In the w4DVar the control variable is the entire trajectory over the window, $\mathbf{x}_{K:0}$, so the corrections (continuous red arrow) are computed at the observation times. In the s4DVar, the control variable is the state at the beginning of the window, \mathbf{x}_0 , and the corrections (dotted red arrow) are computed at observation times but then propagated back to t_0 using the adjoint model (see Eq. (31)). In the 3DVar only the observations at time t_0 are used (the correction is indicated with the dashed arrow) and the analysis consists in the state at that time.

3.2.3 Comments on the variational methods

The Gaussian hypothesis has not just allowed to get an analytic expression for the cost-function but it also offered a statistical, and physically plausible, interpretation of the analyzed trajectory. Given the unimodality of the Gaussian pdf, the most likely state is also the

mean of the pdf, that is to say the minimum variance estimate. Without unimodality the mean state, while still having minimum variance, may well be of scarce relevance (it may fall in very low probability region) or not have physical plausibility at all.

In deriving the 4DVar, either in the weak or strong constraint formulations, no assumptions have been made about the features of the dynamical or observational models, that can, in fact, even be nonlinear. Nevertheless, whether or not the latter is actually the case it has enormous consequences on the accuracy of the 4DVar analysis, as well as on the complexity of the algorithms used to solve it. When both models are linear and all errors are Gaussian, mutually uncorrelated and white-in-time, the 4DVar cost-function is quadratic and the gradient, that will depend linearly on the control variable, will correctly point to its global minimum. In this linear case, the 4DVar solution will match exactly the mean solution of a KS, Eq. (21), to which the same input statistics are provided, and it will thus represent an alternative way to get the best mean estimate without the explicit need to compute inverse matrices as in the KS⁶⁹.

In the general nonlinear case however an exact solution cannot be obtained. The approximate analysis will be the outcome of the minimization process and the degree of its accuracy will strongly depend on the degree of nonlinearity in the dynamical and observational models, even if the initial condition and observational error are Gaussian. The cost function will no longer be quadratic and it may possess multiple minima to which the minimization procedure can wrongly be trapped. A number of fixes have been proposed and put in place to overcome this issue, so as to render the cost-function "more quadratic", notably by the use of a precondition under the form of a suitable invertible control variable transformation⁷⁰. It is beyond our scopes to expand further on this subject, but the readers can find more details in the literature^{4,56}.

The variational approach does not automatically solve the complete Gaussian estimation problem: it does not provide the two moments, the mean and the covariance, of the posterior distribution, but only the first one. It is possible to show that the analysis error covariance is indeed given, exactly/approximately for the linear/nonlinear case respectively, by the inverse Hessian matrix of the cost function; at its minimum the (inverse) Hessian must be positive definite (see Sect. 3.2.1), consistently with a feature of a covariance matrix. Nevertheless,

estimating the Hessian matrix for a realistic geophysical applications is extremely difficult, and usually the same (fixed in time) error covariance matrix is used to characterize the background errors at the beginning of each DA cycle. When solving the s4DVar the background error covariance is implicitly evolved within the window so that, effectively, a dynamically evolved estimate of the prior error is used at the observation times⁵⁸, but such an updated covariance is not explicitly accessible to initialize the next cycle.

This inherent limitation of the variational approach marks a key distinction with respect to sequential methods like KF and KS, which are able to provide a time-dependent estimate of the uncertainty associated to the state estimate. This aspect has largely (but not uniquely) contributed to the popularity of KF-like approaches for DA with chaotic models⁷¹ where a time dependent description of the estimation error is highly desirable (cf. Sect. 5.1). We will see in Sect. 4.5 that the recent promising efforts toward hybrid variational-ensemble methods are also aiming to cope with this issue, thus endowing the 4DVar with a flow-dependent estimate of the error covariance^{72–74}.

3.3 Some popular approximations

We describe briefly some of the early successful approximations of the Kalman filter and of the variational approach that have made their implementation possible in the geosciences.

3.3.1 Extended Kalman filter

The *extended Kalman filter* (EKF) represents a first-order expansion of the KF and extends its use to nonlinear dynamics¹³. As the KF, it is sequential: the systems state and associated error covariance are updated at discrete observation times and evolved in between them. In the EKF, the mean state estimate is propagated by the full nonlinear model, but the error covariance evolution is approximated using the tangent linear one. The linearization is taken around the nonlinear model solution, so that the Jacobian of the model is evaluated upon it and it is thus state dependent.

As with the standard KF for linear dynamics, the EKF also assumes that errors are all Gaussian distributed. Nevertheless, under the action of the nonlinear dynamics, even

a possible initial Gaussian error covariance will not stay Gaussian, and the EKF will only provide an approximate description of the actual estimation error distribution. In general, the accuracy of the EKF scales with the degree of nonlinearity in the model⁷⁵. For instance, Evensen⁷⁶ implemented the EKF with a multilayer ocean model finding that the tangent linear operator led to unbounded error growth since the nonlinear saturation that should occur at climatological level is contained in higher order moments of the error covariance equations, and those are all neglected in the closure used in the EKF.

The EKF has been successful in a number of pioneering applications of DA for meteorology^{77,78} and oceanography⁷⁹. It has also been used in one of the early study of coupled DA (cf. Sect. 6.2) with an atmosphere-ocean model of intermediate complexity⁸⁰. The joint state and parameter estimation is possible with the EKF using the state-augmentation approach and its efficiency for this purpose has been demonstrated in the context of DA for seasonal forecasts⁸¹ or land surface DA (see, e.g., de Rosnay et al.⁸²). A formulation of the EKF for parameter estimation in the presence of time correlated model error has been proposed by Carrassi and Vannitsem⁸³ and later applied to a soil model⁸⁴.

Along with the linear assumption on which it is built, another limitation of the EKF is due to the enormous computational requirements of the error covariance propagation. This involves the storage of full covariance matrices, the derivation of the tangent linear model, and its application a number of times twice the state vector dimension⁴.

3.3.2 Incremental 4DVar and 3DVar

The *incremental formulation*⁸⁵ employs a linearization of the problem around the background trajectory: both the dynamical and observational models are linearized and the cost function of the incremental (strong-constraint) 4DVar reads

$$\mathcal{J}^{\text{s4DVar-Incr}}(\delta\mathbf{x}_0) = \frac{1}{2} \sum_{k=0}^K \|\mathbf{v}_k - \mathbf{H}_k \mathbf{M}_{k:0} \delta\mathbf{x}_0\|_{\mathbf{R}_k}^2 + \frac{1}{2} \|\delta\mathbf{x}_0\|_{\mathbf{B}^{-1}}^2, \quad (32)$$

where the increment, $\delta\mathbf{x}_0 = \mathbf{x}_0 - \mathbf{x}^b$, is now the control variable for the minimization, and $\mathbf{v}_k = \mathbf{y}_k - \mathcal{H}_k(\mathbf{x}_k) = \mathbf{y}_k - \mathcal{H}_k \circ \mathcal{M}_{k:0}(\mathbf{x}_0)$ is the innovation vector (cf. Sect. 3.1.3).

The cost function is now quadratic, it possesses a unique absolute minimum, and it can be minimized much more easily. The minimization can be carried out by first computing the

innovations (outer loop) using the nonlinear models, \mathcal{H} and \mathcal{M} . In the inner loop, Eq. (32) is evaluated using the linearized models, \mathbf{H} and \mathbf{M} , and then the gradient using the adjoint \mathbf{M}^T . This procedure returns the analysis increment, $\delta\mathbf{x}_0$, to be used for the next outer loop and so on until convergence. The incremental 4DVar allows thus to deal with small nonlinearities in an incremental way, given that the linearized models are cyclically updated when a new outer loop trajectory is computed. Usually a simplified version of the model (coarser resolutions, simplified physics, etc.) is used in the inner loop⁸⁶, and this feature along with the quadratic form of the cost function, have been pivotal for the operational implementation of the incremental 4DVar (see, e.g., Courtier et al.⁸⁵).

3DVar is a special case of the 4DVar where the time dimension is removed and only the observations at the analysis time are assimilated (see Fig. 2 and Kalnay⁶).

4 Ensemble methods

A Monte Carlo approach is at the basis of a class of algorithms referred to as *ensemble-based methods*⁷ of which the *ensemble Kalman filter*, EnKF, and the *ensemble Kalman smoother*, EnKS, are the most celebrated examples. The EnKF and EnKS are still based on the Gaussian hypothesis: their analysis update steps are based only on the mean and covariance. The transition probability is, however, approximated using an ensemble of realizations of the kernel, in practice by running an ensemble of trajectories of the model dynamics. The EnKF and its variants (see Asch et al.⁴, Evensen⁷ and cf. Sect. 4.1–4.2) are nowadays among the most popular approaches for DA in high-dimensional systems, and have been successfully applied in atmospheric and oceanic contexts. Evidence has emerged that a small number of particles, typically 100, is sufficient in many applications, hence making EnKF feasible in situations where the forward step of the DA is computationally expensive. A version of the EnKF is operational for the atmospheric model at the Canadian Meteorological Centre, CMC⁸⁷, and for the ocean system TOPAZ (see Sect. 5.4) developed at NERSC⁸⁸ and exploited operationally by MET Norway as the official Arctic Ocean, sea ice and ecosystem forecasts in the Copernicus Marine Services (www.marine.copernicus.eu).

There have been numerous alternative EnKF-like methods, and we will not attempt here

to discuss or revise them all; a recent review of the EnKF for atmospheric DA is given by Houtekamer and Zhang⁸⁹. However the many different formulations fall almost all into two main categories, namely the *stochastic* and the *square-root* (also called *deterministic*) ones, and this is the subject of the next sections. We shall then discuss the EnKS in Sect. 4.3 and devote Sect. 4.4 to the description of the important fixes that must be put in place to make the EnKF and EnKS working in realistic high-dimensional nonlinear cases. This part of the article closes by presenting an outlook of the current frontier of the hybrid ensemble-based and variational methods in Sect. 4.5.

4.1 Stochastic ensemble Kalman filter

The EnKF as introduced by Evensen⁹⁰, Burgers et al.⁹¹, Evensen⁹² is based on the use of an ensemble representation for error statistics. Thus, instead of storing a full covariance matrix, we can represent the same error statistics using an appropriate ensemble of model states. Given an error covariance matrix, an ensemble of finite size provides an approximation to the error covariance matrix, and, as the size N of the ensemble increases, the errors in the Monte Carlo sampling decrease proportionally to $1/\sqrt{N}$.

The derivations that follow assume a linear observation operator for the sake of simplicity. However ensemble-based methods can straightforwardly incorporate a generic nonlinear operator, \mathcal{H}^7 .

4.1.1 Representation of error statistics

It is convenient to introduce the forecast/analysis ensemble matrix at time t_k

$$\mathbf{E}_k^{\text{f/a}} = [\mathbf{x}_{[1],k}^{\text{f/a}}, \dots, \mathbf{x}_{[N],k}^{\text{f/a}}] \in \mathbb{R}^{m \times N}, \quad (33)$$

which contains the ensemble members, $\mathbf{x}_{[n],k}^{\text{f/a}}$ ($1 \leq n \leq N$), along its columns. The error covariance matrices \mathbf{P}_k^{f} and \mathbf{P}_k^{a} for the predicted and analyzed estimate in the KF are defined in terms of the true state in the KF Eqs. (16–19). However, since the true state is not known, we define the ensemble-anomaly covariance matrices around the ensemble mean, $\bar{\mathbf{x}}_k^{\text{f/a}} = \mathbf{E}_k^{\text{f/a}} \mathbf{1}/N = \frac{1}{N} \sum_{n=1}^N \mathbf{x}_{[n],k}^{\text{f/a}}$, with $\mathbf{1} = [1, \dots, 1]^T \in \mathbb{R}^N$ and

$$\mathbf{X}_k^{\text{f/a}} = \frac{1}{\sqrt{N-1}} [\mathbf{x}_{[1],k}^{\text{f/a}} - \bar{\mathbf{x}}_k^{\text{f/a}}, \dots, \mathbf{x}_{[N],k}^{\text{f/a}} - \bar{\mathbf{x}}_k^{\text{f/a}}] \in \mathbb{R}^{m \times N}. \quad (34)$$

We can now write the ensemble based forecast and analysis error covariances

$$(\mathbf{P}^e)_k^f = (\mathbf{X}_k^f)(\mathbf{X}_k^f)^T, \quad (35)$$

$$(\mathbf{P}^e)_k^a = (\mathbf{X}_k^a)(\mathbf{X}_k^a)^T, \quad (36)$$

where the superscript “e” denotes that the quantities (e.g., matrices in Eqs. (35) and (36)) are estimated based on the ensemble. Having defined the ensemble members, mean, and covariance matrix, for both the forecast and the analysis, we now further simplify the notation by omitting the superscript ”f”, so that for instance we have $\mathbf{X}_k^f = \mathbf{X}_k$, and the convention applies for \mathbf{E} , \mathbf{P}^e , \mathbf{x} and $\bar{\mathbf{x}}$.

Equations (35) and (36) embed an interpretation where the ensemble mean is the best estimate and the spread of the ensemble around the mean is a natural definition of the error in the ensemble mean. Clearly, an ensemble of model states could be seen as a Monte Carlo representation of the pdf $p(\mathbf{x}_0)$ in Eq. (7).

4.1.2 Prediction of error statistics

Given a pdf $p(\mathbf{x}_0)$ at time t_0 , then the joint pdf from time t_0 to t_k is given by Eq. (7), which involves multiplication with the transition density defined in Eq. (4). It was shown in Evensen⁹⁰ that if the pdf $p(\mathbf{x}_0)$ at time t_0 is represented by an ensemble of model states, then the multiplication with the transition density is equivalent to integrating each realization of \mathbf{x} according to the model equations as defined in Eq. (1). Thus, from a finite ensemble of model states we can compute an ensemble approximation of the joint pdf $p(\mathbf{x}_{k:0})$ for the time interval t_0 to t_k .

4.1.3 Analysis scheme

The novel idea of Evensen⁹⁰ was to design an alternative update scheme that could work directly on the ensemble and where it was not necessary to compute the full covariances as defined by Eqs. (35) and (36). For the sake of clarity the time index k is omitted in the equations that follow. It was shown that by updating each individual ensemble member according to the standard KF Eqs. (17) and (18) the updated ensemble will have the correct mean and covariance matrix for the update in agreement with Eq. (19) in the standard KF.

As shown by Burgers et al.⁹¹ it is essential that the observations are treated as random variables having a distribution with mean equal to the observed value and covariance equal to \mathbf{R} . Thus, we start by defining an ensemble of observations

$$\mathbf{y}_{[n]} = \bar{\mathbf{y}} + \boldsymbol{\epsilon}_{[n]} \quad 1 \leq n \leq N, \quad (37)$$

and $\bar{\mathbf{y}} = \mathbf{y}$ from Eq. (14). By subtracting any nonzero mean from the N samples $\boldsymbol{\epsilon}_{[n]}$, it is ensured that the simulated random measurement errors have mean equal to zero and thus the random perturbations do not introduce any bias in the update. Next we define the ensemble covariance matrix of the measurement errors as

$$\mathbf{R}^e = \mathbb{E}[\boldsymbol{\epsilon}\boldsymbol{\epsilon}^T], \quad (38)$$

with \mathbb{E} denoting the expectation operator over the ensemble, and $\mathbb{E}(\boldsymbol{\epsilon}) = 0$. In the limit, $N \rightarrow \infty$, of infinite ensemble size, this matrix converges to the prescribed error covariance matrix \mathbf{R} used in the KF.

The analysis step in the EnKF consists of updates performed on each of the ensemble members, as given by

$$\mathbf{x}_{[n]}^a = \mathbf{x}_{[n]} + \mathbf{P}^e \mathbf{H}^T \left(\mathbf{H} \mathbf{P}^e \mathbf{H}^T + \mathbf{R}^e \right)^{-1} \left(\mathbf{y}_{[n]} - \mathbf{H} \mathbf{x}_{[n]} \right) \quad 1 \leq n \leq N. \quad (39)$$

With a finite ensemble size, the use of the ensemble covariances introduces an approximation of the true covariances. Furthermore, if the number of measurements is larger than the number of ensemble members, then the matrices $\mathbf{H} \mathbf{P}^e \mathbf{H}^T$ and \mathbf{R}^e are singular, and a pseudo inversion must be used.

Equation (39) implies that

$$\bar{\mathbf{x}}^a = \bar{\mathbf{x}} + \mathbf{P}^e \mathbf{H}^T \left(\mathbf{H} \mathbf{P}^e \mathbf{H}^T + \mathbf{R}^e \right)^{-1} \left(\bar{\mathbf{y}} - \mathbf{H} \bar{\mathbf{x}} \right), \quad (40)$$

where $\bar{\mathbf{y}} = \mathbf{y}$ since the measurement perturbations have ensemble mean equal to zero. Thus, the relation between the analyzed and predicted ensemble mean is identical to the relation between the analyzed and predicted state in the standard KF, apart from the use of \mathbf{P}^e and \mathbf{R}^e instead of \mathbf{P}^f and \mathbf{R} .

If the ensemble updates $\mathbf{x}_{[n]}^a$ and $\bar{\mathbf{x}}^a$ from Eqs. (39) and (40) are inserted into Eq. (36), it was shown by Evensen⁹⁰ and Burgers et al.⁹¹ that

$$(\mathbf{P}^e)^a = (\mathbf{I} - \mathbf{K}^e \mathbf{H}) \mathbf{P}^e, \quad (41)$$

with \mathbf{K}^e being the ensemble-based Kalman gain matrix (cf. Sect. 3.1.1 and Eq. (17)). The result in Eq. (41) gives a consistency between the original KF and the EnKF (cf. Eq. (19)).

It should be noted that the EnKF analysis scheme is approximate in the sense that non-Gaussian contributions in the predicted ensemble are not properly accounted for. In other words, the EnKF analysis scheme does not solve the Bayesian update equation for non-Gaussian pdfs. On the other hand, the EnKF analysis scheme is not just a re-sampling of a Gaussian posterior distribution. Only the updates defined by the right hand side of Eq. (39), which are added to the prior non-Gaussian ensemble, are linear. Thus, the updated ensemble inherits many of the non-Gaussian properties from the forecast ensemble. In summary, we have a computationally efficient analysis scheme where we avoid re-sampling of the posterior.

4.1.4 Formulation in terms of the ensemble

In Evensen⁹² it is shown that the EnKF analysis scheme can be formulated in terms of the ensemble without reference to the ensemble covariance matrix, which allows for efficient numerical implementation and an alternative interpretation of the method. We follow the slightly updated formulation from Evensen⁷.

Let us define the matrix $\mathbf{Y}^o \in \mathbb{R}^{d \times N}$ whose columns are the perturbed measurements $\mathbf{y}_{[n]} \in \mathbb{R}^d$, and the corresponding matrix of the normalized anomaly ensemble of the observations, $\dot{\mathbf{Y}}^o \in \mathbb{R}^{d \times N}$

$$\mathbf{Y}^o = [\mathbf{y}_{[1]}, \dots, \mathbf{y}_{[N]}] \in \mathbb{R}^{d \times N}, \quad (42)$$

$$\dot{\mathbf{Y}}^o = \frac{1}{\sqrt{N-1}} [\mathbf{y}_{[1]} - \bar{\mathbf{y}}, \dots, \mathbf{y}_{[N]} - \bar{\mathbf{y}}] \in \mathbb{R}^{d \times N}. \quad (43)$$

The analysis equation (39), expressed in terms of the ensemble matrices, is

$$\mathbf{E}^a = \mathbf{E} + \mathbf{X} \mathbf{X}^T \mathbf{H}^T \left(\mathbf{H} \mathbf{X} \mathbf{X}^T \mathbf{H}^T + \left(\dot{\mathbf{Y}}^o \right) \left(\dot{\mathbf{Y}}^o \right)^T \right)^{-1} (\mathbf{Y}^o - \mathbf{H} \mathbf{E}), \quad (44)$$

where all references to the error covariance matrices are replaced with their ensemble representations. It was shown in Evensen⁹² that the analysis equation (44) can be written as

$$\mathbf{E}^a = \mathbf{E}\mathbf{T}, \quad (45)$$

with the transformation matrix $\mathbf{T} \in \mathbb{R}^{N \times N}$ defined as

$$\mathbf{T} = \mathbf{I}_N + \mathbf{Y}^T \mathbf{C}^{-1} (\mathbf{Y}^o - \mathbf{H}\mathbf{E}), \quad (46)$$

where we have defined the matrix of the normalized observation anomaly ensemble $\mathbf{Y} \in \mathbb{R}^{d \times N}$

$$\mathbf{Y} = \mathbf{H}\mathbf{X}, \quad (47)$$

and the matrix $\mathbf{C} \in \mathbb{R}^{d \times d}$,

$$\mathbf{C} = \mathbf{Y}\mathbf{Y}^T + \left(\dot{\mathbf{Y}}^o\right) \left(\dot{\mathbf{Y}}^o\right)^T, \quad (48)$$

while $\mathbf{I}_N \in \mathbb{R}^{N \times N}$ is the identity matrix. In practical implementations it is common to also use the full-rank exact measurement error covariance matrix \mathbf{R} or the low-rank representation \mathbf{R}^e defined in Eq. (38) as alternatives to the product of measurement perturbations $\left(\dot{\mathbf{Y}}^o\right) \left(\dot{\mathbf{Y}}^o\right)^T$, although that comes with an additional computational cost unless one assume \mathbf{R} to be diagonal (see also Hoteit et al.⁹³).

The important result from Eq. (45) is that the EnKF update ensemble becomes a combination of the forecast ensemble members, and is searched for in the space spanned by the forecast ensemble. It is clear that the formulation in Eq. (45) is a stochastic scheme due to the use of randomly perturbed measurements. This allows for a natural interpretation of the EnKF as a Monte Carlo algorithm, while making it easy to understand and implement. An illustration is provided in Fig. 3, which shows the EnKF mean solution and estimated error standard deviation, as a function of the model grid and for three successive analysis times.

An efficient and stable numerical implementation of the analysis scheme is discussed in Evensen⁷, including the case in which \mathbf{C} is singular or of low rank, e.g., due to the number of measurements being larger than the number of realizations or if linearly dependent measurements are used.

In practice the ensemble size is critical since the computational cost scales linearly with the number of realizations. That is, each individual realization needs to be integrated forward

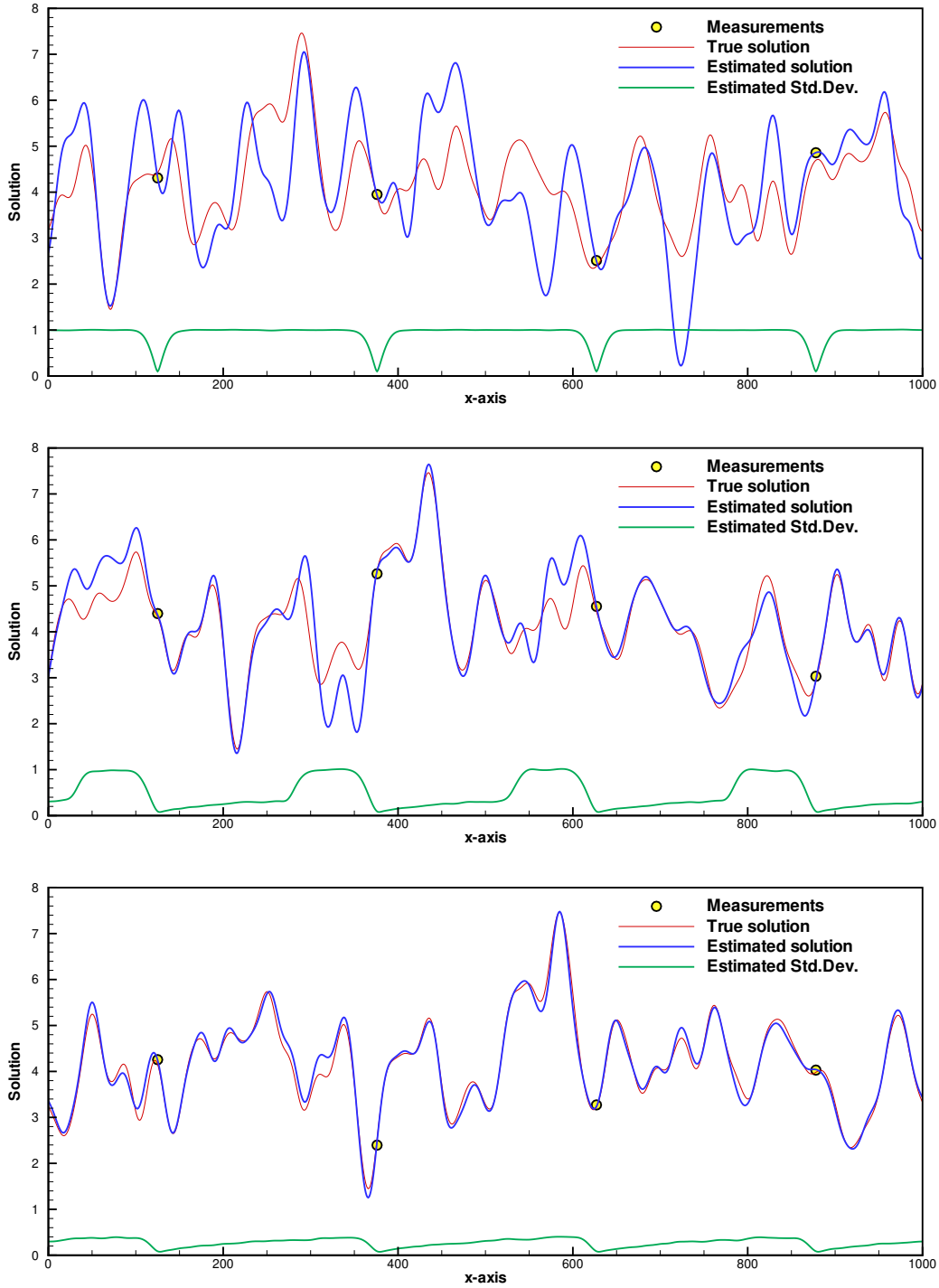


Figure 3: A linear advection equation on a periodic domain illustrates how the KF and/or EnKF estimates the state at three different times, namely, (top) $t = 5$, (middle) $t = 150$, and (bottom) $t = 300$. The plots show the reference solution, measurements, estimate, and standard deviation. The initial condition, observation and model error variance is 1.0, 0.01 and 0.0001 respectively, and the ensemble size is $N = 500$.

in time. The cost associated with the ensemble integration motivates the use of an ensemble with the minimum number of realizations that can provide acceptable accuracy. We will see in Sect. 5.1 how the optimal ensemble size to achieve satisfactory performance is also related to the dynamical properties, notably the degree of instabilities, of the model.

There are two major sources of sampling errors in the EnKF, namely (i) the use of a finite ensemble of model realizations and (ii) the introduction of stochastic measurement perturbations^{7,94}. In addition, stochastic model errors influence the predicted error statistics, which are approximated by the ensemble. The stochastic perturbation of measurements used in EnKF can be avoided using a square-root implementation of the analysis scheme, which is the topic of the next Section.

4.2 Deterministic square-root schemes

The perturbation of measurements used in the EnKF standard analysis Eq. (44) is an additional source of sampling error. However, methods such as the *square-root schemes* compute the analysis without perturbing the measurements and preserve exactly the posterior variance in the update. The square-root schemes such as the ETKF (Ensemble Transform Kalman Filter^{95,96}), the EAKF (Ensemble Adjustment Kalman Filter⁹⁷) or the MLEF (Maximum Likelihood Ensemble Filter⁹⁸) were originally introduced as alternatives to the traditional EnKF.

4.2.1 Updating the mean

In a square-root scheme, the analyzed ensemble mean is computed from the standard KF analysis equation,

$$\bar{\mathbf{x}}^a = \bar{\mathbf{x}} + \mathbf{X}\mathbf{Y}^T\mathbf{C}^{-1}(\bar{\mathbf{y}} - \mathbf{H}\bar{\mathbf{x}}), \quad (49)$$

with the matrix \mathbf{C} defined in Eq. (48) with \mathbf{R} in the place of $(\dot{\mathbf{Y}}^o) (\dot{\mathbf{Y}}^o)^T$, $\mathbf{C} = \mathbf{Y}\mathbf{Y}^T + \mathbf{R}$. The ensemble mean in the square-root formulation is thus computed without the use of perturbed observations.

4.2.2 Updating the ensemble perturbations

The deterministic algorithm used to update the ensemble perturbations is derived starting from the traditional analysis equation for the covariance update, Eq. (19) in the KF, in its ensemble-based representation, Eq. (41), which can be rewritten by making explicit the expression of the Kalman gain matrix

$$(\mathbf{P}^e)^a = \mathbf{P}^e - \mathbf{P}^e \mathbf{H}^T (\mathbf{H} \mathbf{P}^e \mathbf{H}^T + \mathbf{R})^{-1} \mathbf{H} \mathbf{P}^e. \quad (50)$$

Using the ensemble representation of the error covariance matrices, Eqs. (35) and (36), along with Eqs. (47) and (48), we can rewrite Eq. (50) as

$$(\mathbf{X}^a)(\mathbf{X}^a)^T = \mathbf{X}(\mathbf{I}_N - \mathbf{Y}^T \mathbf{C}^{-1} \mathbf{Y}) \mathbf{X}^T = \mathbf{X}(\mathbf{I}_N + \mathbf{Y}^T \mathbf{R}^{-1} \mathbf{Y})^{-1} \mathbf{X}^T, \quad (51)$$

where the second expression is derived by making use of the Sherman-Morrison-Woodbury formula (see Golub and Van Loan⁹⁹, their Sect. 2.1.4). Equation (51) is also known as *right transform* as it applies to the right-hand of the anomalies, in the N -dimensional ensemble space⁴. Similarly, *left transform* expressions exist, that applies on the m -dimensional state-space; see Asch et al.⁴, their Sect. 6.4, for an extensive treatment of the subject.

The square-root filters are based on deriving a factorization of Eq. (51). We note that the expression is symmetrical and the goal is to also use a symmetrical factorization. There are several methods that can be used. The simplest, but not very efficient, approach would be to compute the eigenvalue factorization of the matrix $\mathbf{I}_N - \mathbf{Y}^T \mathbf{C}^{-1} \mathbf{Y} = \mathbf{Z} \mathbf{\Lambda} \mathbf{Z}^T$, and the update

$$\mathbf{X}^a = \mathbf{X} \mathbf{Z} \sqrt{\mathbf{\Lambda}}, \quad (52)$$

would be a factorization that exactly satisfies Eq. (50). It is shown^{100–102} that symmetrical square root preserve the zero mean in the updated perturbations: the update in Eq. (52) needs to be replaced with

$$\mathbf{X}^a = \mathbf{X} \mathbf{Z} \sqrt{\mathbf{\Lambda}} \mathbf{Z}^T, \quad (53)$$

which is also a symmetrical factorization of Eq. (51) (see, e.g., Hunt et al.¹⁰³). The analysis update of the perturbations becomes a symmetric contraction of the forecast ensemble perturbations. Thus, if the predicted ensemble members have a non-Gaussian distribution,

then the updated distribution retains the shape but the variance is reduced (see the review in Raanes et al.¹⁰⁴, their Sect. 4). The importance of the symmetry in the square-root methods was first recognized by Hunt et al.¹⁰³. For the square-root schemes in operational use one has to focus more on numerical stability and efficiency. Here we assumed that \mathbf{C}^{-1} exists, which is generally not the case and particularly not so when the number of measurements is larger than the ensemble size and \mathbf{R} is not full rank (a situation that can however be fixed by eliminating some measurements). For a more elaborate derivation of numerically stable schemes we refer to the initial publications by Bishop et al.⁹⁵, Whitaker and Hamill⁹⁶, Anderson⁹⁷, later reviewed by Tippett et al.¹⁰⁵, while for a recent review on square-root methods see Nerger et al.¹⁰⁶.

A randomization of the analysis update can be used to generate updated perturbations that better resemble a Gaussian distribution, see Evensen⁹⁴. Thus, we write the symmetric square root solution Eq. (53) as

$$\mathbf{X}^a = \mathbf{XZ}\sqrt{\Lambda}\mathbf{Z}^T\Phi^T, \quad (54)$$

where Φ is a mean-preserving random orthogonal matrix, which can be computed using the algorithm from Pham¹⁰⁷ or Sakov and Oke¹⁰⁸. Note again that the random rotation in the square-root filter, contrary to the measurement perturbation used in EnKF, completely eliminates all previous non-Gaussian structures that may be contained in the forecast ensemble. Efficient ways to account for stochastic model noise within square-root EnKF are discussed in Raanes et al.¹⁰⁴.

4.3 Ensemble Kalman Smoother (EnKS)

The EnKS is a straightforward extension of the EnKF in which the output of the latter is used as a prior in the EnKS. Like the EnKF, it uses the ensemble covariances in space to spread the information from the measurements, the EnKS uses the ensemble covariances to spread the information in both space and time (also backward). We reintroduce here the time index for the sake of clarity.

Assume we have measurements available at discrete times t_k , $k = 1, \dots, K$. We then compute the EnKF solution recursively by assimilating the observations when they are available

and then propagate the ensemble till the next measurements (cf. Sec. 4.1). The members of the EnKF can be stored at any time instant when a smoother update is desired.

The analysis update at a time t_k (which does not have to be an observation time) from measurements available at a later time t_j , $1 \leq k < j \leq K$, reads

$$\mathbf{E}_k^a = \mathbf{E}_k + \mathbf{X}_k \mathbf{Y}_j^T \mathbf{C}_j^{-1} (\mathbf{Y}_j^o - \mathbf{Y}_j) \quad 1 \leq k < j \leq K, \quad (55)$$

where \mathbf{Y}_j from Eq. (47), and \mathbf{C}_j from Eq. (48) are evaluated using the ensemble and measurements at t_j . From the right-hand side of Eq. (55) we recognize the product $\mathbf{X}_k \mathbf{Y}_j^T$ as the covariance between the predicted measurements at t_j and the model state at $t_k > t_j$.

It is also seen that the update at the arbitrary time t_k , uses exactly the same combination of ensemble members as was defined by \mathbf{T}_k in Eq. (46) for the EnKF analysis at the time t_k . Thus, we can compactly write the EnKS analysis as

$$\mathbf{E}_k^{\text{a,EnKS}} = \mathbf{E}_k^{\text{a,EnKF}} \prod_{j=\hat{k}}^K \mathbf{T}_j, \quad (56)$$

where \hat{k} corresponds to the first data time t_j with $t_j > t_k$, and t_K is the last measurement time. It is then a simple exercise to compute the EnKS analysis as soon as the EnKF solution has been found. The computation requires only the storage of the coefficient matrices $\mathbf{T}_k \in \mathbb{R}^{N \times N}$, for $k = 1, \dots, K$, and the EnKF ensemble matrices for the times where we want to compute the EnKS analysis. Note that the EnKF ensemble matrices are large, but it is possible to store only specific variables at selected locations where the EnKS solution is needed. The equivalence between the formulation of the EnKS given above with the Rauch-Tung-Striebel smoother (cf. Sect. 3.1.2) even in the nonlinear, non-Gaussian, case is discussed in Raanes¹⁰⁹.

4.4 Making it work: Localization and Inflation

The salutary reduction of dimensionality obtained through the Monte Carlo treatment of the KF that yielded the EnKF comes at a price. Indeed, with a limited number, N , of anomalies, the sample covariance matrix is severely rank-deficient. It is doubtful that such sample error covariance matrix can be a good substitute for the possibly full-rank true one. Assume that

the true covariance matrix is \mathbf{B} . Further define \mathbf{P}^e as the sample covariance matrix meant to approximate \mathbf{B} and obtained from N samples, (as in Eq. (35)) of the normal distribution with covariance matrix \mathbf{B} . Then it can be shown that for two distinct entry indices i and j corresponding to distinct locations:

$$\mathbb{E}([\mathbf{P}^e - \mathbf{B}]_{ij}^2) = \frac{1}{N-1} ([\mathbf{B}]_{ij}^2 + [\mathbf{B}]_{ii}[\mathbf{B}]_{jj}), \quad (57)$$

with \mathbb{E} indicating the expectation operator. In most spatial geophysical systems, $[\mathbf{B}]_{ij}$ is expected to vanish exponentially with the distance between sites corresponding to i and j . Differently, the $[\mathbf{B}]_{ii}$ are the variances and remain finite, so that

$$\mathbb{E}([\mathbf{P}^e - \mathbf{B}]_{ij}^2) \underset{|i-j| \rightarrow \infty}{\sim} \frac{1}{N-1} [\mathbf{B}]_{ii}[\mathbf{B}]_{jj}. \quad (58)$$

Consequently, the right-hand-side arithmetically goes to 0 with the ensemble size N . Unfortunately, since $[\mathbf{B}]_{ij}$ is expected to vanish exponentially with the distance, we would have liked instead $\mathbb{E}([\mathbf{P}^e - \mathbf{B}]_{ij}^2)$ to also vanish exponentially with the distance. Hence, with N finite (and usually $N \ll m$) the sample covariance $[\mathbf{P}^e]_{ij}$ is potentially a bad approximation of the vanishing true covariance, especially for large distances $|i - j|$. This approximation generates spurious correlations in between distant parts of the system, as a manifestation of the rank-deficiency of the sample error covariance matrix.

The errors committed with such an approximation are usually referred to as *sampling errors*. When taking \mathbf{P}^e as the forecast/background error covariance matrix, the accumulation of such errors over the EnKF data assimilation cycles can be detrimental to the stability of the EnKF. Without counter-measures, the divergence of the EnKF in high-dimensional geophysical systems is almost systematic. Fortunately, more or less *ad hoc* fixes meant to address the issue are known: *localization* and *inflation*. They are rather complementary so that both of them are often required.

4.4.1 Localization

Localization fundamentally relies on the exponential decrease of the correlations with the distance in geophysical systems. Under this condition, one can assume that the interdependence of distant parts of a physical system is negligible. Hence, EnKF analyses could be made local^{110–114}. Localization comes in two flavors that we describe in the following.

Covariance localization The first approach, named *covariance localization* (CL), seeks to regularize the sample covariance matrix, with the goal to mitigate the rank-deficiency of \mathbf{P}^e and the appearance of spurious correlations. A mathematical means to achieve this objective is to compute the Schur (or Hadamard) product of \mathbf{P}^e with a well chosen smooth correlation function $\boldsymbol{\rho}$. We assume $\boldsymbol{\rho}$ to have exponentially vanishing correlations for distant parts of the system and to be representative of such dampening of real geophysical systems. The Schur product of $\boldsymbol{\rho}$ and \mathbf{B} is defined by

$$[\boldsymbol{\rho} \circ \mathbf{P}^e]_{ij} = [\boldsymbol{\rho}]_{ij} [\mathbf{P}^e]_{ij}, \quad (59)$$

i.e., a mere point-wise matrix multiplication. The Schur product theorem¹¹⁵ ensures that this product is positive semi-definite, and hence still represents a proper covariance matrix. For sufficiently regular $\boldsymbol{\rho}$, $\boldsymbol{\rho} \circ \mathbf{P}^e$ turns out to be full-rank (hence positive definite). Moreover, the spurious correlations should be exponentially dampened as is obvious from Eq. (59).

To illustrate the CL principle, we consider a multivariate one-dimensional ($m = 100$) Gaussian distribution, with mean, $\mathbf{x}^b = 0$. Its covariance matrix \mathbf{B} is given by $[\mathbf{B}]_{ij} = e^{-|i-j|/L}$, where $i, j = 1, \dots, m$ and $L = 10$ is the correlation length. An ensemble of $N = 20$ members $\{\mathbf{x}_{[n]}\}_{n=1, \dots, N}$ is drawn from this distribution from which we can compute the unbiased sample covariance matrix $\mathbf{P} = \frac{1}{N-1} \sum_{n=1}^N (\mathbf{x}_{[n]} - \bar{\mathbf{x}})(\mathbf{x}_{[n]} - \bar{\mathbf{x}})^T$, with the mean $\bar{\mathbf{x}} = \frac{1}{N} \sum_{n=1}^N \mathbf{x}_{[n]}$, which are approximations of \mathbf{B} and \mathbf{x}^b , respectively. The true and the sample covariance matrices are shown in Fig. 4. The spurious correlations are obvious in panel Fig. 4b. Let us define $\boldsymbol{\rho}$ through the Gaspari-Cohn (GC) function¹¹⁶,

$$G(r) = \begin{cases} \text{if } 0 \leq r < 1: & 1 - \frac{5}{3}r^2 + \frac{5}{8}r^3 + \frac{1}{2}r^4 - \frac{1}{4}r^5, \\ \text{if } 1 \leq r < 2: & 4 - 5r + \frac{5}{3}r^2 + \frac{5}{8}r^3 - \frac{1}{2}r^4 + \frac{1}{12}r^5 - \frac{2}{3r}, \\ \text{if } r \geq 2: & 0, \end{cases}$$

which is a fifth-order piecewise rational function. The cutoff function is defined by $r \in \mathbb{R}^+ \mapsto G(r/c)$ where c is a length scale which is called the localization radius. It mimics a Gaussian distribution but vanishes beyond $r \geq 2c$, which is numerically efficient (G is compactly supported). The Gaspari-Cohn cut-off function is shown in Fig. 4c. Hence, choosing $c = L$, we define $[\boldsymbol{\rho}]_{ij} = G(|i-j|/L)$. The regularized covariance matrix, $\boldsymbol{\rho} \circ \mathbf{P}^e$ is shown in Fig. 4d. As expected, the spurious correlations are tapered.

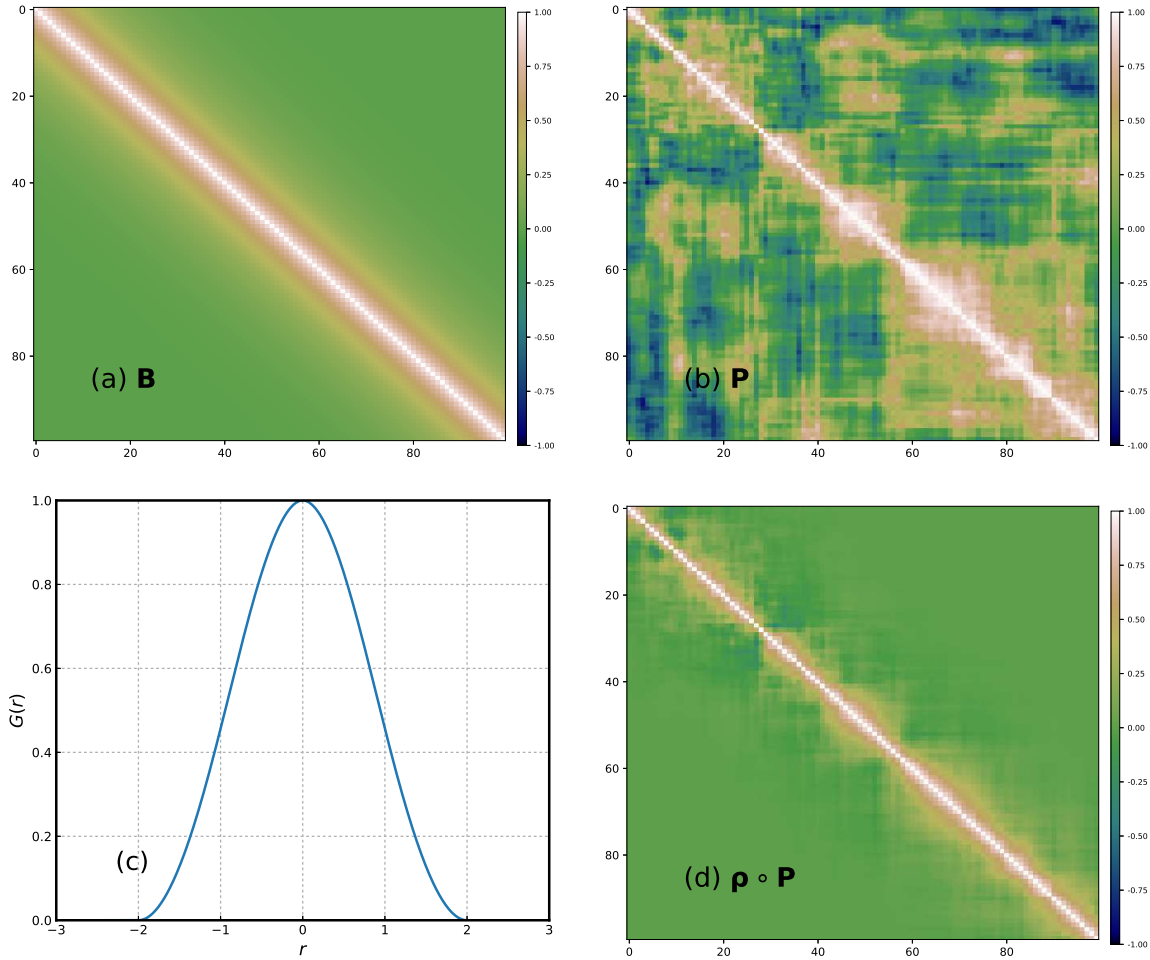


Figure 4: Panel a: True covariance matrix. Panel b: Sample covariance matrix. Panel c: Gaspari-Cohn correlation matrix used for covariance localization. Panel d: Regularized covariance matrix obtained from a Schur product.

One of the drawbacks of covariance localization is that it still leads to huge regularized covariance matrix (a priori in $\mathbb{R}^{m \times m}$). Ways out of this are (i) avoiding the explicit computation and storage of $\boldsymbol{\rho} \circ \mathbf{P}^e$, (ii) combining CL with domain localization (see below), (iii) or transferring the Schur product from state space to observation space for in situ observations. Solution (iii) can for instance be used to compute the Kalman gain (cf. Eq. (17)) in a more efficient manner¹¹⁰.

Domain localization An alternative to covariance localization is the so-called *domain localization* (DL). In DL, one performs the global EnKF analysis as a collection of independent local EnKF analyses, each of them assimilating a subset of the observations. Typically, one seeks to update a state at location/grid-cell x . The EnKF analysis is locally carried out by assimilating observations contained in a disk of radius L centered on x . The number of observations in this local domain should be small enough so that the ensemble can accommodate the information content of these observations, *i.e.*, that \mathbf{P}^e is locally full rank. This is equivalent to setting \mathbf{R} to \mathbf{R}_x where all the entries associated to sites outside the disk are large or infinite, which rules out these outer observations. In DL, both the state vector and anomalies are locally updated. A global analysis is then recovered from this collection of local analyses. Because the subdomains overlap, one hopes that the transition between analyses is smooth enough so that the global updated ensemble remains physically balanced. A way to improve on these transitions, is to obtain \mathbf{R}_x by tapering (Schur product) \mathbf{R}^{-1} with a regularizing cut-off function, typically the GC, that decreases with the distance from x .

Because the number of local EnKF analyses to be carried out scales linearly with the size of the system m , the method may seem numerically doomed. However, on the one hand, all of the analyses can be performed in parallel and, on the other hand, their numerical complexity is significantly reduced as it is driven by the ensemble size and the number of local, not global, observations. The numerical feasibility of the approach has been demonstrated by Hunt et al.¹⁰³.

Sakov and Bertino¹¹⁷ have shown that CL and DL are not mathematically equivalent in general but that they can become so in regimes where the analysis is dominated by the prior. Another important point to mention is the physical imbalance that may result from the gluing of local analyses and from the true long-distance correlations that have necessarily been discarded in the localization process^{118,119}. For chaotic systems, it has been suggested that the ensemble size below which localisation is mandatory is equal to the dimension of the unstable and neutral subspace of the dynamics (see also Sect. 5.1).

4.4.2 Inflation

Using localization addresses the rank-deficiency issue and gets rid of spurious correlations. Unfortunately, sampling errors are not entirely removed in the process. Residual errors are still often sufficient to make the EnKF diverge for long-term runs. Accounting for these residual sampling errors consists in recognizing that the errors are underestimated, which, by accumulation, may lead to the filter’s divergence. One very simple *ad hoc* means to amend this underestimation is to inflate the error covariance matrix by a multiplicative factor $\lambda^2 \geq 1$, $\mathbf{P}^e \rightarrow \lambda^2 \mathbf{P}^e$, which can also be implemented by inflating the anomalies $\mathbf{x}_{[n]} \rightarrow \bar{\mathbf{x}} + \lambda (\mathbf{x}_{[n]} - \bar{\mathbf{x}})$ ^{120,121}. Note that inflation is not only used to cure sampling errors^{122–124}, but is also often used to counteract model error impact.

Inflation can also come in an additive, clearly non-equivalent, form: $\mathbf{x}_{[n]} \rightarrow \mathbf{x}_{[n]} + \boldsymbol{\epsilon}_{[n]}$ with $\mathbb{E} \left[\boldsymbol{\epsilon}_{[n]} (\boldsymbol{\epsilon}_{[n]})^T \right] = \mathbf{Q}$.

As a drawback, inflation often needs to be tuned in order to obtain satisfactory performance of the EnKF, which is numerically costly. Hence, adaptive schemes have been developed to make the task more automatic^{122,124–133}. For instance, a variant of the deterministic EnKF, the DEnKF from Sakov and Oke¹⁰¹, was introduced as an approximation of the EnKF with an implicit inflation.

4.5 Ensemble Variational methods

4DVar and EnKF are now both used in operational meteorological centers as well as in academic studies (see, e.g., Bauer et al.¹³⁴). In spite of apparent similar performances in the context of synoptic scale meteorology, they are not equivalent. 4DVar allows for a nonlinear estimation of the maximum a posteriori of the underlying pdf using nonlinear optimization techniques, while the EnKF only performs a linear update (with the notable exception of the MLEF⁹⁸). The EnKF propagates the statistics of the errors, hence estimating the *errors of the day*, whereas the traditional 4DVar only relies on time-independent statistics of the errors. An important weakness of 4DVar, of technical nature, is the derivation of the adjoint models, which remains a computer sciences challenge, whereas the EnKF estimates the adjoint of the observation operator via the ensemble. These and other pros and cons of both approaches

have been discussed by Lorenc¹³⁵, Kalnay et al.¹³⁶, Yang et al.¹³⁷, Bocquet and Sakov¹³⁸.

Hence, it is tempting to combine both approaches, for theoretical reasons (nonlinear analysis, errors of the day) and technical reasons (no adjoint models). The resulting algorithms are called *ensemble variational* methods (EnVar). They have been reviewed in chapter 7 of Asch et al.⁴ on theoretical grounds and with a focus on operational implementation by Bannister¹³⁹, although the iterative ensemble Kalman smoother (see Sect. 4.5.4) is lacking in this latter review. A classification of these methods and the terminology has been proposed by Lorenc¹⁴⁰.

Here, we distinguish between (i) the hybrid methods, (ii) the methods based on an ensemble of variational data assimilation (EDA), (iii) the so-called 4DEnVar, and (iv) full nonlinear 4D EnVar methods, of which the IEnKS is a deterministic exemplar.

4.5.1 Hybrid methods

Hybrid can refer to the merging of a variational method and of an EnKF method. Yet, it quite often specifically refers to the hybridizing of a static error covariance matrix with a dynamical one sampled from an ensemble. The idea was first introduced by Hamill and Snyder¹⁴¹. The objective was to use the static covariance of a 3DVar and perform a variational analysis to be used for the analysis step of an EnKF. The effective covariance matrix used for the prior is:

$$\mathbf{B} = \alpha\mathbf{C} + (1 - \alpha)\mathbf{X}^f (\mathbf{X}^f)^T, \quad (60)$$

where \mathbf{C} is the static error covariance matrix (as used in 3DVar or optimal interpolation⁶), \mathbf{X}^f is the matrix of the forecast ensemble anomalies, and $\alpha \in [0, 1]$ is a scalar that weights the static and dynamical contributions. The updated ensemble can be obtained within the framework of a stochastic EnKF (cf. Sect. 4.1) using several stochastically perturbed variational problems. On the other hand, if the mean is estimated in a deterministic EnKF framework (cf. Sect. 4.2), the anomalies update has to rely on an approximation due to the necessary reduction of the rank from the hybrid covariance to the new dynamical covariances. There are ways to improve this update, such as using a left-transform update^{117,124}, or Lanczos vectors¹⁴². Note that, as with the EnKF, it may be necessary to enforce localization

of the sample covariances, which would be based on $\mathbf{B} = \alpha\mathbf{C} + (1 - \alpha)\boldsymbol{\rho} \circ [\mathbf{X}^f (\mathbf{X}^f)^T]$, using CL.

4.5.2 Ensemble of data assimilation

Methods known as *ensemble of data assimilations* (EDA) stem from meteorological prediction centers that operate a 4DVar, and in particular Météo-France and the European Centre for Medium-Range Weather Forecasts (ECMWF). The idea is to introduce dynamical errors that are absent in the traditional 4DVar. In order to build on the existing 4DVar systems, one considers an ensemble of N 4D-Var analyses. Each analysis, indexed by i , uses a different first guess \mathbf{x}_0^i , and observations perturbed with $\boldsymbol{\epsilon}_k^i \sim \mathcal{N}(\mathbf{0}, \mathbf{R}_k)$ to maintain statistical consistency. Hence, each analysis i carries out the minimization of (cf. Eq. (30))

$$\mathcal{J}_i^{\text{EDA}}(\mathbf{x}_0) = \frac{1}{2} \sum_{k=0}^K \|\mathbf{y}_k + \boldsymbol{\epsilon}_k^i - \mathcal{H}_k \circ \mathcal{M}_{k:0}(\mathbf{x}_0)\|_{\mathbf{R}_k}^2 + \frac{1}{2} \|\mathbf{x}_0 - \mathbf{x}_0^i\|_{\mathbf{B}^{-1}}^2. \quad (61)$$

The background covariance \mathbf{B} is typically a hybrid one as in Eq. (60) because it still uses the static covariances of the traditional 4DVar and incorporates the sampled covariances from the dynamical perturbations. The procedure yields an updated ensemble, from which it is possible to assess a dynamical part of the error covariance matrix. This is rather close to the idea of the hybrid EnKF-3DVar, but with a 4DVar scheme. The method has been implemented at Météo-France^{143–145} and at the ECMWF^{146,147}. Like for the hybrid method, it may be necessary to localize the sampled part of the hybrid covariances, using for instance CL. In this context, it may be convenient to enforce covariance localization via the so-called $\boldsymbol{\alpha}$ control variable trick^{135,148,149} or using wavelet truncations¹⁴⁵.

4.5.3 4DEnVar

NWP centers which have been using 4DVar were also the ones to offer the most reliable forecasts. But the future of 4DVar as an operational tool is uncertain because of its poor scalability and of the cost of the adjoint model maintenance, although weak-constraint 4DVar has scalable implementations¹⁵⁰. The so-called 4DEnVar, an example of 4D EnVar method, emerged in these centers as a way to circumvent the development of the evolution model

adjoint. The key idea is based on the ability of the EnKF to estimate the sensitivities of the observation to the state variables using the full observation model in place of the tangent linear one and of its adjoint in the computation of the Kalman gain. Liu et al.¹⁵¹ essentially proposed to generalize this idea to the computation of the sensitivities of the observations within a data assimilation window (DAW) to the variables of the initial state. This implies applying the EnKF trick based on the observation operator \mathcal{H} to the composition $\mathcal{H} \circ \mathcal{M}$ defined over the DAW. As a consequence, the sensitivities with respect to the anomalies degrees of freedom can be approximated with

$$\varepsilon^{-1} \mathcal{H}_k \circ \mathcal{M}_{k:0} \left(\bar{\mathbf{x}}_0 \mathbf{1}^T + \varepsilon \mathbf{X}^f \right) \left(\mathbf{I}_m - \frac{\mathbf{1}\mathbf{1}^T}{m} \right), \quad (62)$$

which generates an ensemble of centered perturbations across the DAW. With $0 < \varepsilon \ll 1$, these perturbations can be seen as generated by the tangent linear of $\mathcal{H}_k \circ \mathcal{M}_{k:0}$, whereas with $\varepsilon = \sqrt{m-1}$ these perturbations account for the nonlinearity of $\mathcal{H}_k \circ \mathcal{M}_{k:0}$ as in the EnKF. Since these sensitivities are the basis for the analysis, this idea appears to be quite close to that of the reduced-rank 4DVar put forward in oceanography by Robert et al.¹⁵².

In 4DEnVar, the perturbations are usually generated stochastically, for instance using a stochastic EnKF^{153,154}. Hence, in addition to avoiding the need for a model adjoint, flow-dependent error estimation is introduced. Given that 4DEnVar has been developed in NWP centers using 4DVar which relies on building a sophisticated static background error covariance matrix, the background is usually of hybrid nature. If the perturbations are part of a deterministic scheme, then the method could be seen as similar to the 4D-LETKF¹⁰³.

Because of the introduction of the limited set of perturbations, localization is again needed to mitigate the limited rank of the sample error covariance matrix. However, in a 4D ensemble context and differently from the synchronous EnKF, localization must be applied to covariances that are not only distant in space but also possibly in time within the DAW. Unfortunately localization and the dynamics do not commute in general^{155,156}, yielding inconsistencies in the implementation of a static localization within the flow. A solution is to implement a *covariant* localization that changes in time with the dynamical flow^{157,158}. For instance, if localization is enforced via LA, one would pull-back the influential observations within the DAW using a surrogate, hyperbolic-like, model for the full evolution

model and check in which local domains their antecedent would fall in¹⁵⁷. Note, however, that this issue is circumvented if one possesses the adjoint of the evolution model.

Many variants of the 4DEnVar are possible depending on the way the perturbations are generated, or if the adjoint model is available or not^{154,157,159–162}. Full 4DEnVar operational systems are now implemented or are in the course of being so^{72,73,163–167}.

4.5.4 The iterative ensemble Kalman smoother

Most of these EnVar methods, with the noticeable exception of the more firmly grounded EDA ones (Sect. 4.5.2), have been designed heuristically blending theoretical insights and operational constraints. This led to many variants of the schemes, even when this is not theoretically justified. In contrast, the iterative ensemble Kalman smoother (IEnKS), is a 4D EnVar method that is derived from Bayes’ rule and where all approximations are understood at a theoretical level. It comes from ensemble-based DA and, specifically, extends the iterative ensemble Kalman filter¹⁶⁸ to a full DAW as in 4DVar. The name *smoother* reminds us that the method smooths trajectories like 4DVar. However, it can equally be used for smoothing and filtering. The name also pays an homage to the iterative Kalman smoother of Bell¹⁶⁹ which corresponds to the non-ensemble precursor of the method. Basically, the IEnKS can be seen as an EnKF, for which each analysis corresponds to a nonlinear 4DVar analysis but within the reduced affine space defined by the ensemble. Hence, the associated cost function is of the form

$$\mathcal{J}(\mathbf{w}) = \frac{1}{2} \|\mathbf{w}\|^2 + \sum_{k=L-S+1}^L \frac{1}{2} \|\mathbf{y}_k - \mathcal{H}_k \circ \mathcal{M}_{k:0}(\bar{\mathbf{x}}_0 + \mathbf{X}_0 \mathbf{w})\|_{\mathbf{R}_k}^2, \quad (63)$$

where L is the length of the DAW, and S is the length of the forecast in between cycles (in units of $t_{k+1} - t_k$). Because the IEnKS catches the best of 4DVar (nonlinear analysis) and EnKF (flow-dependence of the error statistics), both parameters turn out to be critical.

The minimization of \mathcal{J} can be performed in the ensemble subspace using any nonlinear optimization method, such as Gauss-Newton (cf. Sect. 3.2.1), Levenberg-Marquardt or trust-region methods^{131,170,171}. The required sensitivities (derivative of the observation with respect to the initial state) are computed using an ensemble forecast within the DAW, as in 4DEnVar. Hence, it does not require the tangent and adjoint models but emulates them,

similarly to 4D-EnVar. The anomalies update is computed using an approximate Hessian of this cost function, using again these sensitivities. The ensemble forecast step is similar to the EnKF but over S time units.

The parameters L and S are constrained to satisfy $1 \leq S \leq L + 1$ if all observations are to be assimilated. In the case $S = L + 1$, with a single iteration of the minimization and further less important restrictions, the IEnKS identifies with the 4D-ETKF¹⁷². In the case $S = 1$ and $L = 0$, it coincides with the MLEF⁹⁸, which can be seen as a precursor to the IEnKF and IEnKS. The IEnKS represents an ideal tool to study deterministic 4D EnVar methods and test new strategies.

In chaotic systems, the IEnKS outperforms any reasonably scalable DA method in terms of accuracy. By construction, it outperforms the EnKF, the EnKS and 4DVar for smoothing but also filtering. This has been checked numerically on several low-order models (Lorenz models^{173–175}), 2D turbulence and quasi-geostrophic models^{156,157}. Figure 5 compares the performance of the IEnKS with that of optimally tuned 4DVar, EnKF and EnKS for filtering and smoothing on the 40-variable Lorenz-95 model¹⁷⁶. As for the other EnVar methods, localization needs to be used in high-dimensional systems. It can be implemented using covariant DL or CL¹⁵⁷.

To conclude this brief review of the EnVar set of techniques, the simplified table 1 summarizes some key properties of a selection of the methods we described.

5 Special topics

This section discusses four selected topics related to the application of DA to the geosciences. The issues for the DA and the countermeasures connected to the chaotic nature of the atmosphere and ocean are the content of Sect. 5.1. Section 5.2 discusses the techniques that allow to deal with non-Gaussian variables in the framework of DA methods originally devised to tackle with Gaussian quantities. The DA for chemical species is the subject of Sect. 5.3: the topic is of great relevance (pollutant dispersion, accidental nuclear release etc.) and has received much attention in recent years. Finally Sect. 5.4 describes one example of operational DA, the TOPAZ system for ocean prediction.

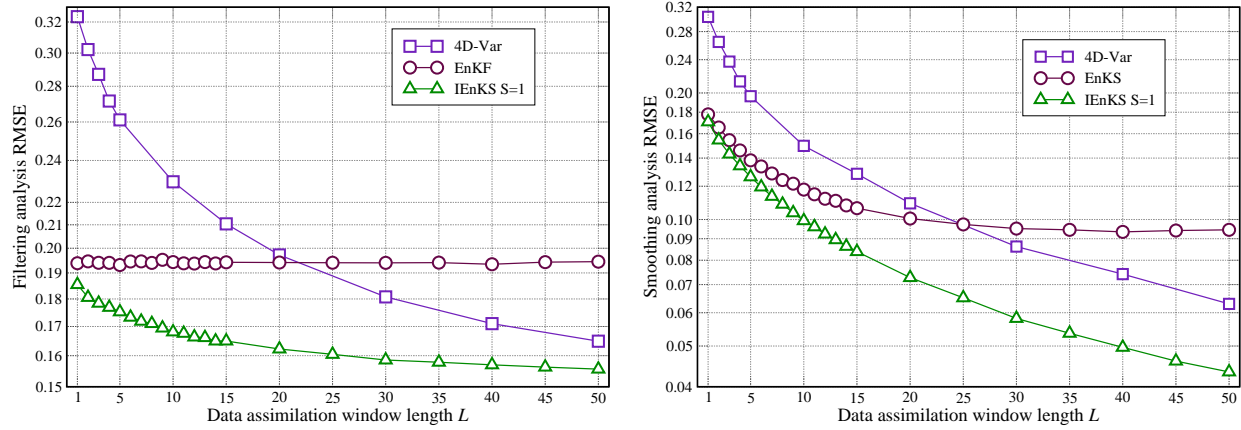


Figure 5: Average root mean square error of several DA methods computed from synthetic experiments with the Lorenz-95 model. The left panel shows the filtering analysis root mean square error of optimally tuned EnKF, 4DVar, IEnKS assimilation experiments, as a function of the length of the DAW. The right panel shows the smoothing analysis root mean square error of optimally tuned EnKS, 4DVar and IEnKS as a function of the length of their data assimilation window. The optimal RMSE is chosen within the window for 4DVar and it is taken at the beginning of the window for the IEnKS. The EnKF, EnKS and IEnKS use an ensemble of $N = 20$, which avoids the need for localization but requires inflation. The length of the DAW is $L \times \Delta t$, where $\Delta t = 0.05$.

Table 1: Comparison of EnVar data assimilation techniques. This table answers the following questions: (i) Is the analysis based on a linear or nonlinear scheme? (ii) Is the adjoint of the evolution model required? (iii) Is the adjoint of the observation operator required? (iv) Is the background flow-dependent? (v) Are the updated perturbations stochastic or deterministic? (vi) Are the updated perturbations fully consistent with the analysis, i.e., are they a faithful representation of the analysis uncertainty? (vii) Is localization of the ensemble analysis required? (viii) Is a static background used? To some extent, all algorithms can accommodate a static background; the answer tells whether the published algorithm has a static background. Blank answers correspond to irrelevant questions.

algorithm	<i>analysis type</i>	<i>evol. model adjoint required?</i>	<i>obs. operator adjoint required?</i>	<i>background flow-dependence?</i>	<i>sto. or det. perturbations?</i>	<i>consistent perturbations?</i>	<i>localization required?</i>	<i>static background</i>
EnKF	linear	no	yes	both	yes	yes	no ³	
3D-Var	nonlinear	yes	no				yes	
4D-Var	nonlinear	yes	yes	no			yes	
EDA with 4D-Var	nonlinear	yes ¹	yes ¹	yes	sto.	yes	part.	yes ³
4D-EnVar	linear	no	no	yes	sto.	no ²	yes	yes ³
IEnKS	nonlinear	no	no	yes	det.	yes	yes	no ⁴
MLEF	nonlinear	no	no	yes	det.	yes	yes	no ⁴
4D-ETKF	linear	no	no	yes	det.	yes	yes	no ⁴

¹ The adjoint models could be avoided considering an EDA of 4D-EnVar.

² It depends on the implementation of 4D-EnVar; the perturbations are often generated by a concomitant EnKF.

³ With an hybridization of the covariances.

⁴ But possible with an hybridization of the covariances.

5.1 Dealing with chaotic dynamics

Many natural systems, including atmosphere and ocean, are examples of chaotic dissipative dynamics¹⁸. Among the characteristic features of this class of system, the one having the largest impact on prediction, is the extreme sensitivity to initial conditions¹⁷³. Infinitesimal errors are bound to grow exponentially in the short time (and later saturate), and the rate and directions of such a growth are themselves highly state-dependent¹⁷⁷. Forecasters have been long aware of this flow-dependent behavior of the forecast uncertainty and "prediction of predictability" (i.e., the prediction of the uncertainty) has become an important issue in NWP^{176,178}. The difficulties inherent to the chaotic nature of the climate on the one hand, and the social pressure to deliver reliable forecast with associated prediction of the uncertainty, on the other, have motivated a huge bulk of research on predictability (see the review by Vannitsem⁷¹ and references therein). In forecasting practice, the problem of predicting uncertainty, thus moving from a "single-realization deterministic forecast" to a "multi-realizations probabilistic forecast", has been tackled by ensemble prediction schemes¹⁷⁹.

Dealing with such a flow-dependent error growth is obviously also a challenge for DA: one must in fact be able to properly track and incorporate this dependency in the DA description of the state estimation error. A situation that is further complicated by the large size of the geophysical models ($m = \mathcal{O}(10^9)$). Nevertheless, the dissipative character (due to friction) of the dynamics, induces an effective dimensional reduction, in the sense that the error dynamics is often confined to a subspace of much smaller dimension, $n_0 \ll m$. This subspace, referred to as the *unstable-neutral subspace*, is defined as the vector space generated by the backward Lyapunov vectors with non-negative Lyapunov exponents, i.e., the space of the small perturbations that are not growing exponentially under the action of the backward dynamics (see Legras and Vautard¹⁸⁰ for a topical review). The full phase-space can thus be seen as split in a (usually much smaller) unstable-neutral subspace and a stable one¹⁸¹. For instance, Carrassi et al.¹⁸² have shown how a quasi-geostrophic atmospheric model of $\mathcal{O}(10^5)$ degrees of freedom possesses an unstable-neutral subspace of dimension as small as $n_0 = 24$.

The existence of this underlying splitting of the phase-space has enormous impact on the skill of DA with chaotic models. In EnKF-like methods, Bocquet and Sakov¹⁵⁶, Carrassi et al.¹⁸³, Ng et al.¹⁸⁴ have studied the relation between the properties of the model dynamics and the performance of DA, and revealed how the knowledge about the former can be used in the design of the square-root EnKF and EnKS: for purely deterministic models, the minimum ensemble size required to achieve good performance must be at least as big as the number, n_0 , of non-negative Lyapunov exponents^{156,183}. Along similar lines, but for variational DA, Pires et al.⁵⁸ showed that the relative projection of the state estimation error on the stable and unstable subspaces depend on the length of the DAW (see Sect. 4.5.3): for long DAW the stable components are all dampened and the error is essentially confined on the unstable subspace.

These results have recently been corroborated by a proper mathematical understanding of the behavior of the KF and KS (cf. Sect. 3.1.1 and 3.1.2) for linear unstable systems in the absence of model noise. It has been proven analytically that the span of the error covariance matrices of the KF and KS tends asymptotically to the unstable-neutral subspace⁴⁶, independently from the initial condition³¹, and that the rate of such convergence is faster for the KS¹⁸⁵. Remarkably, Bocquet and Carrassi¹⁸⁵ have shown that, even in the case of a four-dimensional EnVar method (the IEnKS, cf. Sect. 4.5.4) applied to a noiseless nonlinear system, the full alignment of the ensemble anomaly subspace with the unstable-neutral subspace is accompanied by the maximum reduction of the state estimation error. Figure 6 illustrates this mechanism for the EnKF using the L95 model¹⁷⁴.

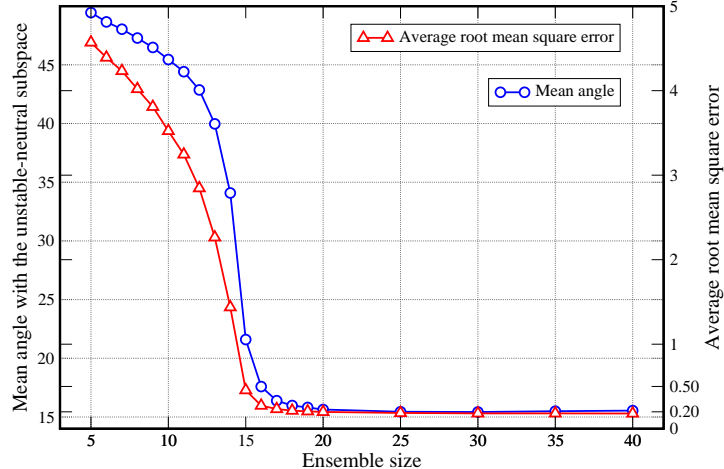


Figure 6: Time- and ensemble- averaged angle (in degree) between an anomaly from the EnKF ensemble and the unstable-neutral subspace as a function of the ensemble size N (left y-axis) and corresponding time-averaged root mean square error of the EnKF (right y-axis). The numerical experiments are performed on the L95 model with $m = 40$ variables¹⁷⁴ and the DA setup is $\mathbf{H} = \mathbf{I}_d$, $\mathbf{R} = \mathbf{I}_d$, observational frequency $\Delta t = 0.05$ and error variance $\sigma = 1$.

These results indicate that, in deterministic chaotic systems, the unstable-neutral subspace fully describes (in an average, asymptotic, sense) the uncertainty in the state estimate. This fact is at the basis of a class of DA algorithms known as *assimilation in the unstable subspace* (AUS) pioneered by Anna Trevisan and collaborators^{186,187}, in which the unstable-neutral subspace (or a suitable numerical approximation of it) is explicitly used in the DA scheme to parametrize the description (both temporally and spatially) of the uncertainty in the state estimate. Given that usually $n_0 \ll m$, AUS represents an interesting alternative to operate DA efficiently on high-dimensional system (large m) by monitoring only n_0 unstable-neutral directions. Applications to large atmospheric¹⁸⁸ and oceanic models¹⁸⁹ have confirmed its capabilities. The AUS paradigm has been successfully incorporated in both the EKF⁴⁷ and the 4DVar¹⁹⁰ and its extension to cope with the deviations from the linear assumption of the error dynamics on which it relies, has been studied recently¹⁹¹.

5.2 Dealing with non Gaussian variables

There are cases for which the linear analysis is sub-optimal. These arise when either the state variables, observations or model parameters are not Gaussian distributed. We consider first the case in which the distribution of at least one variable is not Gaussian, for example it exhibits a clear skewness or kurtosis, but the pdf remains continuous.

Ignoring the non-Gaussian nature of a variable will normally make the least-squares estimator sub-optimal (cf. Sect. 3.1.3): either by systematic biases, by under-estimating the correlation length scales¹⁹², or more visibly by returning nonphysical values (for example negative concentrations of tracer variables). In a DA framework, the state variables (called the "control variable" in this context) need not be exactly defined as in the forward model: nonlinear transformations are allowed and will change the outcomes of the minimization problem¹⁹³.

Transformations of the variables have been practiced extensively in the geostatistical literature under the term *Gaussian anamorphosis* (also known as "normal-score transform"): a nonlinear function is applied to the cumulative pdf in order to make it Gaussian¹⁹⁴. In DA, the Gaussian anamorphosis function can either be applied to the state variables $\tilde{\mathbf{x}} = \phi(\mathbf{x})$ or to the observations $\tilde{\mathbf{y}} = \varphi(\mathbf{y})$ or the model parameters or to all of them at the same time. The prerequisite is that the transformed variables $\tilde{\mathbf{x}}$ and $\tilde{\mathbf{y}}$ should be "more Gaussian" and better suited to a linear analysis update than the original ones. The anamorphosis function must be strictly increasing so that backward transformations from the Gaussian values to the "natural" pdf can be given by ϕ^{-1} and φ^{-1} . Since $\mathbf{E}(\phi^{-1}(\tilde{\mathbf{x}})) \neq \phi^{-1}(\mathbf{E}(\tilde{\mathbf{x}}))$, Monte Carlo techniques are often employed to obtain unbiased statistics. This makes the anamorphosis particularly convenient to apply in conjunction with ensemble techniques¹⁹³.

In practice, the stochastic models (13) and (14) are valid for the transformed $\tilde{\mathbf{x}}$ and $\tilde{\mathbf{y}}$, so that the EnKF and EnKS equations can be re-used with $\tilde{\mathbf{x}}$ and $\tilde{\mathbf{y}}$ in replacement of \mathbf{x} and \mathbf{y} . Equations (33) and (42) become

$$\mathbf{E}^{f/a} = (\tilde{\mathbf{x}}_{[1]}^{f/a}, \tilde{\mathbf{x}}_{[2]}^{f/a}, \dots, \tilde{\mathbf{x}}_{[N]}^{f/a}) \in \mathbb{R}^{m \times N}, \quad (64)$$

$$\mathbf{Y}^o = (\tilde{\mathbf{y}}_{[1]}, \tilde{\mathbf{y}}_{[2]}, \dots, \tilde{\mathbf{y}}_{[N]}) \in \mathbb{R}^{d \times N}. \quad (65)$$

The observations are preferably transformed before perturbing the observations, since

the perturbations are more conveniently applied in the Gaussian space (even when using a deterministic version of the EnKF, the \mathbf{R} matrix characterizes more adequately Gaussian observation errors). After the analysis, the inverse transformation ϕ^{-1} is applied to each member of the analyzed ensemble $\mathbf{x}_i^a = \phi^{-1}(\tilde{\mathbf{x}}_i^a)$ before the next propagation step. If one variable is both an observation and a model state variable, then the same transformation should be applied to both so that the observation operator \mathbf{H} keeps a simple form¹⁹⁵.

There are an infinity of strictly increasing functions: choosing a good anamorphosis function is therefore an open question. When a set of observations is available or a free model run, it is possible to approximate the anamorphosis function based on the histogram of available data, using for example a piecewise linear fit¹⁹⁶. Adaptive types of anamorphosis functions have also then been explored¹⁹⁷, in which the anamorphosis function is fitted to the values present in the ensemble forecast at the assimilation time. These have proven advantageous in twin experiments^{197,198}, but their stability remains to be tested in real cases, where the true density is unknown and the results can become excessively sensitive to the choice of the tails of the distribution¹⁹⁷. In practical cases, simple analytical functions are sometimes preferred like the exponential, gamma or logit functions, which can be supported theoretically knowing the nature of the problem at hand^{199,200}.

One immediate benefit of the Gaussian anamorphosis is the ability to impose positivity constraints in the EnKF which is useful for example in ecosystem models¹⁹⁶. The use of an anamorphosis function has been demonstrated with the EnKF in hydrological models^{198,201}, in joint parameter-state estimation in ocean ecosystem models^{197,200,202}, for the evaluation of covariance length scales in various ocean modeling applications¹⁹² and with moderate success in a coupled ice-ocean model²⁰³. It has been as well introduced in a snow model with an ensemble smoother²⁰⁴.

One limitation of the Gaussian anamorphosis as described above is that it does not consider the multi-Gaussian case: only the marginal distributions of the variables are transformed independently from each other. Although this does not guarantee that the joint distributions become multi-Gaussian, the experience still shows that the multi-Gaussian properties are generally improved after transforming the marginals^{195,205}. The anamorphosis framework can however be further extended by the use of copulas²⁰⁶.

A more serious limitation in many practical cases is that the Gaussian anamorphosis does not lend itself to discontinuous pdf. These are better addressed in the framework of truncated Gaussians: a threshold is defined on the Gaussian distribution, and all values exceeding the threshold are reset to its precise value, generating an atom of probability distribution. Truncated Gaussians were first applied in optimal interpolation, by introducing a Lagrange parameter in the minimization²⁰⁷, only in the cases when assimilated values exceeded the threshold, leading to a two-step interpolation process (detect and constrain). The issue of sampling a multivariate truncated Gaussian in the framework of an EnKF was then explored applying a Gibbs sampler²⁰⁸, under the simplifying assumption of small truncations. Another approach is the use of Quadratic Programming²⁰⁹, more general in the sense that it can accommodate nonlinear constraints. An alternative and inexpensive approach is to "moderate" the strength of DA in order to avoid reaching the discontinuities of the distribution. This has been proposed for assimilation into an ocean model in isopycnic coordinates, for which the values of layer thickness must be positive²¹⁰.

The above examples are extending the Gaussian framework introduced in Sect. 3.1 and extend as well the use of the EnKF and EnKS methods. The Gaussian anamorphosis can be included at almost no additional costs, but the costs of the truncated Gaussian methods are potentially a limitation in realistic cases (a 500% increase of the analysis step is reported with the Gibbs sampler²⁰⁸). Still, these methods benefit from the advantages of the Gaussian framework in high dimensions and represent attractive alternatives to more general Bayesian methods that suffer from the curse of dimensionality (see Sect. 6.1).

5.3 Data assimilation for chemicals

There is a huge literature on the use of DA for chemical constituents of the atmosphere. There are several quasi exhaustive reviews about the advances in this field, such as Carmichael et al.²¹¹, Zhang et al.²¹², Bocquet et al.²¹³. We here briefly explain what chemical DA is, what the motivations for using DA in this field are, and, finally, which methods are used.

The specific set of chemical reactions that prevails in the atmosphere depends on the species but also on the considered spatial and temporal scales. For instance, one typically distinguishes between global atmospheric chemistry and air quality. The former is concerned

with species transported and reacting over long distances and within the whole column of the atmosphere, whereas the latter is more concerned with the complex chemistry within the boundary layer (about 1 km from the ground) at regional scales. As an example of species, greenhouse gases are global pollutants with long life spans considered in the first type of study, even though regional studies of their transport are also of interest. Another example is ozone, which, in the lower troposphere, is studied and forecast in air quality as a harmful pollutant whereas, in the stratospheric layer, or when transported in between continents, is the focus of global studies. Besides the global and regional scales, DA is also nowadays used for chemical studies at urban scale.

Chemistry and transport models are fundamentally multivariate with many species to be accounted for (about a hundred for gaseous species, hundreds when considering aerosols). This also significantly increases the dimensionality of the models compared to atmospheric and ocean models independently. That is why the choice of the control variables (cf. Sect. 3.2) is critical in the feasibility of chemical DA.

One also distinguishes between online and offline models. Offline models (also called CTM for *chemical transport model*) only consider emissions and uptakes, chemistry, loss processes and transport driven by meteorological fields that are supposed to be provided. Online models (also called CCMM for *coupled chemistry meteorology model*) couple meteorology with chemistry and transport. CCMMs are therefore much more costly but allow for two-way coupling between meteorology and chemistry. Most of chemical DA studies are performed offline.

One major difference with atmospheric and ocean models is that the dynamics of CTMs are mostly stable. In practice two model trajectories with distinct initial conditions will coalesce, quite differently from chaotic geofluid dynamics⁷¹. Hence, the initial conditions are rarely the most important control variables in chemical DA. Quite often, the species emissions are the most influential input parameters, if not control variables. More generally, model error is more influential for chemical DA than for geofluids DA. One consequence of this dynamical stability is that air quality forecast are rarely useful beyond 48 hours, even with the help of DA. Another consequence is the importance of all other parameters and input of these models and their uncertainty and hence of error model.

For these many reasons, but also to serve the enforcement of regulations, chemical DA is used for (i) chemical forecast, nowcasting and possibly reanalysis, (ii) inverse modeling of species emission and uptake, and (iii) parameter estimation, such as the boundary conditions, constants of the physical and chemical parametrizations.

The methods used in chemical DA are largely inspired by meteorological DA. Optimal interpolation⁶ has been largely used from the very beginning. Since the beginning of the 2000s, 4DVar has also been used, which can advantageously be adopted for the simultaneous estimation of inputs and model parameters²¹⁴. Methodological advances in chemical DA also had some influence, with the early development of reduced Kalman and ensemble methods in the 90s²¹⁵⁻²¹⁸. Four-dimensional ensemble variational methods have also been tested in this field^{219,220}.

5.4 An example of operational data assimilation and reanalysis: the TOPAZ integrated ice-ocean system

The concept of operational oceanography has gradually arisen in the 1990's under the joint pressure from its users in the navy, the authorities in charge of emergency response (oil spills, search and rescue operations) and the offshore oil and gas industry. Ocean monitoring was becoming possible from remote sensing and increasing in-situ observations to fulfill the needs of both the operational and the climate research communities and the development of ocean models was accelerated. The conditions for ocean DA were then ripe and a community was formed around the international Global Ocean Data Assimilation Experiment (GODAE, now GODAE-OceanView, www.godae-oceanview.org). The EnKF, originally introduced in a QG model, was then extended to a multi-layer isopycnal model (Miami Isopycnal Coordinate Model, MICOM) and then its offspring in generalized vertical coordinates HYCOM (HYbrid Coordinate Ocean model²²¹). The EnKF⁷, SEEK filter²²² as well as the EnKS⁷ were applied successfully to this model to assimilate ocean remote sensing observations from satellite altimeters and sea surface temperatures in a North Atlantic configuration called DIADEM²²³. In parallel, the assimilation of sea ice concentrations in a coupled ice-ocean model was demonstrated²²⁴ as well as the assimilation of remotely sensed ocean color in a coupled

physical-ecosystem model²²⁵, both with the EnKF. These experiments were all using similar settings of the EnKF: same number of members, same sources and statistics of model errors and were therefore encouraging signs that a single integrated system could monitor the ocean, the sea ice and the ocean ecosystem consistently, with the uncertainties of the three components represented by the same ensemble. Such an integrated system for the North Atlantic and the Arctic Oceans was then built and named TOPAZ, including downscaling capabilities to forecast the coastal zones at higher resolution. An illustration showing a typical output from the TOPAZ system is given in Figure 7.

The TOPAZ system has been set in near real-time forecasting mode in January 2003, initially using the perturbed-observations EnKF⁹² (cf. Sect. 4.1), and then moved on to the DEnKF¹⁰¹ (cf. Sect. 4.4.2) in January 2010.

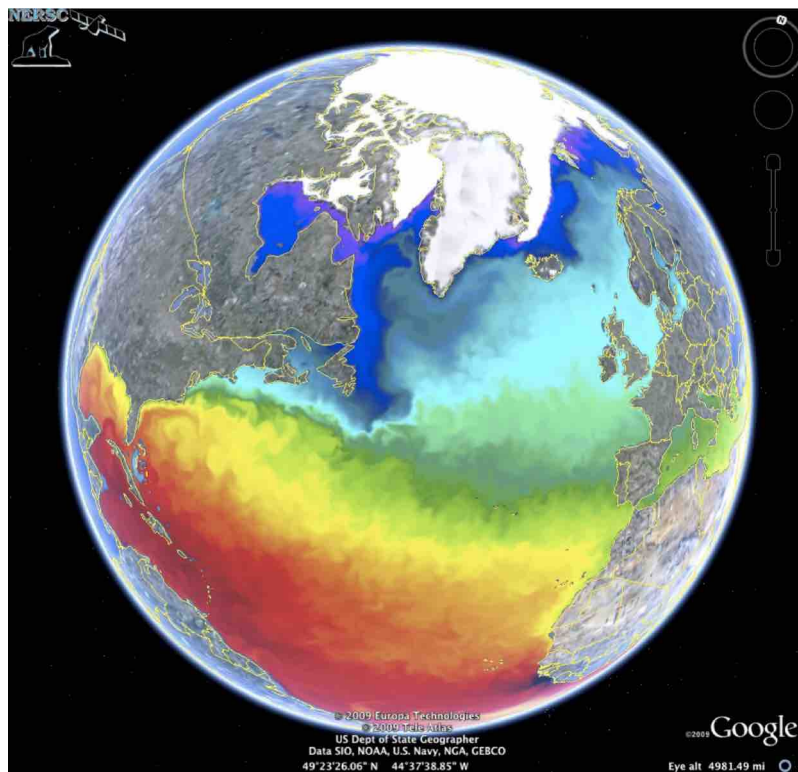


Figure 7: Example of sea surface temperature (in color) and sea ice concentration (in white) real-time analysis by the TOPAZ system on the 28th November 2009.

The HYCOM ocean model uses isopycnic coordinates in the deep stratified ocean, the

following state vector is then the closest possible to the original model prognostic variables¹:

- 3-dimensional variables, defined for each hybrid vertical layer: layer thickness, u- and v-components of the current velocity, temperature and salinity
- 2-dimensional variables: barotropic pressure, u- and v-components of the barotropic velocity, sea ice characteristics (ice concentration, ice thickness, snow depth).
- Static parameters, 2-dimensional bias fields for mean SLA and mean SST.
- If the ecosystem module is coupled:
 - 3-dimensional nutrients concentrations (nitrate, phosphate and silicates in North Atlantic and Arctic regions)
 - 3-dimensional phytoplankton (diatoms and flagellates) and zooplankton species (meso- and microzooplankton).
 - 3-dimensional detritus variable, as well as oxygen and biogenic silicate.
 - 2-dimensional maps of model parameters (different plankton loss rates).

Recalling that the EnKF analysis is conserving linear equilibrium, the above definition of the state vector in generalized (isopycnic) vertical coordinates is advantageous for preserving the geostrophic balance, which relates linearly the velocity vector averaged over one ocean layer to the gradient of the layer thickness⁹². The use of isopycnic coordinates in the state vector has also the advantage of reducing diapycnal mixing during the linear update in Eq. (45) or (54) since the analyzed temperature and salinity tracers are the results of combinations of forecast temperature and salinity from different members but at the same density. The application of the EnKF in the MICOM isopycnic model has also proven to make the assimilation of surface temperature properties more efficient in the context of a climate reanalysis²²⁶.

On the downside, not all the above state variables are Gaussian distributed, so according to the discussion in Sect. 5.2, biological variables are log-transformed¹⁹⁹. However variables

¹A prognostic variable is necessary for carrying out the model calculations.

with discontinuous distributions (sea ice variables, ocean layer thickness) are simply post-processed⁸⁸, and TOPAZ is thus exposed to assimilation biases. Yet, the experience has not revealed strong biases.

TOPAZ has used a local analysis (cf. Sect. 6.1.5) ever since its inception, a global analysis having proven utterly incapable of controlling millions of state variables with only 100 members. The inflation is implicit in the formulation of the DEnKF¹⁰¹ and additionally in the form of a factor applied to the \mathbf{R} matrix, used only in the update of the anomalies⁸⁸. The use of a constant multiplicative inflation (cf. Sect. 4.4.2) of the forecast anomalies has proven problematic in the case of the Arctic due to the inhomogeneous observation coverage, even with a small inflation of 1%.

The present TOPAZ4 physical system with its horizontal resolution of about 12 km and 28 hybrid vertical layers counts about 80 million unknowns. The data assimilated in a weekly cycle count the along-track sea level anomalies from satellite altimeters, the interpolated sea surface temperatures and sea ice concentrations from satellites as well, the Lagrangian sea ice drift from continuous maximum cross-correlation of scatterometer data, and the temperature and salinity profiles from various in-situ platforms, including the Argo autonomous buoys and Ice-Tethered Profilers. This amounts to about 400 thousands observations after super-obing. The altimeter and the sea ice drift data are assimilated asynchronously²²⁷, accounting for time-delayed covariances.

The computer costs of the TOPAZ4 system are mainly related to the propagation of the 100 members (1200 CPU hours per week, but embarrassingly parallel as the 100 members are submitted independently and the HYCOM model is itself parallel, running on 144 CPUs), the analysis step takes 20 hours only, and is also parallelized because all local analysis updates are independent from each other.

The TOPAZ4 reanalysis²²⁸ has been conducted over 24 years (covering the altimeter era 1991-2015) and thus 1250 assimilation steps. During this time, the Arctic observing system has undergone large changes with for example the International Polar Year (IPY, 2007-2009) during which several Ice-Tethered Profilers have been deployed in the Central Arctic, measuring temperature and salinity profiles in areas previously unobserved. The large increase of observations during the IPY is visible in the time series of Fig. 8 and

does, as expected, reduce the bias and root mean square error, but the latter increases again during the 6 months that follow the end of the IPY. This implies that the special observation efforts done on the occasion of the IPY should be the rule rather than the exception for the sake of monitoring the Arctic Ocean. The diagnostics shown for other variables indicate that the reanalysis is stable all through the 1250 assimilation cycles²²⁸ and how much each observation type contributes to the minimization.

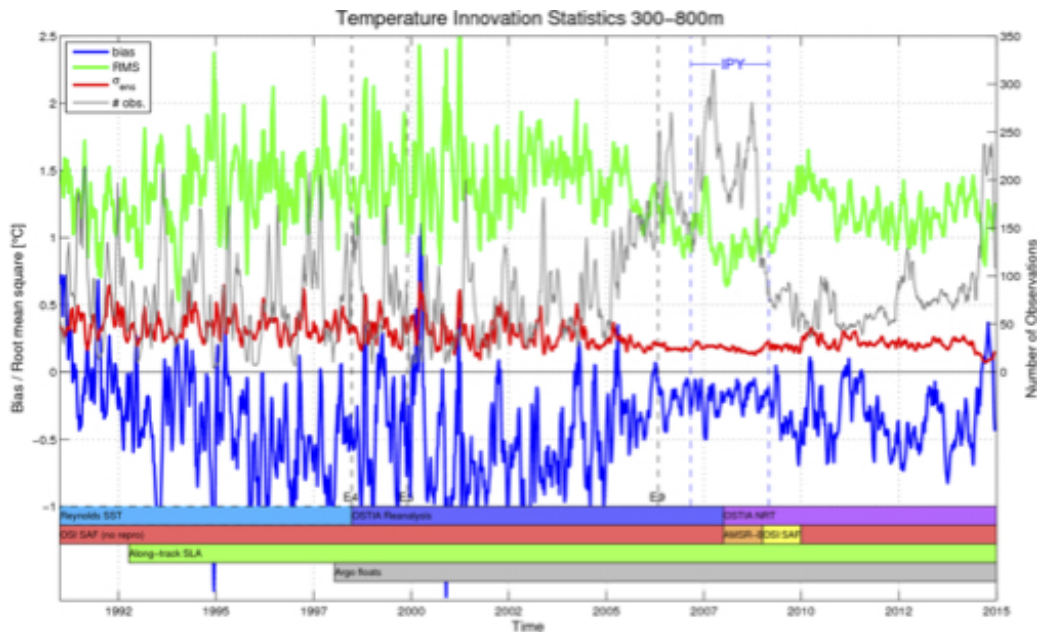


Figure 8: Time series of data assimilation diagnostics across the 24-years reanalysis for all temperature profiles in the depths 300 m to 800 m in the whole Arctic. The blue line is the average of all innovations, the yellow line is the related standard deviation (Root Mean Square Error), the red line is the ensemble spread of \mathbf{S} and the grey line is the number of observations. Vertical dashed lines indicate changes applied to the assimilation system during the reanalysis. The bars in the bottom indicate the succession of input data products assimilated, from top to bottom: SST, sea ice concentrations, SLA and Argo data.

The coupled physical-biological reanalysis with assimilation of surface chlorophyll estimates from remotely-sensed ocean color data is a much more difficult endeavor than the physical reanalysis, both on technical and scientific levels¹⁹⁹.

6 Where we are and where we go: a look at the perspectives

Data assimilation is nowadays a key ingredient of the atmospheric and oceanic prediction machinery and substantial computational power and economical resources are allocated to its maintenance and updates. What are the challenges DA is facing at this present time? Which solutions are being proposed to cope with the requirements of present days climate research? Figure 9 illustrates this quest by displaying the required DA approach as a function of the model resolution (x-axis) and of the prediction horizon (y-axis).

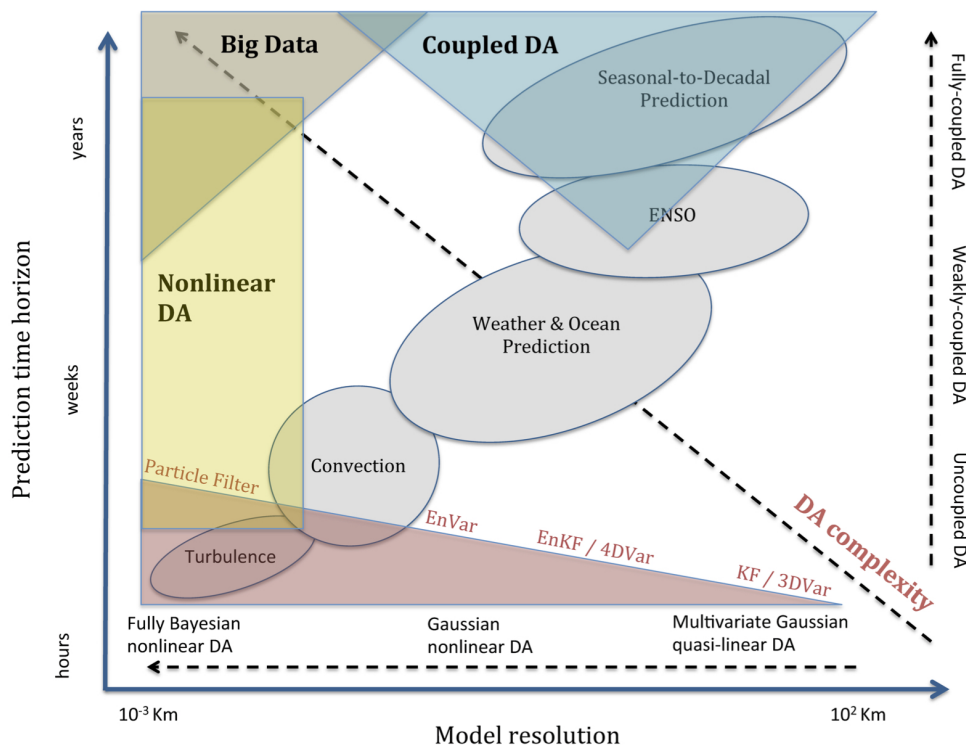


Figure 9: Required DA method versus model resolution and prediction time horizon; examples of corresponding natural phenomena are also shown for illustrative purposes. The degree of sophistication of the DA grows commensurately with the increase in prediction time horizon and the decrease of the model grid size.

The constant increase of the numerical model resolution, i.e., reducing the model grid size, implies resolving more and more small scales processes (e.g., convection or turbulence)

that are often inherently nonlinear and non-Gaussian. The transition toward high-resolution models must thus be accompanied by corresponding DA developments where the Gaussian and linear assumptions are relaxed. This identifies one of the current time more challenging and active line of research in DA: fully Bayesian methods. The horizontal dashed line in Fig. 9 illustrates the DA method required features as a function of the model grid size; particle filters, the subject of Sect. 6.1, are fully Bayesian and nonlinear methods and are placed at the top of the algorithms hierarchy in Fig. 9.

Together with the increase in model resolution, the current era is also characterized by a growing interest in long-term forecasts. Indeed, beyond the meteorological time horizon of two weeks, predictions over seasonal-to-decadal (s2d) time scales potentially bear higher societal relevance: they can guide adaptation to near-term climate change and related risks²²⁹. Such long-term predictability arises from the interactions between the atmosphere and the more slowly varying components of the climate system, like the ocean, land surface and cryosphere, so that predictions are issued using fully coupled models (Earth System Models, ESMs). The fruitful use of DA with coupled models necessitates the development of adequate coupled DA (CDA) methods that allow for a consistent and balanced propagation of the informational content of the observations across all model components (see vertical dashed line in Fig. 9). As will be discussed in Sect. 6.2, this is not straightforward with standard DA methods and substantial efforts are currently being undergone to develop CDA strategies.

In addition to the increase in numerical model resolution and of the prediction time horizon, we are also experiencing a dramatic growth and refinement of the observations suppliers. The Earth is now observed over a wide range of spatial and temporal scales, thanks to an increasingly wider variety of sustained observing systems, which includes satellites, but also new, not stationary, ocean measurements such as floats, drifters and more recently gliders (see, e.g., Kuznetsov et al.²³⁰). The assimilation of data derived from instruments that are not stationary has come to be known as *Lagrangian DA*. These methods have gained popularity as they offer a suitable way to incorporate consistently modern observation suppliers of the ocean, and have experienced a flourishing stream of improvements in the last decade, driven by addressing two main challenges: the use of indirect measurements

of the state variables (see, e.g., Salman et al.²³¹) and the inherent nonlinear character of the underlying dynamics²³². More recently, the Lagrangian dimension of the DA problem has also involved the model component, and not just the data, with the appearance of numerical models discretised on a spatio temporal varying mesh (see, e.g., Rampal et al.²³³ for an example of Lagrangian sea-ice model). This feature represents another methodological challenge for DA that is not longer demanded to update the value of the physical variables on the grid points, but also their positions (see, e.g., Bonan et al.²³⁴).

6.1 Bayesian data assimilation: particle filters

From the Bayesian standpoint, the state estimation problem is best formulated as Eq. (3). We have seen in Sect. 2.2 how to exploit and formulate the sequential estimation problem through the conjunction of Bayes' rule and the Chapman-Kolmogorov equations.

Yet, these formula were claimed to be impractical, at least for high-dimensional models, and we moved on to solutions based on Gaussian approximations. The algebra involved with these approximations is numerically demanding with inversions of covariance matrices in the analysis step, which contrasts with the apparent simplicity of Eq. (3).

A more brutal and direct approach to the DA problem would be to use Monte Carlo methods and draw N samples from Eq. (3). The hope is that in the asymptotic limit, i.e., $N \rightarrow \infty$, one would properly estimate the conditional density $p(\mathbf{x}|\mathbf{y})$. In a sequential context, this approach is called the particle filter (PF), or sequential Monte Carlo.

6.1.1 Bootstrap particle filter and resampling

As a first step, let us see how to solve the filtering problem sequentially with the PF. The forecast pdf $p_{k|k-1}$ from t_{k-1} to t_k is assumed – and this is the main approximation at finite N – to be of the form

$$p_{k|k-1}(\mathbf{x}_k|\mathbf{y}_{k-1}) = \sum_{n=1}^N \omega_{k-1}^n \delta(\mathbf{x}_k - \mathbf{x}_k^n), \quad (66)$$

which is an empirical distribution with delta-Dirac masses. The $\{\mathbf{x}_k^n\}_{n=1,\dots,N}$ are the particles (i.e., the ensemble members or the samples) and the $\{\omega_k^n\}_{n=1,\dots,N}$ are positive weights attached to the particles; \mathbf{x}_k^n is a shortcut for the particle $\mathbf{x}_{[n]}$, as denoted in Sect. 4, at time

t_k . Since $p_{k|k-1}$ is a pdf, the weights need to be normalized to one, $\sum_{n=1}^N \omega_{k-1}^n = 1$.

The analysis at t_k consists in the assimilation of \mathbf{y}_k using Bayes' rule:

$$\begin{aligned} p_{k|k}(\mathbf{x}_k|\mathbf{y}_{k:}) &= \frac{p_k(\mathbf{y}_k|\mathbf{x}_k)}{p(\mathbf{y}_{k:})} p_{k|k-1}(\mathbf{x}_k|\mathbf{y}_{k-1:}) \\ &= \sum_{n=1}^N \omega_{k-1}^n \frac{p_k(\mathbf{y}_k|\mathbf{x}_k)}{p(\mathbf{y}_{k:})} \delta(\mathbf{x}_k - \mathbf{x}_k^n) \\ &\propto \sum_{n=1}^N \omega_{k-1}^n p_k(\mathbf{y}_k|\mathbf{x}_k^n) \delta(\mathbf{x}_k - \mathbf{x}_k^n). \end{aligned} \quad (67)$$

This suggests to define the updated weights as

$$\omega_k^n \propto \omega_{k-1}^n p_k(\mathbf{y}_k|\mathbf{x}_k^n), \quad (68)$$

where the proportionality factor can be determined by the condition that the normalized updated weights should sum up to 1. Hence, the analysis elegantly sums up to a simple multiplication of the weights by the likelihood of each particle.

The forecast step amounts to applying Chapman-Kolmogorov Eq. (9):

$$\begin{aligned} p_{k+1|k}(\mathbf{x}_{k+1}|\mathbf{y}_{k:}) &= \int d\mathbf{x}_{k+1} p(\mathbf{x}_{k+1}|\mathbf{x}_k) p_{k|k}(\mathbf{x}_k|\mathbf{y}_{k:}) \\ &= \sum_{n=1}^N \int d\mathbf{x}_{k+1} p(\mathbf{x}_{k+1}|\mathbf{x}_k) \omega_k^n \delta(\mathbf{x}_k - \mathbf{x}_k^n) \\ &= \sum_{n=1}^N \omega_k^n p(\mathbf{x}_{k+1}|\mathbf{x}_k^n). \end{aligned} \quad (69)$$

If the model, defined by its transition density $p(\mathbf{x}_{k+1}|\mathbf{x}_k)$, as in Eq. (4), is deterministic, the forecast pdf $p_{k+1|k}$ is, as the update pdf $p_{k|k}$, in the form of a delta-Dirac density; otherwise it is not so. To obtain $p_{k+1|k}$ as a delta-Dirac pdf, we need to sample from Eq. (69).

One solution consists, for each particle n , in sampling \mathbf{x}_{k+1}^n from the density $p(\mathbf{x}_{k+1}|\mathbf{x}_k^n)$ by forecasting \mathbf{x}_k^n from t_k to t_{k+1} using the (possibly stochastic) model associated with the transition density $p(\mathbf{x}_{k+1}|\mathbf{x}_k)$, which yields:

$$p_{k+1|k}(\mathbf{x}_{k+1}|\mathbf{y}_{k:}) \approx \sum_{n=1}^N \omega_k^n \delta(\mathbf{x}_{k+1} - \mathbf{x}_{k+1}^n). \quad (70)$$

Alternatively, one can sample particle n from Eq. (69) by randomly selecting one of the particles, say n' , with a probability proportional to its importance weight. Once $\mathbf{x}_k^{n'}$ is selected,

one can forecast it and define \mathbf{x}_{k+1}^n using, as in the previous case, the model associated with the transition density $p(\mathbf{x}_{k+1}|\mathbf{x}_k^n)$, which yields

$$p_{k+1|k}(\mathbf{x}_{k+1}|\mathbf{y}_{k:}) \approx \frac{1}{N} \sum_{n=1}^N \delta(\mathbf{x}_{k+1} - \mathbf{x}_{k+1}^n). \quad (71)$$

The first option corresponds to the so-called *bootstrap* PF²³⁵ or sequential importance sampling (SIS) PF. The second option adds, before forecasting, a so-called *resampling* step that uniformly resets the weights to N^{-1} ; it is called sequential importance resampling (SIR) PF and is depicted in Fig. 10. There are several ways to resample the particles given their weights. Popular resampling schemes include multinomial resampling, residual resampling, and stochastic universal (or systematic) resampling, the latter minimizing the sampling noise introduced in the procedure²³⁶.

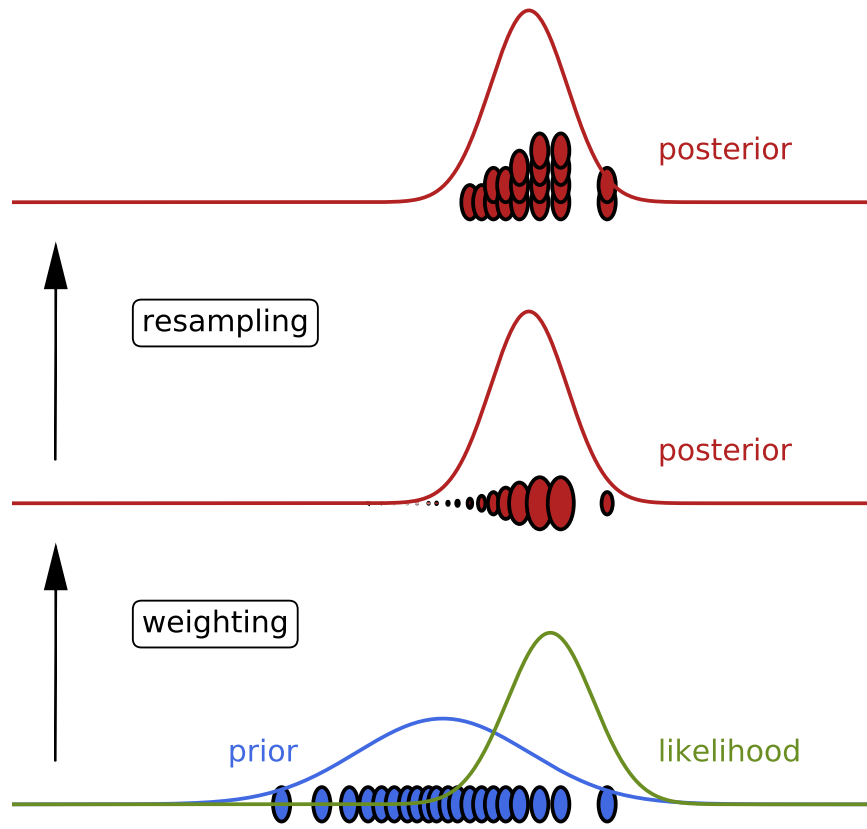


Figure 10: Principle of the SIR particle filter. The lower panel curves are the pdfs of the prior and the observation. The initial equal-weight particles are also displayed. The middle panel shows the weighing of the particles by the likelihood yielding unequal weights. The upper panel shows the outcome of resampling with multiple copies of several of the initial particles.

6.1.2 Importance sampling with a proposal

A richer class of particle filters can be formalized if we consider a density of trajectories $p_{k|k}(\mathbf{x}_{k:}|\mathbf{y}_{k:})$ in place of model states (i.e., the density $p_{k|k}(\mathbf{x}_k|\mathbf{y}_{k:})$), a pdf which is usually associated to a smoothing problem (cf. Sect. 2.2). Now, we assume the existence of a smoothing density $q(\mathbf{x}_{k:}|\mathbf{y}_{k:})$ from which it is easier to sample, instead of the "desired"

$p_{k|k}(\mathbf{x}_k|\mathbf{y}_k)$. It has the following delta-Dirac representation:

$$q(\mathbf{x}_k|\mathbf{y}_k) = \sum_{n=1}^N \omega_k^n \delta(\mathbf{x}_k - \mathbf{x}_k^n). \quad (72)$$

We can exploit this *proposal* density, which is auxiliary to the conditional pdf under study, to compute any statistical moment of the conditional probability $p_{k|k}(\mathbf{x}_k|\mathbf{y}_k)$. If ϕ is a generic test function, we have

$$\mathbb{E}[\phi(\mathbf{x}_k)] = \int d\mathbf{x}_k: \phi(\mathbf{x}_k) p_{k|k}(\mathbf{x}_k|\mathbf{y}_k) \quad (73)$$

$$= \int d\mathbf{x}_k: \phi(\mathbf{x}_k) \frac{p_{k|k}(\mathbf{x}_k|\mathbf{y}_k)}{q(\mathbf{x}_k|\mathbf{y}_k)} q(\mathbf{x}_k|\mathbf{y}_k) \quad (74)$$

$$= \sum_{n=1}^N \omega_k^n \phi(\mathbf{x}_k^n) \frac{p_{k|k}(\mathbf{x}_k^n|\mathbf{y}_k)}{q(\mathbf{x}_k^n|\mathbf{y}_k)}. \quad (75)$$

Hence, the conditional pdf can be represented using weighted samples:

$$p_{k|k}(\mathbf{x}_k|\mathbf{y}_k) \approx \sum_{n=1}^N \frac{p_{k|k}(\mathbf{x}_k^n|\mathbf{y}_k)}{q(\mathbf{x}_k^n|\mathbf{y}_k)} \omega_k^n \delta(\mathbf{x}_k - \mathbf{x}_k^n). \quad (76)$$

We further assume that the proposal density factorizes according to

$$q(\mathbf{x}_k|\mathbf{y}_k) = q(\mathbf{x}_k|\mathbf{x}_{k-1}, \mathbf{y}_k) q(\mathbf{x}_{k-1}|\mathbf{y}_{k-1}) \quad (77)$$

such that it is easy to sample \mathbf{x}_k^n from $q(\mathbf{x}_k|\mathbf{x}_{k-1}^n, \mathbf{y}_k)$.

The particle trajectories $\{\mathbf{x}_{k-1}^n, \omega_{k-1}^n\}_{n=1, \dots, N}$ can then be extended to t_k by sampling \mathbf{x}_k^n from $q(\mathbf{x}_k|\mathbf{x}_{k-1}^n, \mathbf{y}_k)$ so as to obtain $\{\mathbf{x}_k^n, \omega_k^n\}_{n=1, \dots, N}$. Hence, the smoothing conditional pdf at t_k is

$$p_{k|k}(\mathbf{x}_k|\mathbf{y}_k) = \sum_{n=1}^N \frac{p_{k|k}(\mathbf{x}_k^n|\mathbf{y}_k)}{q(\mathbf{x}_k^n|\mathbf{y}_k)} \omega_{k-1}^n \delta(\mathbf{x}_k - \mathbf{x}_k^n) \quad (78)$$

Assuming Markovian dynamics, the sequential evolution of the smoothing pdf decomposes as

$$p_{k|k}(\mathbf{x}_k|\mathbf{y}_k) \propto p(\mathbf{y}_k|\mathbf{x}_k) p(\mathbf{x}_k|\mathbf{x}_{k-1}) p_{k-1|k-1}(\mathbf{x}_{k-1}|\mathbf{y}_{k-1}), \quad (79)$$

which, together with Eq. (77), yields

$$p_{k|k}(\mathbf{x}_k|\mathbf{y}_k) \propto \sum_{n=1}^N \frac{p(\mathbf{x}_k^n|\mathbf{x}_{k-1}^n) p(\mathbf{y}_k|\mathbf{x}_k^n)}{q(\mathbf{x}_k^n|\mathbf{x}_{k-1}, \mathbf{y}_k)} \omega_{k-1}^n \delta(\mathbf{x}_k - \mathbf{x}_k^n). \quad (80)$$

By comparison with the generic Eq. (76), the weights should be updated at t_k according to

$$\omega_k^n \propto \frac{p(\mathbf{x}_k^n | \mathbf{x}_{k-1}^n) p(\mathbf{y}_k | \mathbf{x}_k^n)}{q(\mathbf{x}_k^n | \mathbf{x}_{k-1}, \mathbf{y}_{k:})} \omega_{k-1}^n, \quad (81)$$

up to a normalization to 1 of the updated weights. The filtering solution of the estimation problem is simply obtained without further computation from $\{\mathbf{x}_k^n, \omega_k^n\}_{n=1, \dots, N}$ by marginalization, i.e., keeping the states at t_k with the same weights: $\{\mathbf{x}_k^n, \omega_k^n\}_{n=1, \dots, N}$.

Importantly, if we choose $q(\mathbf{x}_k | \mathbf{x}_{k-1}, \mathbf{y}_{k:}) \equiv p(\mathbf{x}_k | \mathbf{x}_{k-1})$, then we obtain $\omega_k^n \propto p(\mathbf{y}_k | \mathbf{x}_k^n) \omega_{k-1}^n$ and recover the bootstrap PF (cf. Eq. (68)). Furthermore, if we choose $q(\mathbf{x}_k | \mathbf{x}_{k-1}, \mathbf{y}_{k:}) \equiv p(\mathbf{x}_k | \mathbf{y}_k, \mathbf{x}_{k-1})$, then we obtain $\omega_k^n \propto p(\mathbf{y}_k | \mathbf{x}_{k-1}^n) \omega_{k-1}^n$. This corresponds to the so-called *optimal importance proposal* PF²³⁷. It is optimal only in the sense that it minimizes the theoretical variance of each weight ω_k^n conditional on \mathbf{x}_{k-1}^n and $\mathbf{y}_{k:}$; over the realizations of \mathbf{x}_k^n . This variance is actually 0.

6.1.3 Degeneracy of the particle filter

The algebra required by these PFs is very simple and elegant, and in principle offers a nice and asymptotically exact alternative to the Gaussian approximations to DA. Unfortunately, the PF is plagued by the so-called *curse of dimensionality* as the dimensionality of the model is increased. In a sequential scheme, this curse manifests itself by the degeneracy of the weights: one weight will be close to 1, while the others essentially vanish²³⁸. That is to say, the ensemble of particles collapses onto one single particle, while updating the weights via Eq. (68) or Eq. (81). This collapse is very inefficient as far as state estimation is concerned. Resampling does help by resetting to uniform weights, but it is, quite often, not enough to counteract this curse. Moreover, this trend essentially grows exponentially with the dimension of the system. More precisely, it has been shown in very simple but instructive Gaussian models that the particle numbers required to avoid degeneracy should scale like the variance of the likelihood²³⁹:

$$\ln(m) \propto \text{Var} [\ln(p(\mathbf{y} | \mathbf{x}))]. \quad (82)$$

Equation (82) has the merit to show that m could scale exponentially with the size of the simple systems, but the derivation of such scaling is not straightforward in general.

A carefully designed proposal, such as the optimal proposal, and which can be shown to minimize the variance of the weights, does not change the exponential trend. Yet, it does reduce the constant in the exponent^{240,241}. Numerical investigations confirm this trend^{242,243}.

6.1.4 Smarter particle filters for the geosciences

Particle filtering is a well developed field of statistics and engineering^{244–246}. It is very successful with low-dimensional models (such as object tracking). The number of contributions to the topic has substantially grown in geophysical DA in recent years^{242,247}. Yet, the curse of dimensionality remains a major obstacle. That is why appealing schemes have been proposed to reduce its impact.

The implicit particle filter²⁴⁸ combines smoothing and particle filtering over a DAW, similarly to 4DVar or the IEnKS. It stands as a possible extension of the optimal proposal particle filter but over a several-step long DAW.

In order to circumvent the curse of dimensionality, one can restrict the full Bayesian analysis to a limited number of degrees of freedom, while the rest of the control variables are estimated via a Gaussian-based method, typically the EnKF. This strategy has been developed in Lagrangian DA²⁴⁹.

Another strategy relies on mitigating the degeneracy of the PF by hybridizing with the EnKF²⁵⁰. A family of algorithm can be created and parametrized by a mixing coefficient, which can be tuned or adaptively selected^{251–253}.

The equal weight PF and variants thereof^{254,255} build a proposal such that the particles effectively get the same numerical weight out of the analysis, a procedure which is obviously meant to avoid the degeneracy.

6.1.5 Localization

Similarly to the EnKF, a strategy to mitigate the curse of dimensionality that plagues the PF is to reduce the number of degrees of freedom by making local analyses. However, its implementation is trickier than with the EnKF. Indeed, considering a local domain localization, a particle will be given distinct local weights, even though they might vary smoothly in space. Hence, there is no natural updated particle that could emerge from the former if

the local weights are unequal, as opposed to the local EnKF. One should devise a gluing of local parts of particles through resampling and try to avoid nonphysical discontinuities at the intersections of the local domains. Such strategies have recently been proposed and implemented^{256–260}.

6.2 Coupled data assimilation

Data assimilation algorithms have been conceived mainly for NWP applications and have been usually designed for state estimation in systems with a single dominant dynamical scale and/or for an observational network having a dominant spatio-temporal density. The sustained increase of model resolutions, the deployment of more and more observation platforms and the use of coupled ESMs for s2d predictions, altogether bind to a deep re-thinking of the DA procedures. The design of efficient CDA methods, able to keep simultaneously control of all resolved scales and propagate adequately information across the climate system components, has been recently recognized to have primary importance.

Several research groups and institutions, including weather and climate services, are currently studying and developing CDA (see Penny and Hamill²⁶¹ for an updated report on these efforts). Early attempts include the case of sparsely observed flow possessing a wide range of scales with a KF-like procedure²⁶², or a study of the performance of the EnKF in a prototypical nonlinear dynamics possessing two scales of motion²⁶³. On the side of variational methods, Lorenc and Payne²⁶⁴ have nicely illustrated a modification of the 4DVar which might be successfully applied to global high-resolution coupled models.

Seasonal-to-decadal prediction spans time horizons of up to approximately 10 years, falling between NWP and centurial projections²²⁹. Correct initialization of the model is known to improve forecast quality on horizons of several years²⁶⁵, and predictions have been for long initialized with observations of the present climatic state using either the full field (FFI) or the anomaly initialization (AI) (see, e.g., Carrassi et al.²⁶⁶). FFI makes use of the best possible available estimate of the real state: it reduces the initial error, but the unavoidable presence of model deficiencies causes the model trajectory to drift away from the observations (see, e.g., Stockdale²⁶⁷). Anomaly initialization assimilates the observed climate anomalies on top of an estimate of the model mean climate. This initial state, at

the expense of an initial error of the size of the model bias, is expected to be closer to the model attractor (see, e.g., Smith and Murphy²⁶⁸), so that drift is reduced. Comparisons between FFI and AI have revealed respective advantages and drawbacks, the strong regional and model-dependency of the results (see, e.g., Carrassi et al.²⁶⁶, Magnusson et al.²⁶⁹, Smith et al.²⁷⁰, Hazeleger et al.²⁷¹), and the fact that AI is a viable option only when the model and the observed statistics differ largely on their first moments alone (i.e., the bias)²⁷².

However it was made clear that such a decoupled initialization approach induced problems, particularly imbalances at the boundary between the ocean and the atmosphere. To cope with this issue, a solution has shown some success: the *weakly coupled data assimilation (wCDA)*. In the wCDA, a coupled model is used to run the predictions but the observations of the different model compartments (atmosphere, ocean, land and sea-ice) are used independently, so that each component is subject to a separate analysis. A first attempt to create a weakly coupled reanalysis has been done in the USA at the National Center for Environmental Prediction (NCEP)²⁷³ and at the Japanese Agency for Marine-Earth Science and Technology (JAMSTEC)²⁷⁴, based on global ESMs and using 3DVar and 4DVar respectively. The wCDA reanalysis showed a marked improvement over the standard uncoupled formulation. In the JAMSTEC implementation the control variable includes the ocean initial conditions plus a set of parameters related to the air-sea fluxes. The approach acted as a proof-of-concept for producing successfully balanced initial conditions for the coupled system and optimal coupling parameters, and enhancing the skills of the s2d prediction. The UK MetOffice has designed a weakly coupled atmosphere-ocean assimilation using the incremental 4DVar²⁷⁵ (cf. Sect. 3.3.2) and the global coupled model, but the corrections for atmosphere and ocean are calculated independently. Similarly, the ECMWF is producing a 20-th century reanalysis, based on wCDA. The EnKF in a wCDA setting has been recently used to assimilate ocean observations to initialize s2d predictions with the Norwegian Earth System Model (NorESM)²⁷⁶.

Atmosphere and ocean are constrained independently using the ensemble-based approach at the Geophysical Fluid Dynamics Laboratory (GFDL) using the EAKF²⁷⁷. Using the same framework, Lu et al.²⁷⁸ have achieved some success in a controlled simulated scenario using *strongly CDA (sCDA)*, in which the different model compartments are coupled together

also at the analysis times, so that observations on one compartment, say the atmosphere, impact on another, say the ocean. The assimilation reconstructed successfully relevant climate fields over the period of interest and provides automatically the initial conditions to run an ensemble of forecasts. One of the first attempts of sCDA for a coupled ocean and sea-ice model has been used operationally in TOPAZ (cf Sect. 5.4), demonstrating that successful assimilation of sea ice concentrations requires a coupled, multivariate and time-dependent assimilation method⁸⁸. A recent interesting result using sCDA is due to Sluka et al.²⁷⁹ that shows improvements over wCDA in using only atmospheric observations in a coupled atmosphere-ocean model. Coupled data assimilation with the EnKF to recover the Atlantic meridional overturning circulation with simulated observations in a low-order coupled atmosphere-ocean model has been studied by Tardif et al.²⁸⁰, and subsequently with data from a millennial-scale simulation of a comprehensive coupled atmosphere-ocean climate model in Tardif et al.²⁸¹. These studies suggest that atmospheric observations alone, albeit frequent, do not suffice to properly recover the slowly evolving AMOC. Interestingly, it was shown that, in the lack of enough of observations in the ocean, CDA of time-averaged atmospheric measurements can successfully track the AMOC.

A comparison of different CDA approaches in the context of incremental 4DVar (cf. Sect. 3.3.2) using an idealized single-column atmosphere ocean model is given in Smith et al.²⁸², and revealed the benefit of CDA as being able to produce more balanced analysis fields than its uncoupled counter-part, thus reducing initialisation shock and the subsequent predictions. The same idealistic model setup has been used to investigate the impact of the model error and of the window length of the 4DVar showing that while uncoupled DA may reduce the analysis error more than the CDA, the latter better reduces the imbalances and thus reduces the forecasts error.

Coupled data assimilation is one of the main area of research at present time and more advancements can be expected in the coming years; a review on the current status of the field can be found in Penny and Hamill²⁶¹.

7 CONCLUSIONS

From its origin in the context of NWP, DA has later expanded to the broad areas of environmental prediction, including seasonal, interannual and decadal time-scales. The current efforts toward the implementation of seamless predictions, where the same high-resolution coupled models are used from short to long term forecasts, is also accompanied by advancements in DA so as to tackle the nonlinearities emerging by the increase in resolution and the coupling mechanisms giving rise to long term predictability.

Nevertheless, the range of applications of DA have not remained confined to the state (and/or parameters) estimation to initialize prediction, but are progressively involving other problems. A notable example is the detection and attribution of climate change, or climate related events²⁸³, which is the issue of providing evidence for either the existence or the non-existence of a causal relationship between a hypothetical forcing external (e.g., anthropogenic emission) to a system (e.g., the climate) and an observed response (e.g., increase of temperature), for which novel methods based on DA have proven to be very efficient²⁸⁴. More generally, DA can be efficiently used to estimate the marginal likelihood of the data, the so called model evidence²⁸⁵, which is a key statistical metric to perform model selection (see, e.g., Carson et al.²⁸⁶ for an application in the context of glacial-interglacial cycle) and calibration or parameter estimation (see, e.g., Winiarek et al.²⁸⁷, for the estimation of a radiological plume, or, Tandeo et al.²⁸⁸ for the optimization of a subgrid-scale parametrization). DA has been used to reconstruct the climate of the past based on observations proxies (see, e.g., Dubinkina and Goosse²⁸⁹), and, in the solid Earth science, for seismology applications (see, e.g., Fichtner et al.²⁹⁰).

In general the use DA has proven that the consistent data-to-model fusion provides a more insightful view on the phenomena of interest, than any of the two components, the model or the data, independently. Future applications of DA within the geosciences and beyond, are expected to be numerous, and to naturally arise by the improvement of our modelling capabilities, as a result of the increased computational power and physical understanding, on the one hand, and by the progresses of the observing facilities (such as, but not only, satellite) on the other. DA is thus expected to continue playing a central role to bridge

model with data, to maximally exploit their respective informational content.

We hope that this overview may be a first guide for scientists who are confronting with the use of DA methods, and provide them with a complete first outlook of the approaches and of their foundations. The present work is thus to be intended as a detailed introduction to the topic from where interested readers and researchers may later expand their knowledge.

ACKNOWLEDGEMENTS

The authors are thankful to P. N. Raanes (NERSC) and A. Farchi (ENPC) for their comments and suggestions and insightful discussion that have helped improve this review. A. Carrassi has been funded by the project REDDA of the Norwegian Research Council. CEREIA is a member of Institut Pierre-Simon Laplace (IPSL).

References

1. P. J. Van Leeuwen, Y. Cheng, and S. Reich, *Nonlinear data assimilation*, vol. 2 (Springer, 2015).
2. S. Reich and C. Cotter, *Probabilistic Forecasting and Bayesian Data Assimilation* (Cambridge University Press, Cambridge, 2015).
3. K. Law, A. Stuart, and K. Zygalakis, *Data assimilation: a mathematical introduction*, vol. 62 (Springer, 2015).
4. M. Asch, M. Bocquet, and M. Nodet, *Data Assimilation: Methods, Algorithms, and Applications*, Fundamentals of Algorithms (SIAM, Philadelphia, 2016), ISBN 978-1-611974-53-9.
5. R. Daley, *Atmospheric data analysis* (Cambridge university press, 1993).
6. E. Kalnay, *Atmospheric Modeling, Data Assimilation and Predictability* (Cambridge University Press, Cambridge, 2002).

7. G. Evensen, *Data Assimilation: The Ensemble Kalman Filter* (Springer-Verlag/Berlin/Heidelberg, 2009), 2nd ed.
8. J. E. Hoke and R. A. Anthes, *Mon. Weather Rev.* **104**, 1551 (1976).
9. S. Lakshmivarahan and J. M. Lewis, in *Data Assimilation for Atmospheric, Oceanic and Hydrologic Applications (Vol. II)*, edited by S. K. Park and L. Xu (Springer Berlin Heidelberg, 2013), pp. 27–57.
10. D. Auroux and J. Blum, *Nonlin. Processes Geophys.* **15**, 305 (2008).
11. D. Pazo, A. Carrassi, and J. Lopez, *Q J Roy. Meteor. Soc.* **142**, 1290 (2016).
12. G. S. Duane, J. J. Tribbia, and J. B. Weiss, *Nonlin. Proc. Geophys.* **13**, 601 (2006).
13. A. H. Jazwinski, *Stochastic Processes and Filtering Theory* (Academic Press, New-York, 1970).
14. A. Bain and D. Crisan, *Fundamentals of stochastic filtering*, vol. 3 (Springer, 2009).
15. C. Nicolis, *Journal of the Atmospheric Sciences* **60**, 2208 (2003).
16. A. Carrassi and S. Vannitsem, in *Mathematical Paradigms of Climate Science* (Springer, 2016), pp. 175–213.
17. M. Chekroun, E. Simonnet, and M. Ghil, *Physica D* **240**, 1685 (2011).
18. H. Dijkstra, *Nonlinear Climate Dynamics* (Cambridge University Press, Cambridge, 2013).
19. A. C. Lorenc, *Quarterly Journal of the Royal Meteorological Society* **112**, 1177 (1986).
20. T. Janjić, N. Bormann, M. Bocquet, J. A. Carton, S. E. Cohn, S. L. Dance, S. N. Losa, N. K. Nichols, R. Potthast, J. A. Waller, et al., *Q J Roy. Meteor. Soc.* **0**, 0 (2017), accepted for publication.
21. S. E. Cohn, *Journal of the Meteorological Society of Japan. Ser. II* **75**, 257 (1997).

22. G. Evensen, *IEEE Control Systems Magazine* **29**, 83 (2009).
23. N. Wiener, *Extrapolation, Interpolation and Smoothing of Stationary Time Series, with Engineering Applications* (M.I.T. Press, Cambridge, MA, 1949).
24. L. Bengtsson, M. Ghil, and E. Källén, eds., *Dynamic Meteorology: Data Assimilation Methods* (Springer-Verlag, New York/Heidelberg/Berlin, 1981).
25. D. Dee, S. Uppala, A. Simmons, P. Berrisford, P. Poli, S. Kobayashi, U. Andrae, M. Balmaseda, G. Balsamo, P. Bauer, et al., *Quarterly Journal of the royal meteorological society* **137**, 553 (2011).
26. J. Xie, L. Bertino, F. Counillon, K. A. Lisæter, and P. Sakov, *Ocean Science* **13**, 123 (2017).
27. O. Talagrand, *Journal of the Meteorological Society of Japan. Ser. II* **75**, 191 (1997).
28. C. K. Wikle and L. M. Berliner, *Physica D: Nonlinear Phenomena* **230**, 1 (2007).
29. E. Cosme, J. Verron, P. Brasseur, J. Blum, and D. Auroux, *Mon. Weather Rev.* **140**, 683 (2012).
30. R. Fitzgerald, *IEEE Transactions on Automatic Control* **16**, 736 (1971).
31. M. Bocquet, K. S. Gurumoorthy, A. Apte, A. Carrassi, C. Grudzien, and C. K. Jones, *SIAM/ASA Journal of Uncertainty Quantification* **5**, 304 (2017).
32. A. Carrassi, M. Ghil, A. Trevisan, and F. Uboldi, *Chaos* **18**, 023112 (2008).
33. D. P. Dee, *Q J Roy. Meteor. Soc.* **131**, 3323 (2005).
34. D. P. Dee, *Mon. Weather Rev.* **123**, 1128 (1995).
35. G. Ueno and N. Nakamura, *Q J Roy. Meteor. Soc.* **140**, 295 (2014).
36. G. Ueno and N. Nakamura, *Quarterly Journal of the Royal Meteorological Society* **142**, 2055 (2016).

37. D. Dreano, P. Tandeo, M. Pulido, B. Ait-El-Fquih, T. Chonavel, and I. Hoteit, Quarterly Journal of the Royal Meteorological Society (2017).
38. Y. Liu, J.-M. Haussaire, M. Bocquet, Y. Roustan, O. Saunier, and A. Mathieu, Q J Roy. Meteor. Soc. **0**, 0 (2017), accepted for publication.
39. M. Pulido, P. Tandeo, M. Bocquet, A. Carrassi, and M. Lucini, Submitted to PRE (2017).
40. L. M. Stewart, S. Dance, and N. Nichols, International journal for numerical methods in fluids **56**, 1521 (2008).
41. T. Miyoshi, E. Kalnay, and H. Li, Inverse Problems in Science and Engineering **21**, 387 (2013).
42. A. Gelb, *Applied optimal estimation* (MIT press, 1974).
43. R. E. Kalman, Journal of Fluids Engineering **82**, 35 (1960).
44. S. E. Cohn and D. P. Dee, SIAM Journal on Numerical Analysis **25**, 586 (1988).
45. B. Ni and Q. Zhang, Systems & Control Letters **94**, 172 (2016).
46. K. S. Gurumoorthy, C. Grudzien, A. Apte, A. Carrassi, and C. K. Jones, SIAM Journal on Control and Optimization **55**, 741 (2017).
47. A. Trevisan and L. Palatella, Nonlinear Proc. Geoph. **18**, 243 (2011).
48. F.-X. Le Dimet and O. Talagrand, Tellus A **38**, 97 (1986).
49. A. F. Bennett, *Inverse methods in physical oceanography* (Cambridge university press, 1992).
50. F. Uboldi and M. Kamachi, Tellus A **52**, 412 (2000).
51. O. Talagrand and P. Courtier, Q J Roy. Meteor. Soc. **113**, 1311 (1987).
52. M. Fisher and E. Andersson, *Developments in 4D-Var and Kalman filtering* (European Centre for Medium-Range Weather Forecasts, 2001).

53. Y. Sasaki, *Mon. Weather Rev.* **98**, 875 (1970).
54. J. M. Lewis and J. C. Derber, *Tellus A: Dynamic Meteorology and Oceanography* **37**, 309 (1985).
55. J. L. Lions, *Optimal control of systems governed by partial differential equations problèmes aux limites* (Springer, 1971).
56. O. Talagrand, in *Data assimilation: Making Sense of Observations* (Springer, 2010), pp. 41–67.
57. R. Miller, M. Ghil, and F. Gauthiez, *J. Atmos. Sci.* **51**, 1037 (1994).
58. C. Pires, R. Vautard, and O. Talagrand, *Tellus A* **48**, 96 (1996).
59. D. Zupanski, *Monthly Weather Review* **125**, 2274 (1997).
60. P. Vidard, A. Piacentini, and F.-X. Le Dimet, *Tellus A* **56**, 177 (2004).
61. Y. Trémolet, *Q J Roy. Meteor. Soc.* **132**, 2483 (2006).
62. Y. Trémolet, *Q J Roy. Meteor. Soc.* **133**, 1267 (2007).
63. A. Carrassi and S. Vannitsem, *Mon. Weather Rev.* **138**, 3369 (2010).
64. A. K. Griffith and N. K. Nichols, *Flow, turbulence and combustion* **65**, 469 (2000).
65. M. Lindskog, D. Dee, Y. Tremolet, E. Andersson, G. Radnoti, and M. Fisher, *Q J Roy. Meteor. Soc.* **135**, 695 (2009).
66. M. Fisher, Y. Tremolet, H. Auvinen, D. Tan, and P. Poli, *ECMWF Techn. Rep* **655** (2011).
67. H. Ngodock and M. Carrier, *Mon. Weather Rev.* **142**, 2108 (2014).
68. J. Amezcua, M. Goodliff, and P. J. Van Leeuwen, *Tellus A: Dynamic Meteorology and Oceanography* **69**, 1271564 (2017).

69. M. Fisher, M. Leutbecher, and G. Kelly, Quarterly Journal of the Royal Meteorological Society **131**, 3235 (2005).
70. M. Zupanski, Monthly Weather Review **124**, 2562 (1996).
71. S. Vannitsem, Chaos: An Interdisciplinary Journal of Nonlinear Science **27**, 032101 (2017).
72. A. C. Lorenc, N. E. Bowler, A. M. Clayton, S. R. Pring, and D. Fairbairn, Mon. Weather Rev. **143**, 212 (2015).
73. D. T. Kleist and K. Ide, Mon. Weather Rev. **143**, 433 (2015).
74. M. Buehner, R. McTaggart-Cowan, A. Beaulne, C. Charette, L. Garand, S. Heilliette, E. Lapalme, S. Laroche, S. R. Macpherson, J. Morneau, et al., Mon. Weather Rev. **143**, 2532 (2015).
75. R. N. Miller, M. Ghil, and F. Gauthiez, Journal of the atmospheric sciences **51**, 1037 (1994).
76. G. Evensen, J. Geophys. Res. **97**, 17,905 (1992).
77. M. Ghil, S. Cohn, J. Tavantzis, K. Bube, and E. Isaacson, in *Dynamic meteorology: data assimilation methods* (Springer-Verlag, New York, 1981).
78. D. Dee, S. Cohn, A. Dalcher, and M. Ghil, IEEE Trans. Automatic Control **30**, 1057 (1985).
79. M. Ghil and P. Malanotte-Rizzoli, Advances in geophysics **33**, 141 (1991).
80. C. Sun, Z. Hao, M. Ghil, and J. D. Neelin, Monthly weather review **130**, 1073 (2002).
81. D. Kondrashov, C. Sun, and M. Ghil, Monthly Weather Review **136**, 5062 (2008).
82. P. de Rosnay, G. Balsamo, C. Albergel, J. Muñoz-Sabater, and L. Isaksen, Surveys in Geophysics **35**, 607 (2014).
83. A. Carrassi and S. Vannitsem, Q J Roy. Meteor. Soc. **137**, 435 (2011).

84. A. Carrassi, R. Hamdi, P. Termonia, and S. Vannitsem, *Atmos. Sci. Lett.* **13**, 268 (2012).
85. P. Courtier, J.-N. Thépaut, and A. Hollingsworth, *Q J Roy. Meteor. Soc.* **120**, 1367 (1994).
86. A. Lawless, N. Nichols, C. Boess, and A. Bunse-Gerstner, *Monthly Weather Review* **136**, 1511 (2008).
87. P. L. Houtekamer, H. L. Mitchell, G. Pellerin, M. Buehner, M. Charron, L. Spacek, and B. Hansen, *Mon. Weather Rev.* **133**, 604 (2005).
88. P. Sakov, F. Counillon, L. Bertino, K. Lisæter, P. Oke, and A. Korablev, *Ocean Science* **8**, 633 (2012).
89. P. Houtekamer and F. Zhang, *Monthly Weather Review* **144**, 4489 (2016).
90. G. Evensen, *J. Geophys. Res.* **99**, 10,143 (1994).
91. G. Burgers, P. J. van Leeuwen, and G. Evensen, *Mon. Weather Rev.* **126**, 1719 (1998).
92. G. Evensen, *Ocean Dynamics* **53**, 343 (2003).
93. I. Hoteit, D.-T. Pham, M. Gharamti, and X. Luo, *Monthly Weather Review* **143**, 2918 (2015).
94. G. Evensen, *Ocean Dynamics* **54**, 539 (2004).
95. C. H. Bishop, B. J. Etherton, and S. J. Majumdar, *Mon. Weather Rev.* **129**, 420 (2001).
96. J. S. Whitaker and T. M. Hamill, *Mon. Weather Rev.* **130**, 1913 (2002).
97. J. L. Anderson, *Mon. Weather Rev.* **129**, 2884 (2001).
98. M. Zupanski, *Mon. Weather Rev.* **133**, 1710 (2005).
99. G. H. Golub and C. F. Van Loan, *Matrix computations*, vol. 3 (JHU Press, 2013).
100. X. Wang, C. H. Bishop, and S. J. Julier, *Monthly Weather Review* **132**, 1590 (2004).

101. P. Sakov and P. R. Oke, *Tellus, Ser. A* **60**, 361 (2008).
102. D. M. Livings, S. L. Dance, and N. K. Nichols, *Physica D* **237**, 1021 (2008).
103. B. Hunt, E. J. Kostelich, and I. Szunyogh, *Physica D* **230**, 112 (2007).
104. P. N. Raanes, A. Carrassi, and L. Bertino, *Mon. Weather Rev.* **143**, 3857 (2015).
105. M. K. Tippett, J. L. Anderson, C. H. Bishop, T. M. Hamill, and J. S. Whitaker, *Mon. Weather Rev.* **131**, 1485 (2003).
106. L. Nerger, T. Janjić, J. Schröter, and W. Hiller, *Monthly Weather Review* **140**, 2335 (2012).
107. D. T. Pham, *Monthly weather review* **129**, 1194 (2001).
108. P. Sakov and P. R. Oke, *Mon. Weather Rev.* **136**, 1042 (2008).
109. P. N. Raanes, *Q J Roy. Meteor. Soc.* **142**, 1259 (2016).
110. P. L. Houtekamer and H. L. Mitchell, *Mon. Weather Rev.* **129**, 123 (2001).
111. T. M. Hamill, J. S. Whitaker, and C. Snyder, *Mon. Weather Rev.* **129**, 2776 (2001).
112. V. E. Haugen and G. Evensen, *Ocean Dynamics* **52**, 133 (2002).
113. G. Evensen, *Ocean Dynamics* **53**, 343 (2003).
114. E. Ott, B. R. Hunt, I. Szunyogh, A. V. Zimin, E. J. Kostelich, M. Corazza, E. Kalnay, D. J. Patil, and A. Yorke, *Tellus A* **56**, 415 (2004).
115. R. A. Horn and C. R. Johnson, *Matrix analysis* (Cambridge university press, 2012).
116. G. Gaspari and S. E. Cohn, *Q J Roy. Meteor. Soc.* **125**, 723 (1999).
117. P. Sakov and L. Bertino, *Comput. Geosci.* **15**, 225 (2011).
118. J. D. Kepert, *Q J Roy. Meteor. Soc.* **135**, 1157 (2009).

119. S. J. Greybush, E. Kalnay, T. Miyoshi, K. Ide, and B. R. Hunt, *Mon. Weather Rev.* **139**, 511 (2011).
120. D. T. Pham, J. Verron, and M. C. Roubaud, *J. Marine Syst.* **16**, 323 (1998).
121. J. L. Anderson and S. L. Anderson, *Mon. Weather Rev.* **127**, 2741 (1999).
122. M. Bocquet, *Nonlinear Proc. Geoph.* **18**, 735 (2011).
123. J. S. Whitaker and T. M. Hamill, *Mon. Weather Rev.* **140**, 3078 (2012).
124. M. Bocquet, P. N. Raanes, and A. Hannart, *Nonlinear Proc. Geoph.* **22**, 645 (2015).
125. X. Wang and C. H. Bishop, *J. Atmos. Sci.* **60**, 1140 (2003).
126. J. L. Anderson, *Tellus A* **59**, 210 (2007).
127. H. Li, E. Kalnay, and T. Miyoshi, *Q J Roy. Meteor. Soc.* **135**, 523 (2009).
128. X. G. Zheng, *Adv. Atmos. Sci.* **26**, 154 (2009).
129. J.-M. Brankart, E. Cosme, C.-E. Testut, P. Brasseur, and J. Verron, *Mon. Weather Rev.* **138**, 932 (2010).
130. T. Miyoshi, *Mon. Weather Rev.* **139**, 1519 (2011).
131. M. Bocquet and P. Sakov, *Nonlinear Proc. Geoph.* **19**, 383 (2012).
132. X. Liang, X. Zheng, S. Zhang, G. Wu, Y. Dai, and Y. Li, *Q J Roy. Meteor. Soc.* **138**, 263 (2012).
133. M. Ying and F. Zhang, *Q J Roy. Meteor. Soc.* **141**, 2898 (2015).
134. P. Bauer, A. Thorpe, and G. Brunet, *Nature* **525**, 47 (2015).
135. A. C. Lorenc, *Q J Roy. Meteor. Soc.* **129**, 3183 (2003).
136. E. Kalnay, H. Li, T. Miyoshi, S.-C. Yang, and J. Ballabrera-Poy, *Tellus A* **59**, 758 (2007).

137. S.-C. Yang, M. Corazza, A. Carrassi, E. Kalnay, and T. Miyoshi, *Monthly Weather Review* **137**, 693 (2009).
138. M. Bocquet and P. Sakov, *Nonlinear Proc. Geoph.* **20**, 803 (2013).
139. R. N. Bannister, *Q J Roy. Meteor. Soc.* **143**, 607 (2017).
140. A. Lorenc, *Recommended Nomenclature for EnVar Data Assimilation Methods* (Available at:http://www.wcrp-climate.org/WGNE/BlueBook/2013/individual-articles/01_Lorenc_Andrew_EnVar_nomenclature.pdf, 2013).
141. T. M. Hamill and C. Snyder, *Mon. Weather Rev.* **128**, 2905 (2000).
142. T. Auligné, B. Ménétrier, A. C. Lorenc, and M. Buehner, *Mon. Weather Rev.* **144**, 6773696 (2016).
143. L. Raynaud, L. Berre, and G. Desroziers, *Q J Roy. Meteor. Soc.* **135**, 1177 (2009).
144. L. Raynaud, L. Berre, and G. Desroziers, *Q J Roy. Meteor. Soc.* **137**, 607 (2011).
145. L. Berre, H. Varella, and G. Desroziers, *Q J Roy. Meteor. Soc.* **141**, 2803 (2015).
146. M. Bonavita, L. Raynaud, and L. Isaksen, *Q J Roy. Meteor. Soc.* **137**, 423 (2011).
147. M. Bonavita, L. Isaksen, and E. Hólm, *Q J Roy. Meteor. Soc.* **138**, 1540 (2012).
148. M. Buehner, *Q J Roy. Meteor. Soc.* **131**, 1013 (2005).
149. X. Wang, C. Snyder, and T. M. Hamill, *Mon. Weather Rev.* **135**, 222 (2007).
150. M. Fisher and S. Gürol, *Q J Roy. Meteor. Soc.* **143**, 1136 (2017).
151. C. Liu, Q. Xiao, and B. Wang, *Mon. Weather Rev.* **136**, 3363 (2008).
152. C. Robert, S. Durbiano, E. Blayo, J. Verron, J. Blum, and F. X. Le Dimet, *Journal of Marine Systems* **57**, 70 (2005).
153. C. Liu, Q. Xiao, and B. Wang, *Mon. Weather Rev.* **137**, 1687 (2009).

154. M. Buehner, P. L. Houtekamer, C. Charette, H. L. Mitchell, and B. He, *Mon. Weather Rev.* **138**, 1550 (2010).
155. D. Fairbairn, S. R. Pring, A. C. Lorenc, and I. Roulstone, *Q J Roy. Meteor. Soc.* **140**, 281 (2014).
156. M. Bocquet and P. Sakov, *Q J Roy. Meteor. Soc.* **140**, 1521 (2014).
157. M. Bocquet, *Q J Roy. Meteor. Soc.* **142**, 1075 (2016).
158. G. Desroziers, E. Arbogast, and L. Berre, *Q J Roy. Meteor. Soc.* **142**, 3171 (2016), accepted for publication.
159. M. Buehner, P. L. Houtekamer, C. Charette, H. L. Mitchell, and B. He, *Mon. Weather Rev.* **138**, 1567 (2010).
160. M. Zhang and F. Zhang, *Mon. Weather Rev.* **140**, 587 (2012).
161. A. M. Clayton, A. C. Lorenc, and D. M. Barker, *Q J Roy. Meteor. Soc.* **139**, 1445 (2013).
162. J. Poterjoy and F. Zhang, *Mon. Weather Rev.* **143**, 1601 (2015).
163. M. Buehner, J. Morneau, and C. Charette, *Nonlinear Proc. Geoph.* **20**, 669 (2013).
164. N. Gustafsson, J. Bojarova, and O. Vignes, *Nonlinear Proc. Geoph.* **21**, 303 (2014).
165. G. Desroziers, J.-T. Camino, and L. Berre, *Q J Roy. Meteor. Soc.* **140**, 2097 (2014).
166. M. Buehner, R. McTaggart-Cowan, A. Beaulne, C. Charette, L. Garand, S. Heilliette, E. Lapalme, S. Laroche, S. R. Macpherson, J. Morneau, et al., *Mon. Weather Rev.* **143**, 2532 (2015).
167. N. E. Bowler, A. M. Clayton, M. Jardak, E. Lee, A. C. Lorenc, C. Piccolo, S. R. Pring, M. A. Wlasak, D. M. Barker, G. W. Inverarity, et al., *Q J Roy. Meteor. Soc.* **n/a**, n/a (2017).
168. P. Sakov, D. S. Oliver, and L. Bertino, *Mon. Weather Rev.* **140**, 1988 (2012).

169. B. M. Bell, *SIAM J. Optim.* **4**, 626 (1994).
170. J. Mandel, E. Bergou, S. Gürol, S. Gratton, and I. Kusanický, *Nonlinear Proc. Geoph.* **23**, 59 (2016).
171. E. D. Nino Ruiz and A. Sandu, *Journal of Computational and Applied Mathematics* **293**, 164 (2016).
172. B. R. Hunt, E. Kalnay, E. J. Kostelich, E. Ott, D. J. D. J. Patil, T. Sauer, I. Szunyogh, J. A. Yorke, and A. V. Zimin, *Tellus A* **56**, 273 (2004).
173. E. Lorenz, *J. Atmos. Sci.* **20**, 130 (1963).
174. E. N. Lorenz and K. A. Emanuel, *J. Atmos. Sci.* **55**, 399 (1998).
175. E. N. Lorenz, *J. Atmos. Sci.* **62**, 1574 (2005).
176. E. N. Lorenz, in *Seminar on Predictability* (1996), vol. 1.
177. A. Trevisan and L. Palatella, *International Journal of Bifurcation and Chaos* **21**, 3389 (2011).
178. E. Kalnay and A. Dalcher, *Monthly weather review* **115**, 349 (1987).
179. M. Leutbecher and T. N. Palmer, *Journal of Computational Physics* **227**, 3515 (2008).
180. B. Legras and R. Vautard, in *Proceedings 1995 ECMWF Seminar on Predictability* (Citeseer, 1996), vol. 1, pp. 143–156.
181. P. V. Kuptsov and U. Parlitz, *J. Nonlinear Sci.* **22**, 727 (2012).
182. A. Carrassi, A. Trevisan, and F. Uboldi, *Tellus A* **59**, 101 (2007).
183. A. Carrassi, S. Vannitsem, D. Zupanski, and M. Zupanski, *Tellus A* **61**, 587 (2009).
184. G.-H. C. Ng, D. McLaughlin, D. Entekhabi, and A. Ahanin, *Tellus A* **63**, 958 (2011).
185. M. Bocquet and A. Carrassi, *Tellus A: Dynamic Meteorology and Oceanography* **69**, 1304504 (2017).

186. A. Trevisan and F. Uboldi, *J. Atmos. Sci.* **61**, 103 (2004).
187. L. Palatella, A. Carrassi, and A. Trevisan, *J. Phys. A: Math. Theor.* **46**, 254020 (2013).
188. A. Carrassi, A. Trevisan, L. Descamps, O. Talagrand, and F. Uboldi, *Nonlinear Proc. Geoph.* **15**, 503 (2008).
189. F. Uboldi and A. Trevisan, *Nonlinear Proc. Geoph.* **16**, 67 (2006).
190. A. Trevisan, M. D'Isidoro, and O. Talagrand, *Q J Roy. Meteor. Soc.* **136**, 487 (2010).
191. L. Palatella and A. Trevisan, *Phys. Rev. E* **91**, 042905 (2015).
192. J.-M. Brankart, C.-E. Testut, D. Béal, M. Doron, C. Fontana, M. Meinvielle, P. Brasseur, and J. Verron, *Ocean Sci.* **8**, 121 (2012).
193. L. Bertino, G. Evensen, and H. Wackernagel, *International Statistical Review* **71**, 223 (2003).
194. J. P. Chilès and P. Delfiner, *Geostatistics: Modeling Spatial Uncertainty* (Wiley, New York, 1999).
195. J. Amezcua and P. J. Van Leeuwen, *Tellus A* **66**, 1 (2014), ISSN 1600-0870.
196. E. Simon and L. Bertino, *Ocean Sci.* **5**, 495 (2009), ISSN 1812-0822.
197. E. Simon and L. Bertino, *J. Mar. Syst.* **89**, 1 (2012).
198. L. Li, H. Zhou, H. J. Hendricks Franssen, and J. J. Gómez-Hernández, *Hydrol. Earth Syst. Sci.* **16**, 573 (2012), ISSN 10275606.
199. E. Simon, A. Samuelsen, L. Bertino, and S. Mouysset, *J. Mar. Syst.* **152**, 1 (2015), ISSN 09247963.
200. M. Gharamti, A. Samuelsen, L. Bertino, E. Simon, A. Korosov, and U. Daewel, *J. Mar. Syst.* **168**, 1 (2017), ISSN 09247963.
201. H. Zhou, L. Li, H.-J. Hendricks Franssen, and J. J. Gómez-Hernández, *Math. Geosci.* **44**, 169 (2012), ISSN 1874-8953.

202. M. Gharamti, J. Tjiputra, I. Bethke, A. Samuelsen, I. Skjelvan, M. Bentsen, and L. Bertino, *Ocean Model.* **112**, 65 (2017), ISSN 14635003.
203. A. Barth, M. Canter, B. van Schaeybroeck, S. Vannitsem, F. Massonnet, V. Zunz, P. Mathiot, A. Alvera-Azcarate, and J.-M. Beckers, *Ocean Model.* **93**, 22 (2015), ISSN 14635003.
204. K. Aalstad, S. Westermann, L. Bertino, and J. Boike (2017).
205. H. Wackernagel, *Multivariate Geostatistics* (Springer Verlag, Berlin, 2003), 3rd ed.
206. C. Schölzel and P. Friederichs, *Nonlinear Process. Geophys.* **15**, 761 (2008), ISSN 16077946.
207. C. Thacker, *Ocean Model.* **16**, 264 (2007).
208. C. Lauvernet, J.-M. Brankart, F. Castruccio, G. Broquet, P. Brasseur, and J. Verron, *Ocean Model.* **27**, 1 (2009), ISSN 1463-5003.
209. T. Janjić, D. McLaughlin, S. E. Cohn, and M. Verlaan, *Mon. Weather Rev.* **142**, 755 (2014), ISSN 0027-0644.
210. Y. Wang, F. Counillon, and L. Bertino, *Q. J. R. Meteorol. Soc.* **142** (2016), ISSN 1477870X.
211. G. R. Carmichael, A. Sandu, T. Chai, D. Daescu, E. Constantinescu, and Y. Tang, *J. Comp. Phys.* **227**, 3540 (2008).
212. Y. Zhang, M. Bocquet, V. Mallet, C. Seigneur, and A. Baklanov, *Atmos. Environ.* **60**, 656 (2012).
213. M. Bocquet, H. Elbern, H. Eskes, M. Hirtl, R. Zabkar, G. R. Carmichael, J. Flemming, A. Inness, M. Pagowski, J. L. Pérez Camaño, et al., *Atmos. Chem. Phys.* **15**, 5325 (2015).
214. H. Elbern, A. Strunk, H. Schmidt, and O. Talagrand, *Atmos. Chem. Phys.* **7**, 3749 (2007).

215. R. G. Hanea, G. J. M. Velders, A. J. Segers, M. Verlaan, and A. W. Heemink, *Mon. Weather Rev.* **135**, 140 (2007).
216. E. M. Constantinescu, A. Sandu, T. Chai, and G. R. Carmichael, *Q J Roy. Meteor. Soc.* **133**, 1229 (2007).
217. E. M. Constantinescu, A. Sandu, T. Chai, and G. R. Carmichael, *Q J Roy. Meteor. Soc.* **133**, 1245 (2007).
218. L. Wu, V. Mallet, M. Bocquet, and B. Sportisse, *J. Geophys. Res.* **113**, D20310 (2008).
219. J.-M. Haussaire and M. Bocquet, *Geosci. Model Dev.* **9**, 393 (2016).
220. E. Emili, S. Gurol, and D. Cariolle, *Geosci. Model Dev.* **9**, 3933 (2016).
221. R. Bleck, *Ocean Model.* **37**, 55.88 (2002).
222. D. T. Pham, J. Verron, and M. C. Roubaud, *Journal of Marine systems* **16**, 323 (1998).
223. K. Brusdal, J. Brankart, G. Halberstadt, G. Evensen, P. Brasseur, P. J. van Leeuwen, E. Dombrowsky, and J. Verron, *J. Marine. Sys.* **40-41**, 253 (2003).
224. K. A. Lisæter, J. Rosanova, and G. Evensen, *Ocean Dynamics* **53**, 368 (2003).
225. L. J. Natvik and G. Evensen, *J. Marine. Sys.* **40-41**, 127 (2003).
226. F. Counillon, N. Keenlyside, I. Bethke, Y. Wang, S. Billeau, M. L. Shen, and M. Bentsen, *Tellus A* **68**, 1 (2016), ISSN 1600-0870.
227. P., G. Evensen, and L. Bertino, *Tellus Ser A* **62A**, 24 (2010).
228. J. Xie, L. Bertino, F. Counillon, K. A. Lisæter, and P. Sakov, *Ocean Sci.* **13**, 123 (2017), ISSN 1812-0792.
229. F. J. Doblas-Reyes, J. García-Serrano, F. Lienert, A. P. Biescas, and L. R. Rodrigues, *Wiley Interdisciplinary Reviews: Climate Change* **4**, 245 (2013).
230. L. Kuznetsov, K. Ide, and C. K. Jones, *Monthly Weather Review* **131**, 2247 (2003).

231. H. Salman, L. Kuznetsov, C. Jones, and K. Ide, *Monthly Weather Review* **134**, 1081 (2006).
232. A. Apte and C. K. Jones, *Nonlinear Processes in Geophysics* **20**, 329 (2013).
233. P. Rampal, S. Bouillon, E. Ólason, and M. Morlighem, *Cryosphere* **10** (2016).
234. B. Bonan, N. K. Nichols, M. J. Baines, and D. Partridge, *Nonlinear Processes in Geophysics Discussions* **2016**, 1 (2016).
235. N. J. Gordon, D. J. Salmond, and A. F. M. Smith, *IEE Proc.-F* **140**, 107 (1993).
236. R. Douc and O. Cappé, in *Image and Signal Processing and Analysis, 2005. ISPA 2005. Proceedings of the 4th International Symposium on* (2005), pp. 64–69.
237. A. Doucet, S. Godsill, and C. Andrieu, *Stat. Comput.* **10**, 197 (2000).
238. A. Kong, J. S. Liu, and W. H. Wong, *Journal of the American statistical association* **89**, 278 (1994).
239. C. Snyder, T. Bengtsson, P. Bickel, and J. L. Anderson, *Mon. Weather Rev.* **136**, 4629 (2008).
240. D. J. C. MacKay, *Information Theory, Inference and Learning Algorithms* (Cambridge University Press, Cambridge, 2003).
241. C. Snyder, T. Bengtsson, and T. Morzfeld, *Mon. Weather Rev.* **143**, 4750 (2015).
242. M. Bocquet, C. Pires, and L. Wu, *Mon. Weather Rev.* **138**, 2997 (2010).
243. L. Slivinski and C. Snyder, *Mon. Weather Rev.* **144**, 861 (2016).
244. A. Doucet, N. de Freitas, and N. Gordon, eds., *Sequential Monte Carlo Methods in Practice* (Springer-Verlag New York Inc., 2001).
245. S. Arulampalam, S. Maskell, N. Gordon, and T. Clapp, *IEEE Trans. on Signal Processing* **50**, 174 (2002).

246. Z. Chen, *Statistics* **182**, 1 (2003).
247. P. J. van Leeuwen, *Mon. Weather Rev.* **137**, 4089 (2009).
248. M. Morzfeld, X. Tu, E. Atkins, and A. J. Chorin, *J. Comp. Phys.* **231**, 2049 (2012).
249. L. Slivinski, E. Spiller, A. Apte, and B. Sandstede, *Mon. Weather Rev.* **143**, 195 (2015).
250. N. Santitissadeekorn and C. Jones, *Monthly Weather Review* **143**, 2028 (2015).
251. A. S. Stordal, H. A. Karlsen, G. Nævdal, H. J. Skaug, and B. Vallès, *Comput. Geosci.* **15**, 293 (2011).
252. M. Frei and H. R. Künsch, *Biometrika* **100**, 781 (2013).
253. N. Chustagulprom, S. Reich, and M. Reinhardt, *SIAM/ASA Journal on Uncertainty Quantification* **4**, 592 (2016).
254. M. Ades and P.-J. van Leeuwen, *Q J Roy. Meteor. Soc.* **141**, 484 (2015).
255. M. Zhu, P.-J. van Leeuwen, and J. Amezcua, *Q J Roy. Meteor. Soc.* **142**, 1904 (2016).
256. S. Reich, *SIAM J. Sci. Comput.* **35**, A2013 (2013).
257. J. Poterjoy, *Mon. Weather Rev.* **144**, 59 (2016).
258. S. G. Penny and T. Miyoshi, *Nonlinear Proc. Geoph.* **23**, 391 (2016).
259. S. Robert and H. R. Künsch, *Tellus A* **69**, 1282016 (2017).
260. A. Beskos, D. Crisan, A. Jasra, K. Kamatani, and Y. Zhou, *Advances in Applied Probability* **49**, 24 (2017).
261. S. G. Penny and T. M. Hamill, *Bulletin of the American Meteorological Society* (2017).
262. J. Harlim and A. J. Majda, *Monthly Weather Review* **138**, 1050 (2010).
263. J. Ballabrera-Poy, E. Kalnay, and S.-C. Yang, *Tellus A* **61**, 539 (2009).

264. A. C. Lorenc and T. Payne, *Quarterly Journal of the Royal Meteorological Society* **133**, 607 (2007).
265. A. Carrassi, V. Guemas, F. Doblas-Reyes, D. Volpi, and M. Asif, *Climate Dynamics* **47**, 3693 (2016).
266. A. Carrassi, R. Weber, V. Guemas, F. Doblas-Reyes, M. Asif, and D. Volpi, *Nonlinear Processes in Geophysics* **21**, 521 (2014).
267. T. N. Stockdale, *Monthly Weather Review* **125**, 809 (1997).
268. D. M. Smith and J. M. Murphy, *Journal of Geophysical Research: Oceans* **112** (2007).
269. L. Magnusson, M. Alonso-Balmaseda, S. Corti, F. Molteni, and T. Stockdale, *Climate dynamics* **41**, 2393 (2013).
270. D. M. Smith, R. Eade, and H. Pohlmann, *Climate dynamics* **41**, 3325 (2013).
271. W. Hazeleger, V. Guemas, B. Wouters, S. Corti, I. Andreu-Burillo, F. Doblas-Reyes, K. Wyser, and M. Caian, *Geophysical Research Letters* **40**, 1794 (2013).
272. R. J. Weber, A. Carrassi, and F. J. Doblas-Reyes, *Monthly Weather Review* **143**, 4695 (2015).
273. S. Saha, S. Moorthi, H.-L. Pan, X. Wu, J. Wang, S. Nadiga, P. Tripp, R. Kistler, J. Woollen, D. Behringer, et al., *Bulletin of the American Meteorological Society* **91**, 1015 (2010).
274. N. Sugiura, T. Awaji, S. Masuda, T. Mochizuki, T. Toyoda, T. Miyama, H. Igarashi, and Y. Ishikawa, *Journal of Geophysical Research: Oceans* **113** (2008).
275. P. Laloyaux, M. Balmaseda, D. Dee, K. Mogensen, and P. Janssen, *Quarterly Journal of the Royal Meteorological Society* **142**, 65 (2016).
276. F. Counillon, I. Bethke, N. Keenlyside, M. Bentsen, L. Bertino, and F. Zheng, *Tellus A: Dynamic Meteorology and Oceanography* **66**, 21074 (2014).

277. S. Zhang, M. Harrison, A. Rosati, and A. Wittenberg, *Monthly Weather Review* **135**, 3541 (2007).
278. F. Lu, Z. Liu, S. Zhang, and Y. Liu, *Monthly Weather Review* **143**, 3823 (2015).
279. T. C. Sluka, S. G. Penny, E. Kalnay, and T. Miyoshi, *Geophysical Research Letters* **43**, 752 (2016).
280. R. Tardif, G. J. Hakim, and C. Snyder, *Climate dynamics* **43**, 1631 (2014).
281. R. Tardif, G. J. Hakim, and C. Snyder, *Climate Dynamics* **45**, 1415 (2015).
282. P. J. Smith, A. M. Fowler, and A. S. Lawless, *Tellus A: Dynamic Meteorology and Oceanography* **67**, 27025 (2015).
283. P. Stott, M. Allen, N. Christidis, R. Dole, M. Hoerling, C. Huntingford, P. Pall, J. Perlwitz, and D. Stone, in *Climate Science for Serving Society: Research, Modelling and Prediction Priorities*. G.R. Asrar and J. W. Hurrell (Eds.) (Springer, 2013).
284. A. Hannart, A. Carrassi, M. Bocquet, M. Ghil, P. Naveau, M. Pulido, J. Ruiz, and P. Tandeo, *Climatic Change* **136**, 155 (2016).
285. A. Carrassi, M. Bocquet, A. Hannart, and M. Ghil, *Quarterly Journal of the Royal Meteorological Society* **143**, 866 (2017).
286. J. Carson, M. Crucifix, S. Preston, and R. D. Wilkinson, *Journal of the Royal Statistical Society: Series C (Applied Statistics)* (2017).
287. V. Winiarek, J. Vira, M. Bocquet, M. Sofiev, and O. Saunier, *Atmos. Environ.* **45**, 2944 (2011).
288. P. Tandeo, M. Pulido, and F. Lott, *Q J Roy. Meteor. Soc.* **141**, 383 (2015).
289. S. Dubinkina and H. Goosse, *Climate of the Past* **9**, 1141 (2013).
290. A. Fichtner, H.-P. Bunge, and H. Igel, *Physics of the Earth and Planetary Interiors* **157**, 105 (2006).